

AFFDL-TM-75-147-FXM

AIR FORCE FLIGHT DYNAMICS LABORATORY
DIRECTOR OF SCIENCE & TECHNOLOGY
AIR FORCE SYSTEMS COMMAND
WRIGHT-PATTERSON AIR FORCE BASE OHIO

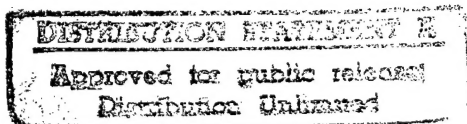


WEAPONS BAY TURBULENCE
REDUCTION TECHNIQUES

Rodney L. Clark

Aerodynamics and Airframe Branch
Aeromechanics Division
Air Force Flight Dynamics Laboratory

December 1975



Project 1476

19980113 253

DTIC QUALITY INSPECTED 2

Approved for public release, 20 Nov 85, ASD 85 2185

FOREWORD


This report documents an in-house wind tunnel test program conducted by the Aerodynamics and Airframe Branch, Aeromechanics Division, Air Force Flight Dynamics Laboratory, Wright Patterson AFB, Ohio 45433. The work was performed from June 1973 to November 1975 under Project 14760313.

This effort was supported by the Air Force Weapons Laboratory under Project Order 73-159 which funded procurement of the wind tunnel model.

The author wishes to acknowledge AFFDL/FXN and AFFDL/FYA for their contributions to this effort. Mr. Richard D. Talmadge, AFFDL/FYA, deserves a special thanks for his expert advice and assistance during the planning and data reduction phases of this effort.

In addition Mr. Richard D. Dyer and Capt. William A. Sotomayer of AFFDL/FXM participated in the planning, model design, test and data analysis phases of this effort. Their efforts were of major assistance.

This report has been reviewed and is approved.


ALFRED C. DRAPER
Asst for Research & Technology
Aeromechanics Division

This Document Contains Missing
Page/s That Are Unavailable In
The Original Document

ERRATUM SHEET FOR AFFDL-TM-75-147-FXM

The following figure titles and information were omitted or unreadable in the printed copies.

- Page 36 - Figure 12. Close up of Configuration 1 with Fence I and Rounded Aft Lip
- Page 85 - Figure 9A. Effect of Blowing at the Forward Lip on Static Pressure Distribution, Configuration 1.
- Page 87 - Figure 11A. Effect of Blowing over Aft Curved Lip on Static Pressure Distribution, Configuration 1.
- Page 93 - Figure 17A. Mach Effects on Static Pressure Distribution with Single BDU-8 in Bay, Configuration 2.
- Page 99 - Figure 23A. Effect of Fence I with and without Store L in Forward Bay, Configuration 3.
- Page 92 - The ☐ symbol represents data with Fence I.
The ☐ symbol represents data without a fence.



RODNEY L. CLARK
Aerodynamics and Airframe Branch
Aeromechanics Division
Air Force Flight Dynamics Laboratory

ABSTRACT

This effort was directed toward experimental investigation of the static and dynamic pressure levels within shallow weapons bay cavities. Several turbulence reduction techniques and various bay geometry features were investigated. These included forward and aft blowing slots, fences positioned at the upstream cavity lip, and rounded cavity lips. Installation of a 50% porosity fence at the forward lip was determined to be the single most effective technique.

LIST OF ILLUSTRATIONS

<u>Figure</u>	<u>Title</u>	<u>Page</u>
1	Weapons Bay Wind Tunnel Model Installed in AFFDL Tri-sonic Gasdynamic Facility	2
2a	Weapons Bay Model Prior to Wind Tunnel Installation	16
2b	Weapons Bay Model Prior to Wind Tunnel Installation	17
3	Comparison of Configurations 1 and 2 (Cross Hatched Areas Indicate Config. 2)	18
4	Cross Section View, Configuration 1	19
5	Cross Section View, Configuration 3 (Tandem Bay)	20
6	Turbulence Reduction Fences	21
7	Detail View Showing Location of Nozzles and Lip Geometry	22
8	Instrumentation Schematic (See Table I)	23
9	Boundary Layer Profiles with and without Boundary Layer Trip	33
10	Angle of Attack Effects on Turbulence with and without Boundary Layer Trip, Configuration 3, Bays Empty	34
11	Configuration 1 with Fence I Prior to Tunnel Installation	35
12	Close up of Configuration 1 with Fence I and Rounded Aft Lip	36
13	View of Configuration 1 with Rounded Aft Lip and B. L. Trip	37
14	Angle of Attack Effects (Alpha) on Turbulence Distribution, Configuration 1	38
15	Angle of Attack Effects (Alpha) on Turbulence Distribution, Configuration 1	39
16	Angle of Attack Effects (Alpha) on Turbulence Distribution, Configuration 1	40
17	Angle of Attack Effects (Alpha) on Turbulence Distribution, Configuration 1	41
18	Angle of Attack Effects (Alpha) on Turbulence Distribution, Configuration 1	42

LIST OF ILLUSTRATIONS (Cont.)

<u>Figure</u>	<u>Title</u>	<u>Page</u>
19	Angle of Attack Effects (Alpha) on Turbulence Distribution, Configuration 1	43
20	Mach Effects on Turbulence Distribution, Configuration 1	44
21	Mach Effects on Turbulence Distribution, Configuration 1	45
22	Overlay of Cavity Turbulence Distributions at Three Mach Numbers and Two R_N 's, Configuration 1	46
23	Comparison of Fences I = IV with the Basic (No Fence) Turbulence Distribution of Configuration 1	47
24	Effect of Cavity Lip Shape on Cavity Turbulence Distribution, Configuration 1	48
25	Effect of Cavity Lip Shape on Turbulence Distribution, Configuration 1	49
26	Angle of Attack Effect on Cavity with Rounded Aft Lip and Fence I at Leading Edge of Cavity	50
27	Effect of Aft Lip Shape Turbulence Distribution with Fence I at Leading Edge of Cavity	51
28	Effect of Blowing at the Forward Lip on Turbulence Distribution, Configuration 1	52
29	Effect of Blowing Over Aft Bulkhead on Turbulence Distribution, Configuration 1	53
30	Effect of Blowing Over Aft Bulkhead with Rounded Lip, Configuration 1	54
31	Combined Effect of Fence I with Curved Aft Lip	55
32	Angle of Attack Effects on Turbulence Distribution, Configuration 2	56
33	Angle of Attack Effects on Turbulence Distribution with and without Store Installed on Left Side of Bay	57
34	Reynold's Number Effect on Turbulence Level, Configuration 2	58
35	Turbulence Distributions in Configuration 2	59

LIST OF ILLUSTRATIONS (Cont.)

<u>Figure</u>	<u>Title</u>	<u>Page</u>
36	Mach Effects on Turbulence with and without Single BDU-8 Store, Configuration 2	60
37	Mach Effects on Turbulence with Fence I, with and without BDU-8 in Bay; Configuration 2	60
38	Angle of Attack Affects on Turbulence Level in Forward and Aft Bays of Configuration 3	61
39	Reynold's Number Effects on Turbulence Level, Configuration 3; Bays Empty	62
40	Angle of Attack Effects on Turbulence with and without Store L in Forward Bay, Configuration 3	63
41	Mach Effects on Peak Turbulence Level in Forward Bay of Configuration 3, with and without Store L and Fence I	64
42	Comparison of Turbulence Levels Measured on Centerline (Roof) with Sidewall of Configuration 3	65
43	Summary of Angle of Attack Effects (Mach \approx .8) Comparing Representative Turbulence Levels in the Three Bay Configurations, Bays Empty	66
44	One Third Octave Band Spectra from Test Point Nr 38, Transducer Nr 6, X/L = .55	67
45	One Third Octave Band Spectra from Test Point Nr 109 Transducer Nr 6, X/L = .55	68
46a	One Third Octave Band Spectra from Test Point Nr 140, Transducer Nr 5, X/L = .45	69
46b	One Third Octave Band Spectra from Test Point Nr 140, Transducer Nr 39	70
47a	Cavity Resonant Modes, Comparison of Calculated with Experimental Results	71
47b	Cavity Resonant Modes, Comparison of Calculated with Experimental Results	72
47c	Cavity Resonant Modes (Tandem Bays), Comparison of Calculated with Experimental Results	73

LIST OF SYMBOLS

P_{RMS}	Root mean square dynamic pressure, psf
D	Cavity depth, in
L	Cavity length, 8.375 in
S	Reference area, area of cavity, .145 ft ²
h	Fence height, in
M	Free stream Mach number
Q	Free stream dynamic pressure, psf
P	Local static pressure, psf
P_o	Free stream static pressure, psf
C_p	Pressure coefficient, $(P - P_o)/Q$
C_J	Jet thrust coefficient
X	Distance from cavity lip, positive aft, in
Y	Distance from model centerline, positive to right looking upstream, in
Z	Distance from model surface, positive up, into cavity, in
g	Acceleration of gravity, 32.18 ft/sec ²
R	Gas constant for air, 53.34, ft/ ⁰ R
T	Air supply total temperature, ⁰ R
P_M	Air supply total pressure, psf
ρ	Air supply density, lb _M /ft ³
γ	Ratio of specific heats for air, 1.4
f	Frequency, Hz
U	Free stream velocity, ft/sec
S_1	Strouhal number, fL/U
α	Empirical phase delay parameter
k_v	Vortex velocity/free stream velocity
m	Frequency mode number, integer

I INTRODUCTION

This report documents an exploratory investigation of the aero-acoustic environment in and around a generic weapons bay at Mach numbers from .7 to .9. High dynamic (oscillatory) pressure levels are experienced in modern aircraft weapon bays. High fatigue stresses can result which can cause both weapon and aircraft structural and equipment failures. Historically, the problems associated with internal carriage and delivery of air droppable and air launched weapons have increased significantly as flight velocities have increased.

This report describes an AFFDL wind-tunnel test of several weapons bay geometries, including a tandem bay arrangement, and various turbulence reduction techniques. The latter included fences; blowing from the forward bulkhead over the cavity and blowing over the rear bulkhead; and lip shaping. The weapons bay model installation is shown in Figure 1.

The objectives of this effort were to evaluate the technical validity of conducting weapons bay turbulence investigations in the AFFDL Trisonic Gasdynamic Facility utilizing a relatively low cost, small scale weapons bay model; and to evaluate experimentally several turbulence reduction techniques. The data from this test will be correlated with similar data from tests of a 1/15 Scale F-111 model and flight test data obtained in the weapons bay of an F-111 aircraft.

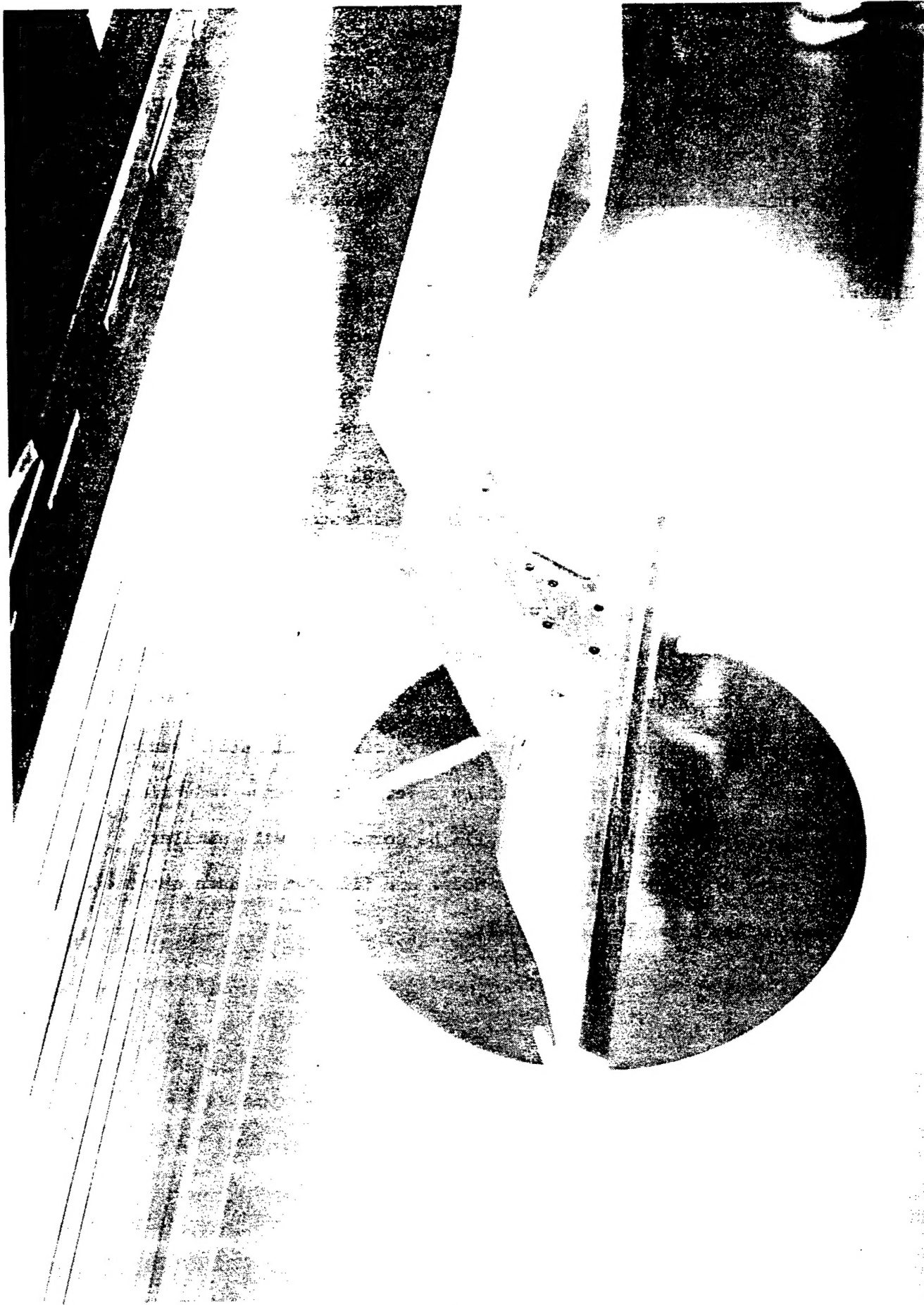


Figure 1. Weapons Bay Wind Tunnel Model Installed in AFFDL Trisonic Gasdynamic Facility.

II TEST APPARATUS AND DATA ANALYSIS PROCEDURES

1. Model Description

The weapons bay wind tunnel model was designed for transonic and supersonic testing up to Mach 3.0 and a maximum dynamic pressure (q) of 1300 psf. The bay cavity was located in a flat plate model designed to produce as nearly as possible two dimensional flow entering the cavity. Figure 1 shows the model installed in the AFFDL Trisonic Gas Dynamic Facility. The uninstalled model along with the various inserts used to reconfigure the model can be seen in Figure 2. Also in Figure 2, the two store shapes, a single BDU-8 and a high solidity launcher simulation designated store L, boundary layer rake and one of the four turbulence reduction fences (See Figure 6) can be identified. The tandem bay insert is shown with store L positioned in the forward bay. Figure 3 compares the geometries of configurations 1 and 2. Typical cross sections of Configurations 1 and 3 are presented in Figures 4 and 5.

The flat surface of the model is 18 in. long and 5 in. wide with a sharp, wedge (6°) shaped leading edge designed to accommodate the low supersonic design condition, Mach 1.3. When installed in the transonic test section described below, the model produced a blockage of 4.4%.

The various bay geometry changes can be accomplished with a minimum effect on the model instrumentation. Three basic bay geometries were tested. Configuration 1 consisted of a simple rectangular cavity; Configuration 2 was similar to the weapons bay shape of the

F-111 aircraft; and Configuration 3 was a tandem bay arrangement. Effects of weapon bay doors were not investigated in this test; however, Reference 1 reports on a related effort during which the effect of bay doors were evaluated on an F-111 model and found to increase the level of the dynamic pressures (turbulence level) in the cavity.

Two blowing slots were provided for Configuration 1 each with a span of 2.5 in. and a width of .03 in. (Figure 7 shows the location of these nozzles as well as the rounded lip inserts.) The forward bulkhead nozzle was canted upward at an angle of 5.5° relative to the surface of the model. The aft nozzle was located in the roof directly ahead of the rear bulkhead.

2. Model Instrumentation

The primary instrumentation consisted of non-screened Kulite CQ-080-25 differential pressure transducers. Figure 8 depicts the location of the pressure transducers along with the secondary static pressure tap and thermocouple instrumentation. The dimensional and non-dimensional location of the pressure instrumentation is listed in Table I. Iron/constantan thermocouples were located on the centerline of the bay roof at $X = 1.125$ in. and $X = 7.625$ in.

The model was designed for a total of 22 transducers and 35 static surface taps. A total of 25 Kulite transducers were procured; however, at the start of the test program only 15 were functional due either to electrical failures or damage to the silicon crystal diaphragm. The model as delivered also had several inoperable static pressure taps. These taps had internal leaks which apparently occurred

at the epoxy bond line between the pressure tubes and the model. Repair would have required complete model disassembly which was not feasible prior to entry into the wind tunnel. The primary data loss which resulted was definition of the local static pressure and as a result the local Mach number entering the cavity.

It must be emphasized that transducer failures prior to the start and during this test program significantly reduced the information gained relative to the distribution of turbulence throughout the cavity. While centerline turbulence distributions are presented in Section III, the relatively large spacing between some of the transducers is a significant concern. The data are considered valid for comparison purposes between configurations at the same relative cavity position.

3. Data Recording and Reduction Procedures

The electrical output of the Kulite pressure transducers was processed in two ways. All transducer signals were amplified and overall signal levels obtained on line using a Hewlett-Packard Model 3400 RMS (Root Mean Square) Volt Meter. Ten channels were simultaneously recorded on FM tape for further off-line data processing. The overall signal levels from the RMS meter were converted off line to pressure (P_{RMS} , psf) and P_{RMS}/Q , as presented in Section III.

The recorded FM data tapes were processed by the Aero-Acoustics Branch (AFFDL/FYA). Third octave frequency plots were provided along with the integrated pressure levels over the frequency range up to 8000 Hz. In addition, AFFDL/FXN personnel performed narrow band spectral frequency analysis of selected data points.

The static pressure data was recorded using IBM card punch equipment. Subsequent data reduction was performed on the CDC 6600 computer and representative Calcomp plots are presented in Appendix 1 along with a brief discussion of the data.

Table II presents a comparison of P_{RMS}/Q turbulence levels as measured with the RMS meter and derived from the third octave analysis. Generally good agreement was observed. The meter values were used as the primary source of turbulence level. Turbulence levels were not available for all transducers from the tapes for a number of runs because high amplifier gain settings resulted in clipped signals.

Data Reduction Equations:

Root Mean Square Dynamic Pressure:

$$P_{RMS, psf} = \frac{(RMS, volts) \times (Transducer constant, volts/psi)}{(144, in^2/ft^2)}$$

Jet Thrust or Momentum Coefficient:

$$C_J = \frac{\text{Isentropic Thrust}}{QS}$$

$$C_J = \left[\frac{(\text{Airflow, ft}^3/\text{sec})^\rho \sqrt{\gamma RTg}}{QSg} \right] \left[\sqrt{\left(\frac{2}{\gamma-1}\right) (1 - P_o/PM)^{\gamma-1/\gamma}} \right]$$

4. Test Facility Description

The AFFDL Trisonic Gasdynamic Facility is a closed circuit continuous flow wind tunnel. Flow in the circuit is maintained at a low dew point and at a constant total temperature of approximately 100 degrees Fahrenheit. The total pressure is variable allowing the maintenance of a constant Reynolds number over a large Mach number range.

For transonic testing in this facility a 15 in. square variable porosity slotted test section insert is used. Both slotted and solid sidewalls are available for this insert. The solid sidewalls were used during this test to permit Schlieren pictures to be obtained through the windows in these sidewalls. The windows were removable permitting easy model access for model changes. During this test, the floor and roof porosity was set at the maximum open (12%) setting. The plenum of the test section is aspirated by variable angle diffusing/converging plates (flaps) at the section exit plane. These plates were maintained at the full open position during this test.

Observation of the flow field around the model using the Schlieren system revealed a flow anomaly originating from the leading edge of the model with the flat plate aligned with the tunnel centerline ($\alpha = \text{zero}$). A small nose up α of $3/4$ of a degree eliminated this flow condition. Therefore, this α , $3/4$ degree positive, was selected as α zero for this test.

TABLE I. Location of Pressure Instrumentation

1. Dynamic Pressure Transducers

Configuration 1

Transducer	X(in) (1)	X/L	Y(in) (1)	Y/L	Z(in) (1)	Z/L
1	.125	-.02	0	0	0	0
2*	0	0	0	0	.375	.05
3*	.188	.02	↓	↓	1.5	.18
4*	.875	.10			↓	↓
5	3.8	.45				
6	4.56	.55				
7	7.937	.95			↓	↓
8*	8.375	1.0	↓	↓	.75	.09
9*	8.375	1.0			.375	.05
10**	8.625	1.03			0	0
11	.188	.02	1.25	.15	.75	.09
12	3.8	.45	↓	↓	↓	↓
13	6.250	.75	↓	↓		
14	3.8	.45	-1.25	-1.5		
15	7.937	.95	-1.25	-1.5		

* Transducers are covered when rounded lips installed.

** Transducers are relocated 7/8 in aft when aft rounded lip installed.

(1) See Figure 3 for definition of coordinate system.

TABLE I. (cont)

Configuration 2 (Note: Identical to Configuration 1 except as indicated).

Transducer	X(in)	X/L	Y(in)	Y/L	Z(in)	Z/L
4	.89	.11	0	0	.77	.09
5	3.8	.45	↓	↓	1.075	.13
6	4.6	.55			1.1	.13
7	7.99	.95			1.235	.15
13(2)	8.375	1.0			.375	.05
12	3.8	.45	1.25	.15	.75	.09
15	7.937	.95	1.25	-.15	.75	.09

- (2) Transducer #13 relocated to aft bulkhead following Configuration 1 test phase.

Note: Transducers # 2,3,8,9,10,11, and 14 failed or were damaged prior to initiation of Configuration 2 tests.

TABLE I. (Cont)

Configuration 3 (Note: Identical to Configuration 1 except as indicated).

Transducer	X(in)	X/L	Y(in)	Y/L	Z(in)	Z/L
13(2)	8.375	1.0	0	0	.375	0
12	3.8	.45	.9	.11	.8	.10
15	7.937	.95	-.9	-.11	.8	.10

- (2) Transducer # 13 relocated to aft bulkhead following Configuration 1 test phase.

Note: Transducers # 3 and 4 failed during model reconfiguration.
Data from #13 and 15 were questionable.

TABLE I. (cont)

2. Static Pressure Tap Locations

Configuration 1

Static Tap	X(in)	X/L	Y/(in)	Y/L	Z(in)	Z/L
1	-1.0	-.119	1.6	.191	0	0
4*	0	0	0	0	.625	.075
5*	0	0	0	0	1.25	.149
6*	.348	.042	0	0	1.50	.179
7*	.737	.088	↓	↓	↓	↓
8	1.514	.181				
9	2.016	.241				
11	3.312	.395				
12	3.662	.437				
13	4.412	.527				
15	5.687	.679				
17	6.750	.806				
18	7.375	.881				
19	7.787	.930				
21*	8.375	1.0	↓	↓	1.25	.149
22*	8.375	1.0			.625	.075
24**	8.516	1.017			0	0
25**	8.902	1.063			↓	↓
26**	9.408	1.123				
27**	9.375	1.12	1.6	.191	↓	↓
28	8.1	.967	1.25	.149	.75	.09
29	6.1	.728	↓	↓	↓	↓
30	3.662	.437				
31	2.02	.241				
32	3.48	.042	↓	↓	↓	↓
33	4.19	.5	1.6	.191	0	0
34	1.6	.191	-1.6	-.191	↓	↓
35	6.8	.812	-1.6	-.191	↓	↓

TABLE I. (cont)

Configuration 2 (Note: Identical to Configuration 1 except as indicated.)

Static Tap	X/(in)	X/L	Y(in)	Y/L	Z(in)	Z/L
6	.35	.04	0	0	.71	.09
7	.75	.09	↓	↓	.77	.09
8	1.52	.18			.86	.10
9	2.0	.24			.92	.11
11	3.34	.40			1.06	.13
12	3.69	.44			1.08	.13
13	4.53	.54			1.1	.13
15	5.8	.69			1.15	.14
17	6.84	.82			1.2	.14
18	7.45	.89			1.21	.14
19	7.86	.94			1.23	.15
30	3.662	.44	1.14	.14	.75	.09
31	2.18	.26	1.03	.12	.75	.09
32	No tap 32 in Configuration 2					

TABLE I. (cont)

2. Static Pressure Tap Locations (cont)

Note: Static Taps 2,3,10,14,16,20, and 23 were inoperative due to leaks or data system failures during this test.

* These taps are covered when rounded lips installed

** These taps are relocated aft 7/8 in when rounded aft lip installed.

TABLE I. (cont)

Configuration 3 (Note: Identical to Configuration 1 except as indicated)

Static Tap	X/(in)	X/L	Y(in)	Y/L	Z(in)	Z/L
28-32	U.C	U.C	.93	.111	.8	.096

U.C. - Unchanged

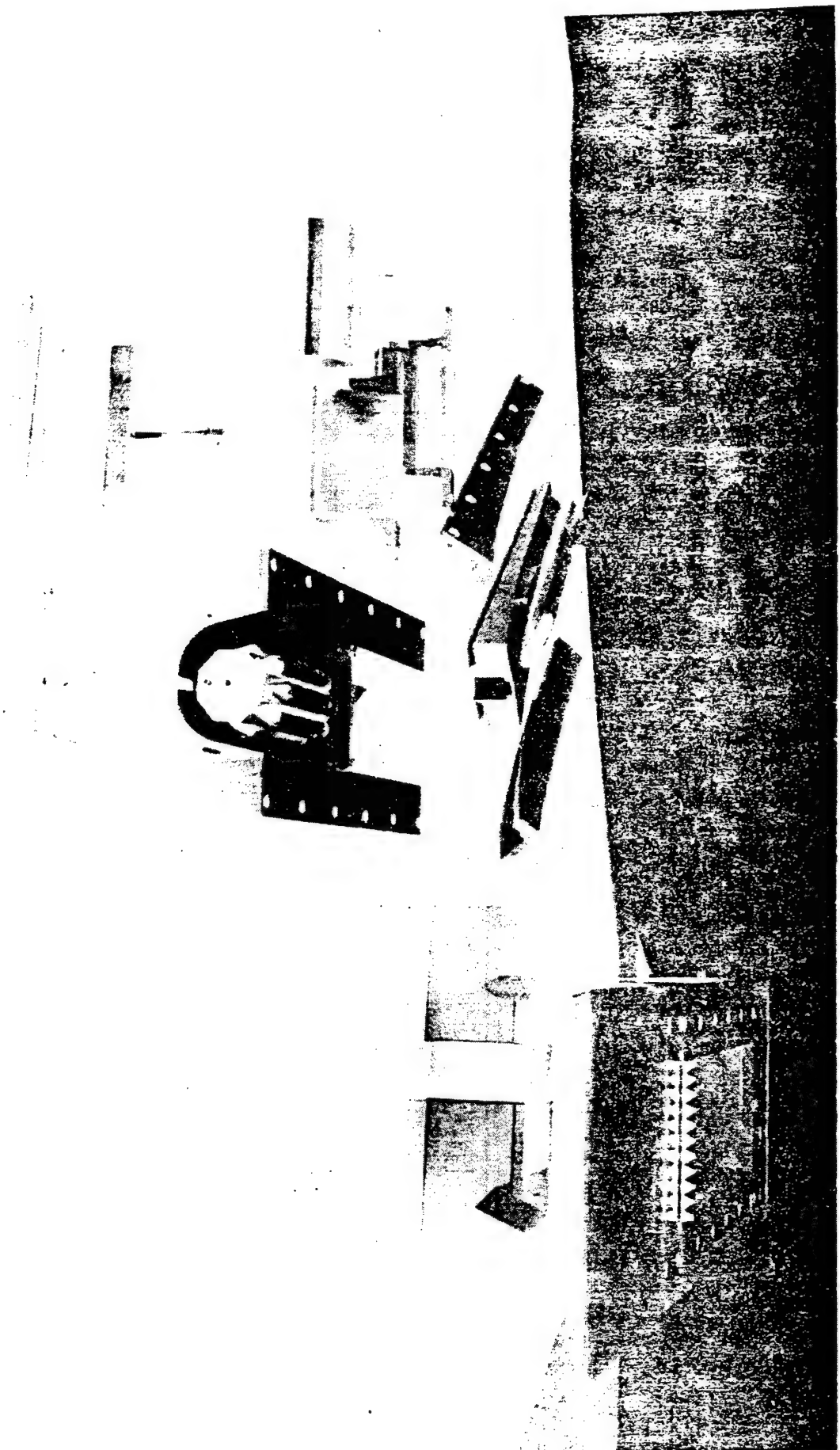
TABLE II. Comparison of Turbulence Levels Measured with RMS Meter
VS. Integrated Values Obtained from 1/3rd Octave Analysis

Test Point/ Config.	Mach	Q(psf)	Reynolds Number X10 ⁻⁶	PRMS/ Q (Meter)					Remarks
				*#1	#4	#5	#6	#7	
30/ ₁	.88	503	3.0	.032 .031	.040 .040	.080 .081	.093 .094	.189 .168	Aft Rounded Lip Installed
34/ ₁	.69	707	5.0	.042 .041	.045 .046	.088 .090	.097 .105	.202 .180	
72/ ₁	.79	778	5.0	.025 .024	.029 -	.057 .058	.074 .074	.143 .143	
120/ ₂	.79	460	3.0	.005 .005	.010 .010	.025 .023	.029 .031	.052 .051	
121/ ₂	.88	500	3.0	.005 .005	.011 .010	.023 .023	.029 .031	.054 .054	

* Transducer Number

Note: Alpha = 3 degrees for all of above Test Points

Figure 2a. Weapons Bay Model Prior to Wind Tunnel Installation



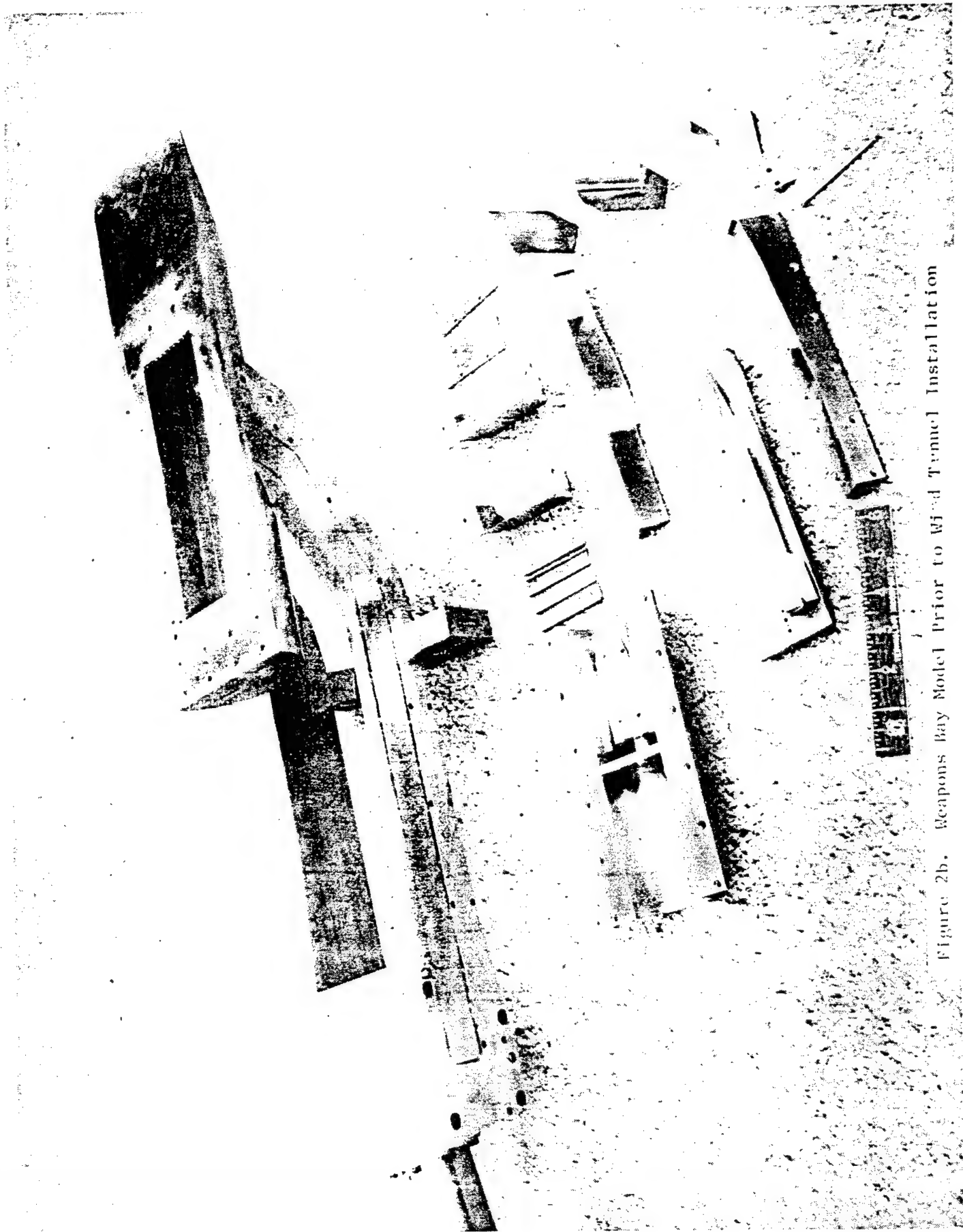


Figure 2b. Weapons Bay Model Prior to Wind Tunnel Installation

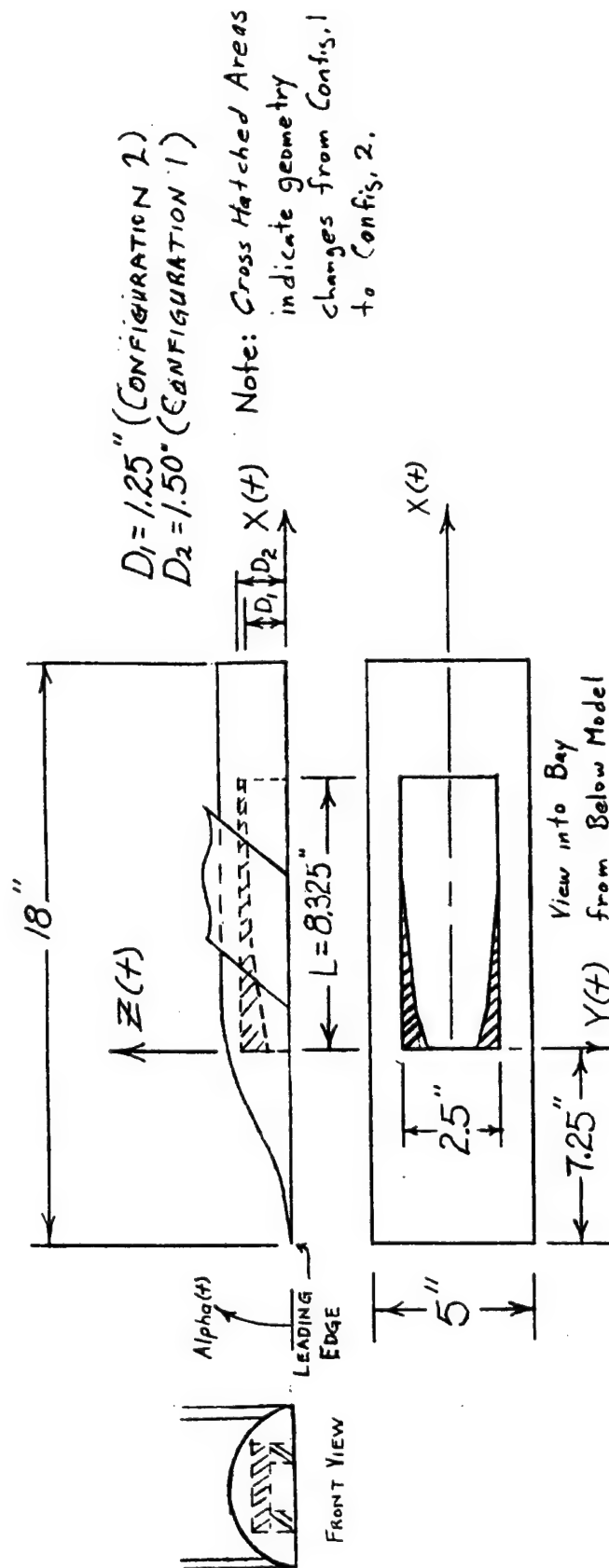


Figure 3. Comparison of Configurations 1 and 2
 (Cross Hatched Areas Indicate Config. 2)

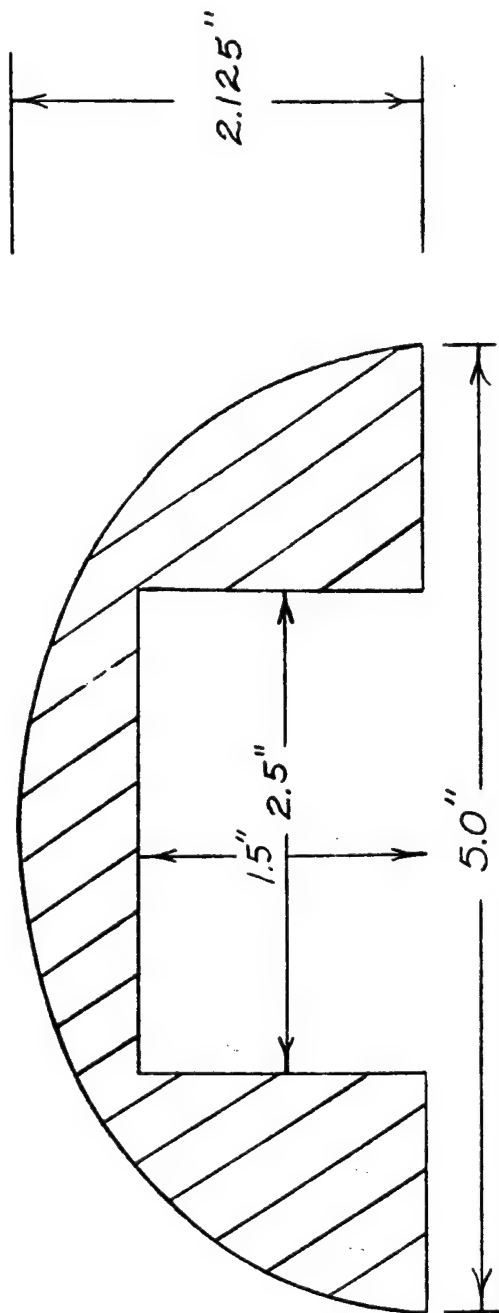


Figure 4. Cross Section View, Configuration 1.

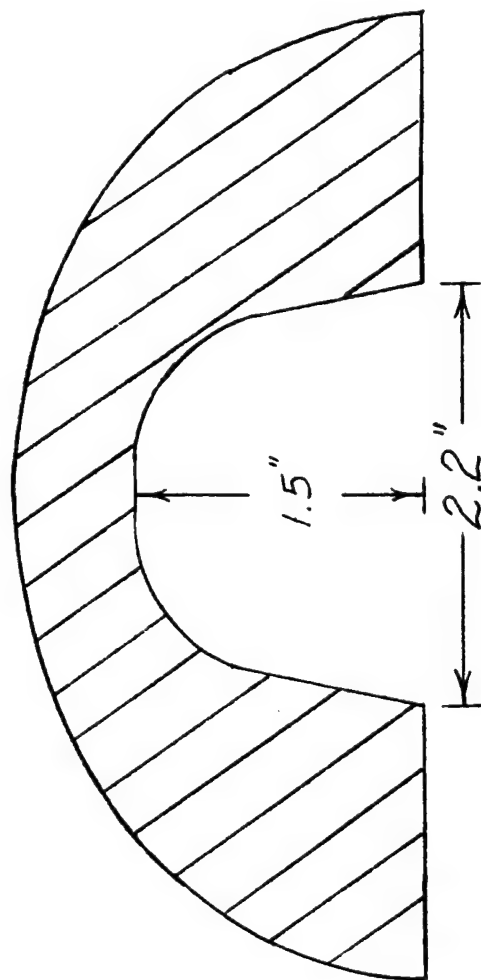


Figure 5. Cross Section View, Configuration 3 (Tandem Bay)

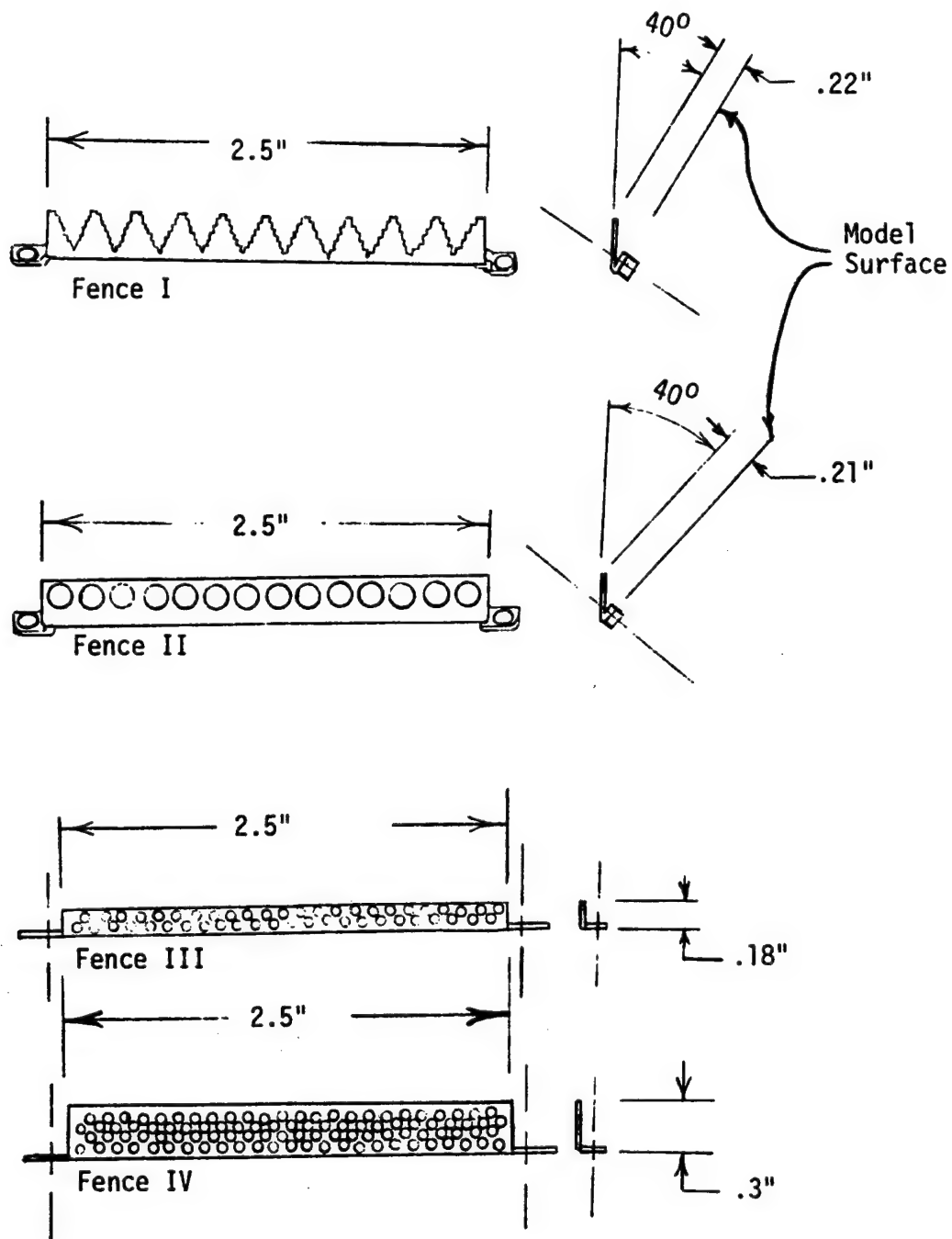
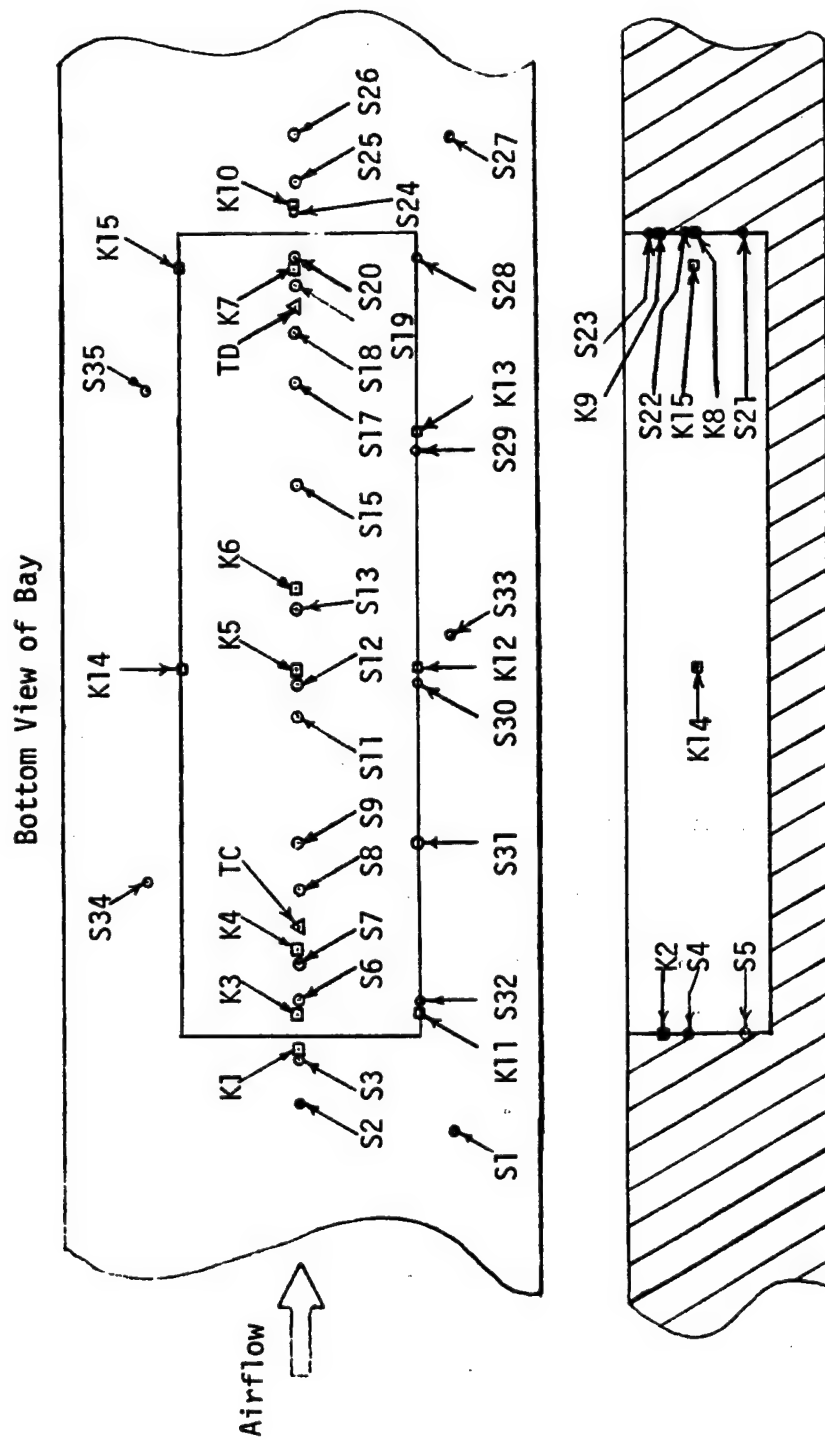


Figure 6. Turbulence Reduction Fences



S - Static Tap K - Kulite Dynamic Pressure Transducer T - Thermocouple

Figure 8. Instrumentation Schematic (See Table I)

III TEST RESULTS

1. Oil Flow and Boundary Layer Survey Results

The flow properties on the model were first evaluated using an oil flow technique and a closed weapons bay cavity. This configuration was obtained by fabricating a flat plate which completely covered the lower flat side of the model. This plate had a sharp leading edge which formed a glove around the actual model leading edge. Oil drops were distributed over the model surfaces and flow of this oil was observed under various Mach and angle of attack conditions. Flow on the flat plate was two-dimensional for all test conditions with no evidence of flow around the corners of the model in either direction. Based upon these results, flow conditions with the bay open were assumed to be two-dimensional at the entrance to the bay cavity.

Following removal of the plate described above, a boundary layer rake was installed at the leading edge of the bay and boundary layer (B.L.) profiles obtained with and without a cellophane tape B.L. trip located approximately an inch behind the model leading edge. Figure 9 presents profiles for Mach .7 and .9, and at Reynolds numbers of 3 and 5 million per foot. Turbulent boundary layers were observed with and without the B.L. trip. The trip was installed for the remaining runs except for the last six which were used to isolate the effect of the trip upon the turbulence levels (P_{RMS}/Q) in the tandem bay (Configuration 3). Figure 10 presents these results which show a small effect at an angle of attack of 6 degrees in the forward bay and no effect on the aft bay.

2. Turbulence Level Test Results

a) Configuration 1

The basic weapons bay, Configuration 1, has a rectangular shape with length to depth ratio (L/D) of approximately 5.6 ($L = 8.375$ in., $D = 1.5$ in.). Figure 11 shows this configuration with Fence I installed. Figure 12 is a close up view of this configuration with the rounded aft lip installed. Details of the model instrumentation can be seen. Figure 13 is an installation view showing the location of the B.L. trip.

Figures 14 through 31 present turbulence distributions for Configuration 1 along the cavity center line as a function of X/L , pressure transducer position (measured from the forward cavity lip) non-dimensionalized value obtained by overall cavity length ($L = 8.375$ in.) This parameter is used throughout this report to relate location of turbulence level measurements between the three configurations tested.

Figures 14 through 22 present the effects of angle of attack, Mach number and Reynolds number on the turbulence level of this configuration. No significant trends are noted as a function of these variables over the ranges investigated; i.e. angle of attack from 0 to 6 degrees, Mach numbers from .7 to .9 and Reynolds's numbers of 3 and 5 million per foot. These data can be characterized as showing sharp increases in turbulence level from front to back in the cavity with peak levels observed on the aft bulkhead or just aft of the cavity. The rear cavity roof ($X/L = .95$) experiences the next highest turbulence level.

The peak level observed on the rear bulkhead at Mach = .8, $R_N = 3$ million/ft and $\alpha = 0$ degrees was a P_{RMS}/Q of a .290. A P_{RMS}/Q level of .303 was observed just aft of the bay at Mach = .69, $R_N = 5$ million/ft, and $\alpha = 0$ and 3 degrees. The highest roof level ($P_{RMS}/Q = .212$) was observed at Mach .69, $R_N = 5$ million/ft, and $\alpha = 6$ degrees.

Figure 23 compares the effects of the fences shown in Figure 6 on the cavity turbulence level. The fences had a porosity of approximately 50%. All of the fences were effective in reducing the turbulence level throughout the cavity. Fence IV ($h/L = .036$) was the largest and most effective turbulence reduction fence. The least effective and smallest was Fence III ($h/L = .021$). Fences I ($h/L = .026$) and II ($h/L = .025$) produced essentially identical results. Fence I was selected as representative and used in all subsequent runs evaluating fence effects.

The second turbulence reduction technique evaluated was installation of rounded cavity lips. Figures 24 and 25 show that installation of the aft lip produced favorable results; while, the addition of the forward lip negated the benefit of the aft lip curvature. Figure 26 presents results with the rounded aft lip and Fence I over an angle of attack range of 0 to 6 degrees. Figure 27 compares the combination of Fence I/rounded aft lip versus Fence I/square aft lip. The former produced slightly lower turbulence levels.

The next turbulence reduction technique evaluated was slot blowing from the forward lip over the cavity. The jet sheet was directed

downward at an angle of approximately 5.5 degrees in an attempt to deflect the shear layer away from the cavity. Figure 28 shows that P_{RMS}/Q levels increased within the cavity; however, a reduction is noted aft of the cavity.

Blowing was also evaluated over the rear bulkhead with the basic square and rounded lip shapes. Again turbulence levels generally increased. A small turbulence reduction was noted relative to the non-blowing level at an $X/L = .95$ (Figure 29) with the basic bulkhead at $C_J = .142$. Aft of the cavity, turbulence levels decreased for both the basic and rounded configurations (Figure 29). Figure 30 shows that the level at $X/L = .95$ was decreasing slowly as C_J was increased from .034 to .124.

Figure 31 shows the combined benefit of Fence I and rounded aft lip relative to the basic geometry of Configuration 1. This represents nearly an 80% reduction in the turbulence level measured at the .95 X/L location on the cavity roof. This combination of fence and aft lip rounding produced the lowest turbulence levels observed with Configuration 1 during this test program.

Additional investigations of blowing is considered necessary to completely evaluate this technique. Specifically, higher blowing rates and a larger forward nozzle injection angle relative to the free stream should be evaluated. Increasing the forward nozzle angle to 20 or 30 degrees may result in deflection of the shear layer away from the cavity in a way similar to a fixed fence.

b) Configuration 2

This configuration is geometrically similar to the internal weapons bay of the F-111 aircraft; however, the bay doors were not modeled. (The effect of the F-111 bay doors on the turbulence level in the bay has been investigated in a related effort, Reference 2. The doors were found to increase the turbulence level in the bay.)

The L/D of the Configuration 2 weapons bay was 6.7 (L = 8.375, D = 1.25 in.). The general geometry of the bay can be seen in Figure 3, the roof and side wall inserts are shown in Figure 2. The forward portion of the bay is tapered in width and depth. These features along with the overall reduction in depth of the bay were the only changes relative to Configuration 1. The 4.6% BDU-8 store model is shown mounted to the roof insert in Figure 2.

As observed with Configuration 1, Figures 32 through 34 show no significant angle of attack, Mach number or Reynolds number effects over the range investigated. Figure 33b also shows the effect of angle of attack on the turbulence distribution with a scale model of a BDU-8 store mounted on the left side of the bay. The store slightly lowers the turbulence level in the rear portion of the bay.

The peak cavity turbulence levels again were observed on the rear bulkhead. (The transducer mounted aft of the bay was inoperable during this test phase.) The peak level observed was a P_{RMS}/Q of .0825 as compared with a peak level of .29 with Configuration 1 at the same aft bulkhead location. This significantly lower turbulence level can only be attributed to the bay geometry changes; however,

the specific effects of L/D, tapered width, and roof contour were not isolated.

Configuration 2 was also evaluated with Fence I installed with the bay empty and with a single store in the bay. Figure 35a shows the substantial improvement in the bay environment with a fence installed. Figure 35b shows the effect of adding the single BDU-8 to be small relative to the empty bay configuration.

Figure 36 does show that over the Mach range investigated the store does reduce the turbulence level in the rear roof position without a fence while Figure 37 shows essentially no store effect on turbulence at the Mach conditions evaluated with the fence installed.

The overall effect of Fence I is a reduction of the peak turbulence level on the aft bulkhead from .08 to less than .02 or approximately a 75% reduction.

c) Configuration 3

Figure 5 is a typical cross section view of Configuration 3. This configuration models a tandem bay with the combined length (8.375 in.) equal to the length of Configurations 1 and 2. Since the same instrumentation is used, X/L values are based upon a length of 8.375 in.; however, the actual length of each bay was approximately 4.06 in. and the depth was 1.5 in. which results in an L/D of 2.7. The number of transducers which were operable at this stage of the test program was insufficient to permit presentation of meaningful turbulence level distributions; therefore, data are presented for the .45 and .95 X/L locations only. These locations correspond to the rear roof position

of the forward and aft bays respectively and should represent peak roof turbulence levels for each bay.

Figure 38 compares the turbulence levels in the forward and aft bay locations at several Mach numbers as a function of angle of attack. The forward bay is clearly more sensitive to angle of attack and Mach number than the aft bay. The turbulence level appears to reach a peak in the forward bay at an angle of attack of 3 degrees and a Mach number of .84.

Effect of Reynolds number variation is shown in figure 39. A turbulence level peak in the forward bay for a Mach number of approximately .84 is evident, but Reynolds number effect is insignificant.

The installation of store L (See Figure 2) in the forward bay is shown in Figure 40 to have a moderating effect on the turbulence level; however, the turbulence level trend with angle of attack is the same with or without store L installed. (Store L is an attempt to represent a rotary launcher or bomb cluster; however, the solidity of the store is much too high and the resulting effects are more representative of a very large single store.)

Figure 41 shows the effect of Fence I with and without store L in the forward bay. The addition of the fence produces a turbulence level reduction from a P_{RMS}/Q level of .19 to .055 or a nearly 70% reduction. With the fence installed the turbulence level is essentially the same with or without store L.

All of the data discussed above, refers to turbulence levels on the model centerline. Figure 42 presents data comparing the $X/L = .45$ centerline location with the corresponding sidewall location in

Configuration 3. The empty bay is seen to have a somewhat higher/turbulence level on the sidewall; however, installation of store L, reverses this comparison. The centerline and sidewall P_{RMS}/Q values are essentially equivalent with Fence I installed. It should be noted that this fence has a width of 2.5 in. compared with a bay width of 2.2 in. for Configuration 3.

3. Comparison of Alpha Effects Between Configurations

Figure 43 compares the three configurations over the angle of attack range. Only the forward bay of Configuration 3 shows a significant alpha effect. Configuration 1 has the highest turbulence level while Configuration 2 has the lowest. The forward bay of Configuration 3 approaches the turbulence level of Configuration 1 at the 6 degree alpha condition.

4. Frequency Analysis Results

Two types of frequency analysis were performed. Third octave analysis provided frequency distributions and turbulence level measurements for comparison with turbulence levels obtained using the on-line RMS meter.

The second technique, narrowband power spectral density (PSD) analysis, was used to more accurately determine the cavity mode frequencies.

Figures 44, 45 and 46 show typical third octave plots for Configurations 1, 2 and 3. Turbulence levels derived from 1/3 octave plots are presented in Table II along with the comparable levels obtained using the RMS meter. Generally, good agreement is observed. (See also Section II, Paragraph 3.)

Figure 47 compares the calculated cavity mode frequencies with the measured values determined from PSD plots. The calculation method developed by Rossiter (Reference 2), which appears below, was used. Good agreement was obtained for all three model configurations using a α of .25 which is applicable to a cavity L/D of 4.0.

Rossiter Equation:

$$S_1 = \text{Strouhal number} = fL/U$$

$$S_1 = \frac{m - \alpha}{M + 1/k_v}$$

f = Mode frequency

m = Frequency mode number

α = Empirical phase delay parameter

$\alpha = 0.25$ for cavity L/D = 4.0 (Ref. 3)

$K_v = 0.57$ (Ref. 3)

SYM	$R_N \times 10^{-6}$	Trip
○	3.0	Off
▽	3.0	On
◇	5.0	Off
△	5.0	On

Alpha = -75°

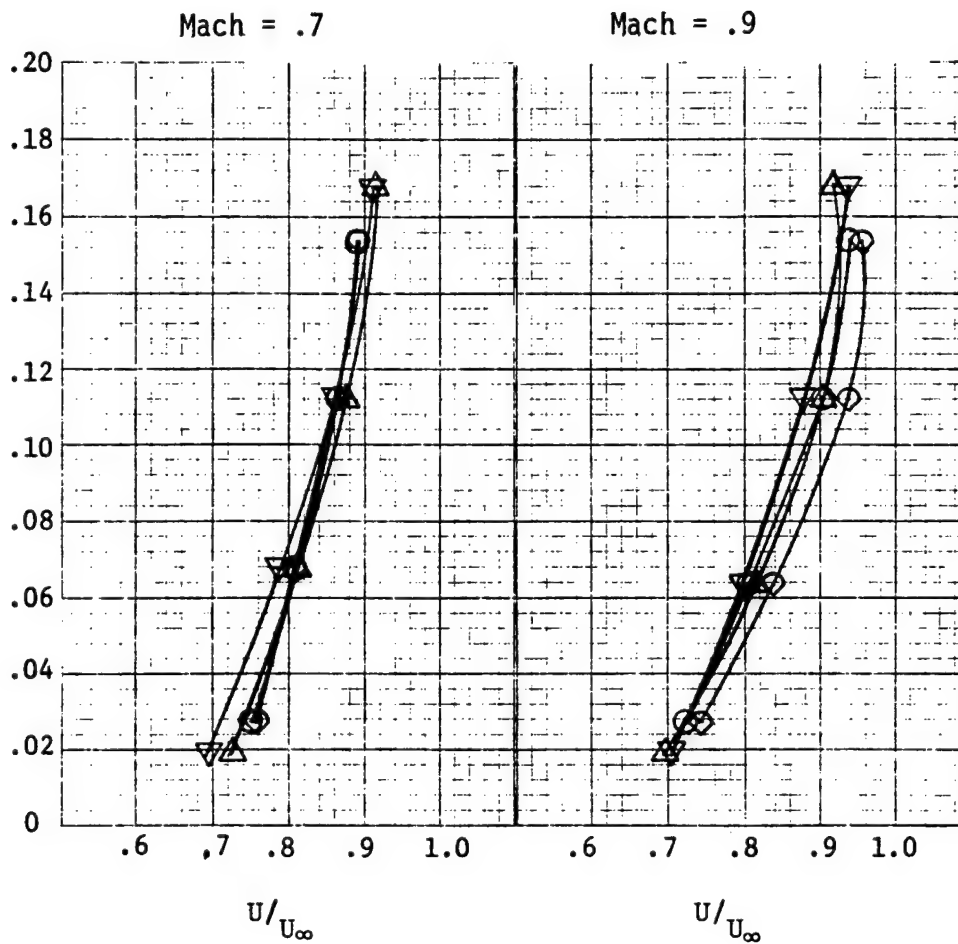


Figure 9. Boundary Layer Profiles with and without Boundary Layer Trip

(1) Note: Alpha of -75 is true tunnel geometric zero.
See discussion on page 7.

SYM	MACH	$R_N \times 10^{-6}$	Trip
Δ	.79	4.9	Off
\circ	.79	4.9	On

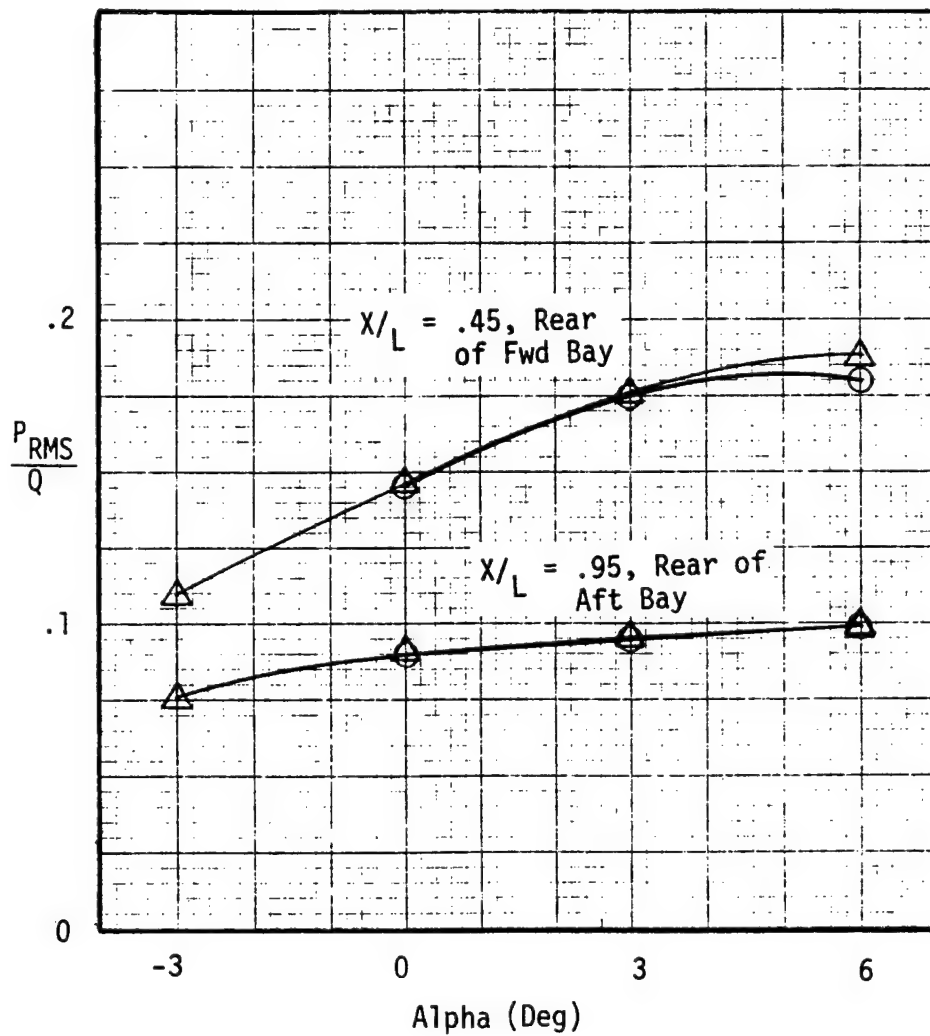


Figure 10. Angle of Attack Effects on Turbulence with and without Boundary Layer Trip, Configuration 3, Bays Empty.

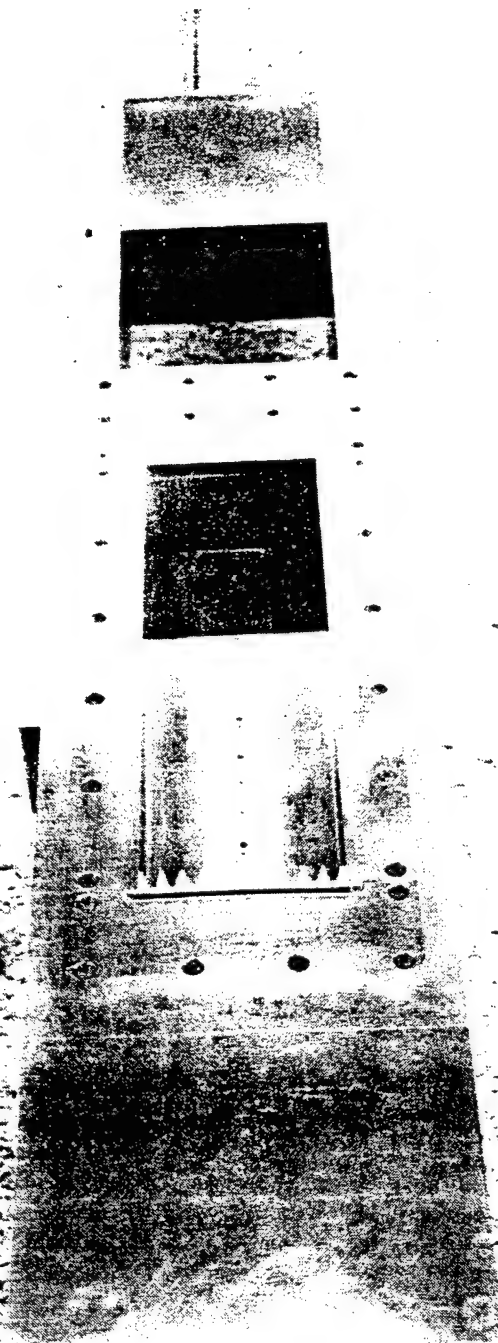
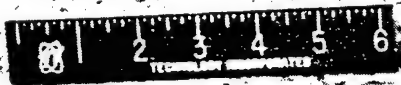




Figure 1. Close-up of configuration of die with fence and rounded



Figure 13. View of Configuration 1 with Rounded Aft Lip and
B. I. Trip

SYM	TP	MACH	ALPHA(DEG)	$R_N \times 10^{-6}/Ft$
○	40	.7	0	3.0
□	41	.7	3	3.0
△	42	.7	6	3.0

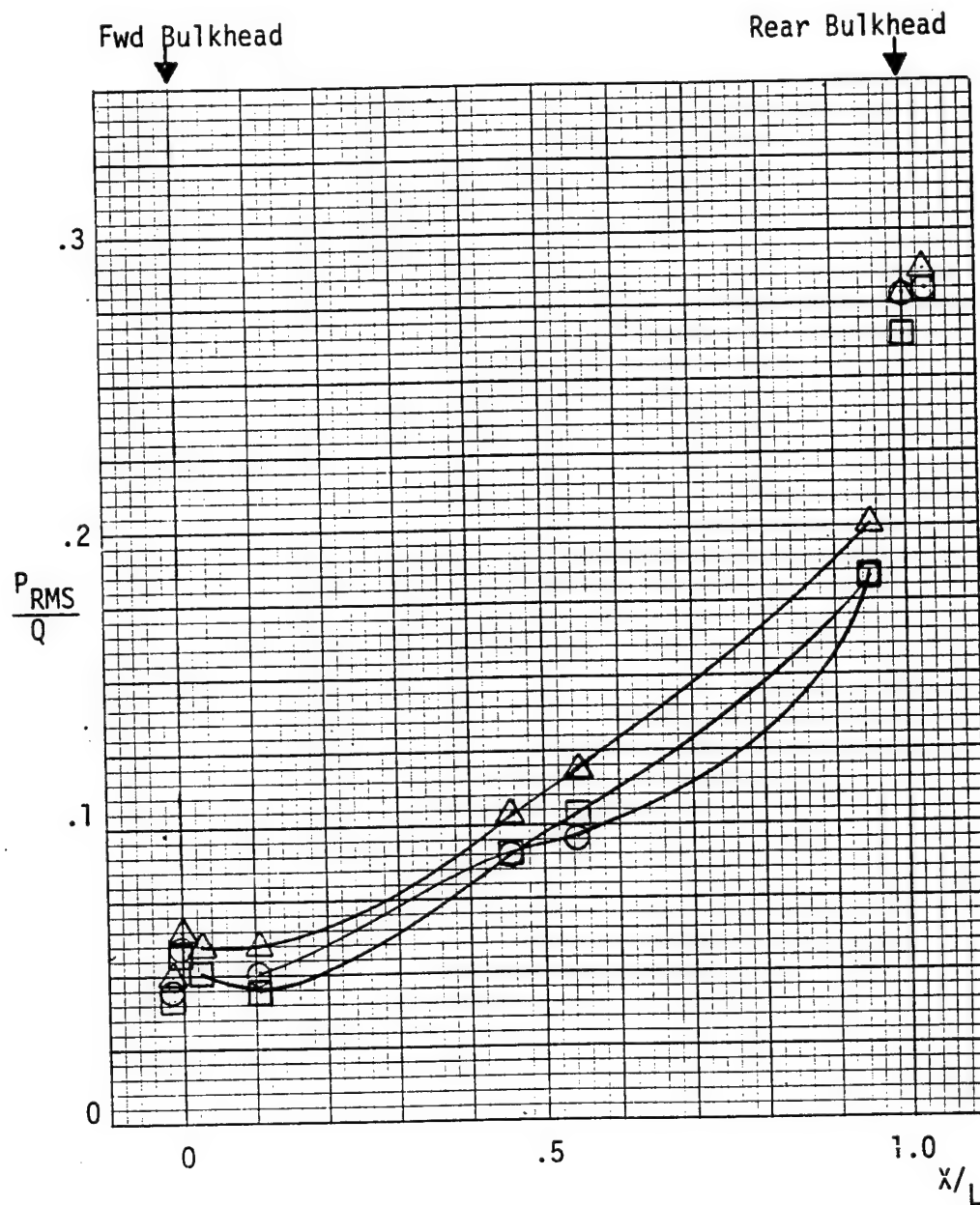


Figure 14. Angle of Attack Effects (Alpha) on Turbulence Distribution, Configuration 1.

SYM	TP	MACH	ALPHA(DEG)	$R_N \times 10^{-6}/FT$
○	33	.69	0	5.0
□	34	.69	3	5.0
△	35	.69	6	5.0

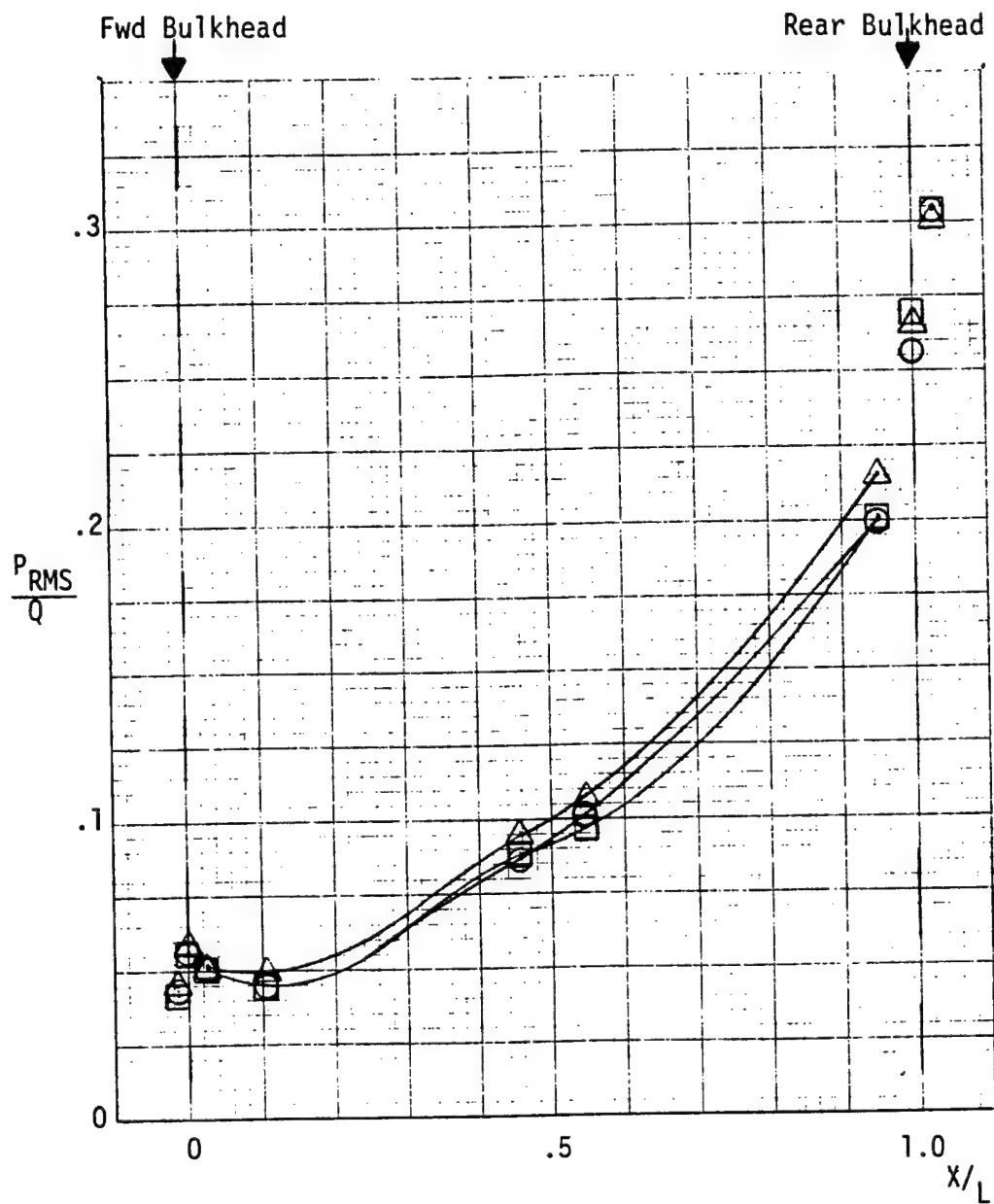


Figure 15. Angle of Attack Effects (Alpha) on Turbulence Distribution, Configuration 1.

SYM	TP	MACH	ALPHA(DEG)	$R_N \times 10^{-6}/Ft$
○	45	.8	0	3.0
□	44	.8	3	3.0
△	43	.8	6	3.0

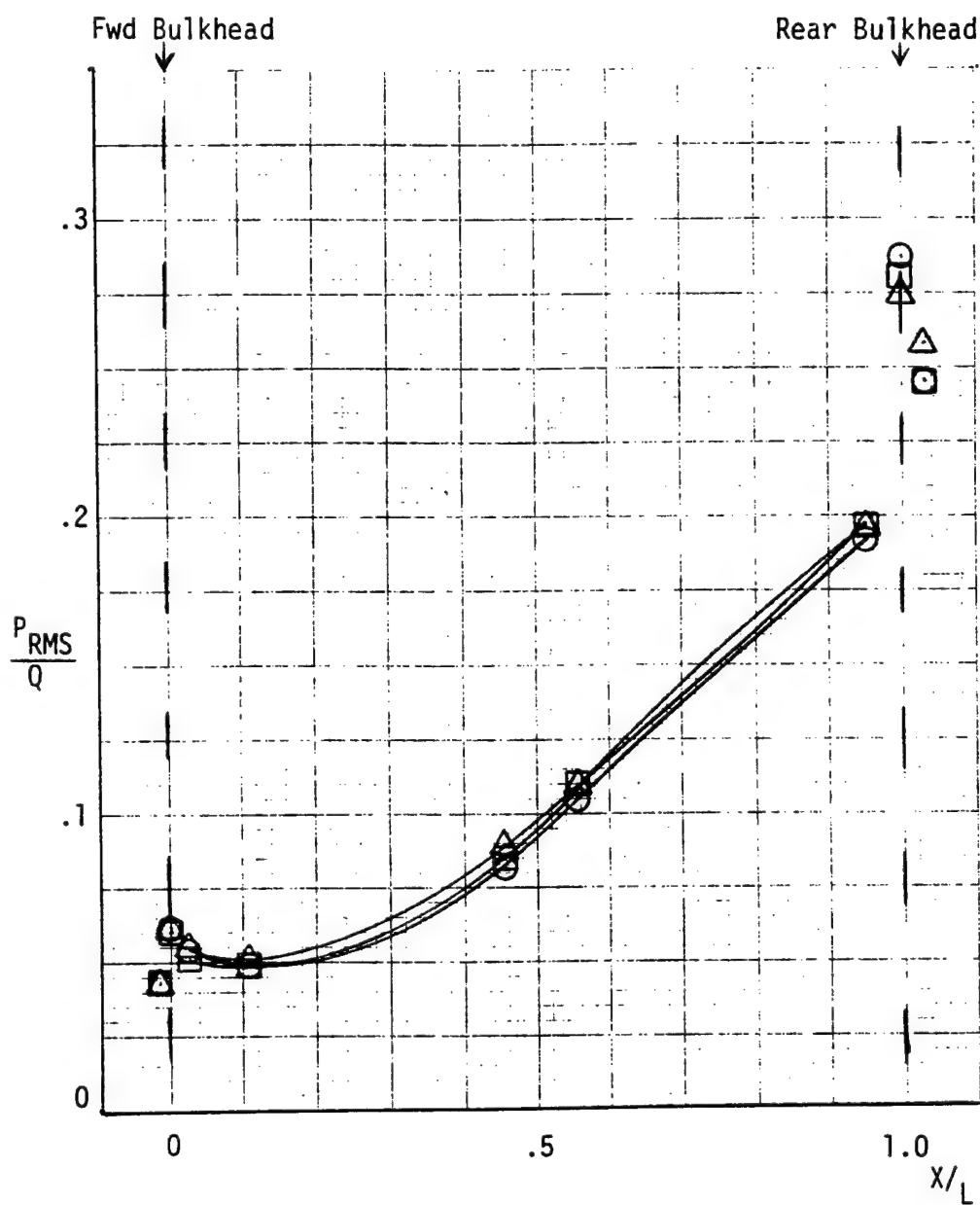


Figure 16. Angle of Attack Effects (Alpha) on Turbulence Distribution, Configuration 1.

SYM	TP	MACH	ALPHA(DEG)	$R_N \times 10^{-6}/Ft$
○	37	.8	0	5.0
□	38	.8	3	5.0
△	39	.8	6	5.0

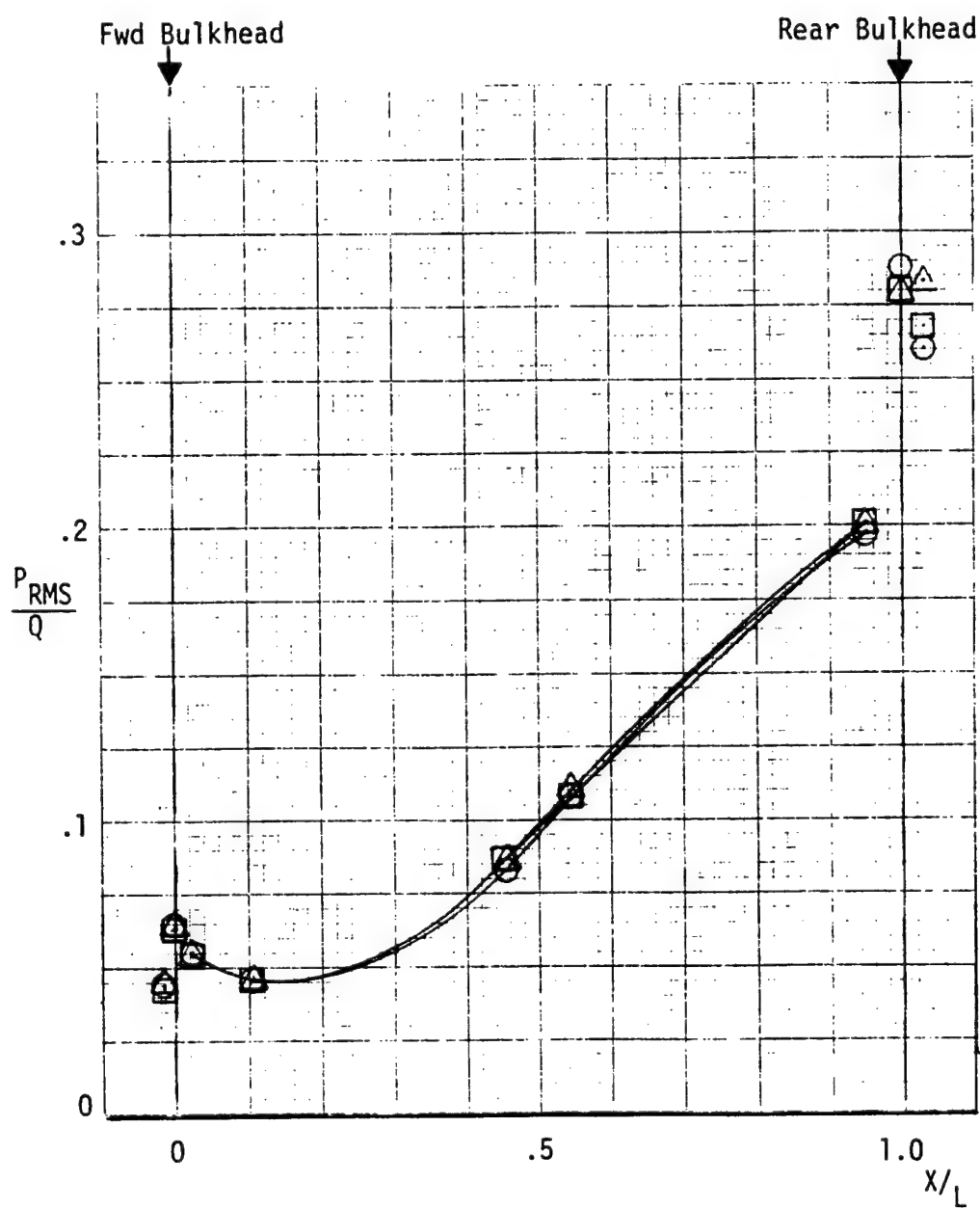


Figure 17. Angle of Attack Effects (Alpha) on Turbulence Distribution, Configuration 1.

SYM	TP	MACH	ALPHA (DEG)	$R_N \times 10^{-6}/Ft$
○	29	.88	0	3.0
□	30	.88	3	3.0
△	31	.88	6	3.0

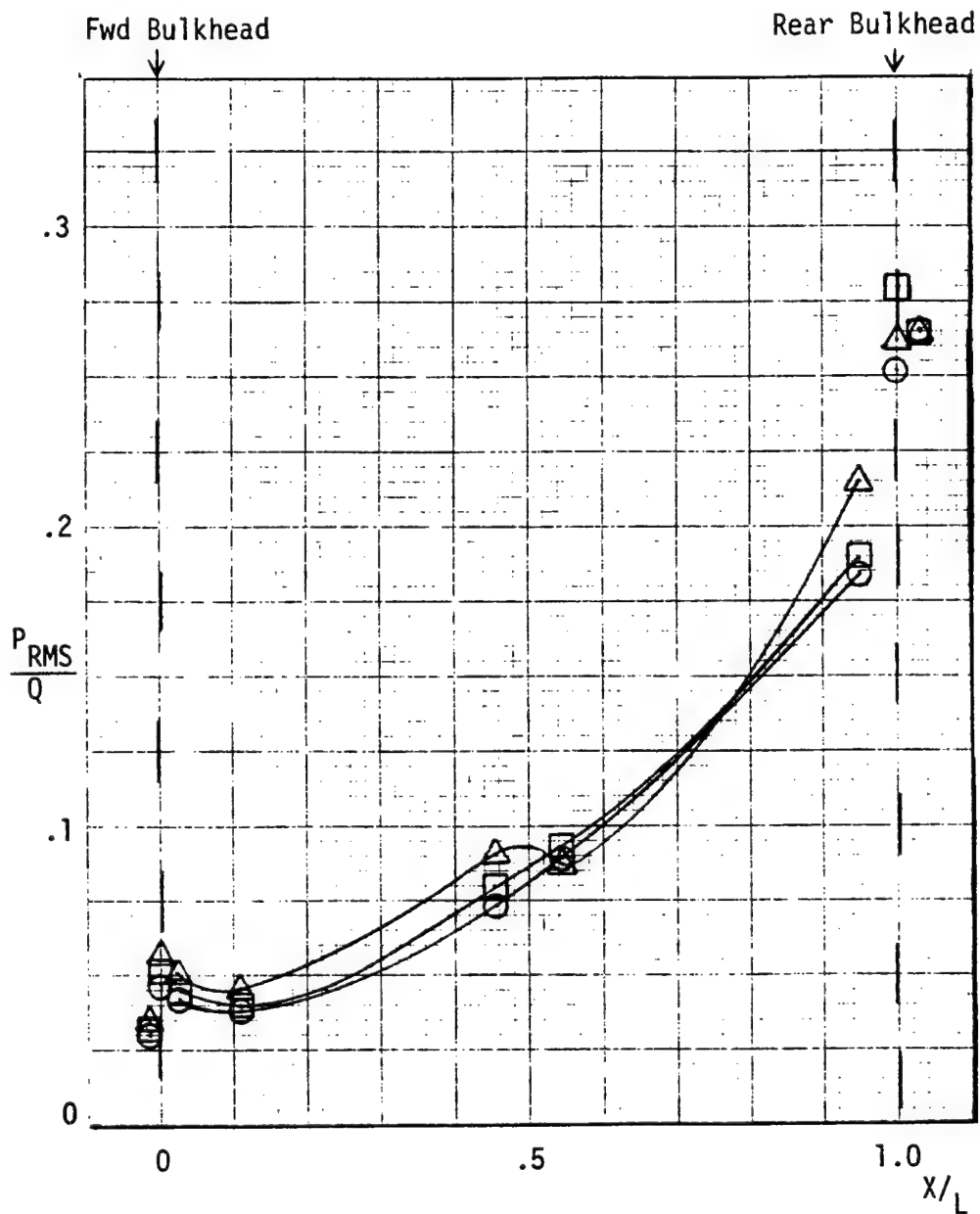


Figure 18. Angle of Attack Effects (Alpha) on Turbulence Distribution, Configuration 1.

SYM	TP	MACH	ALPHA(DEG)	$R_N \times 10^{-6}/Ft$
○	47	.9	0	5
□	48	.9	3	5

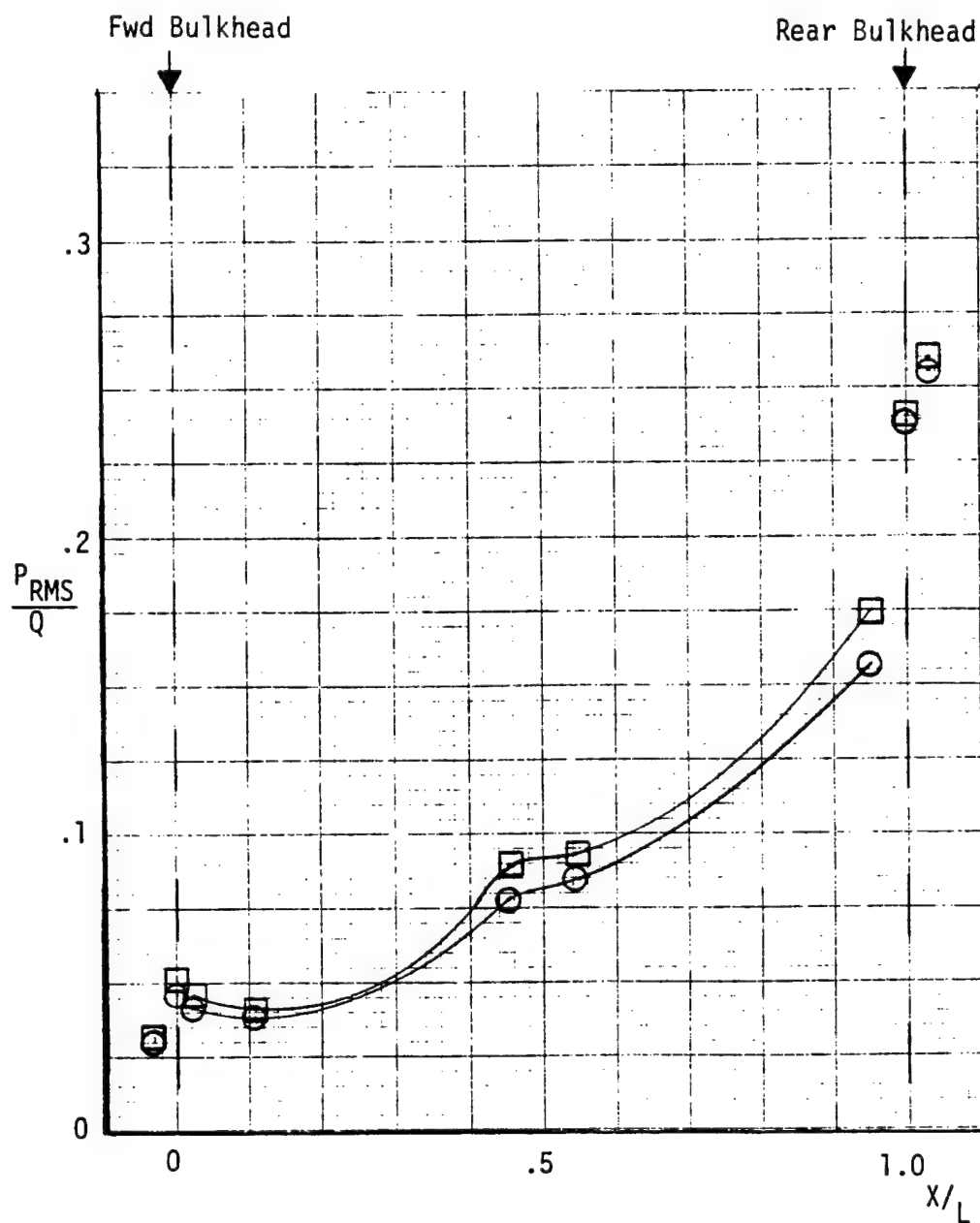


Figure 19. Angle of Attack Effects (Alpha) on Turbulence Distribution, Configuration 1.

SYM	TP	MACH	ALPHA(DEG)	$R_N \times 10^{-6}/Ft$
○	41	.7	3	3.0
□	44	.8	3	3.0
△	30	.9	3	3.0

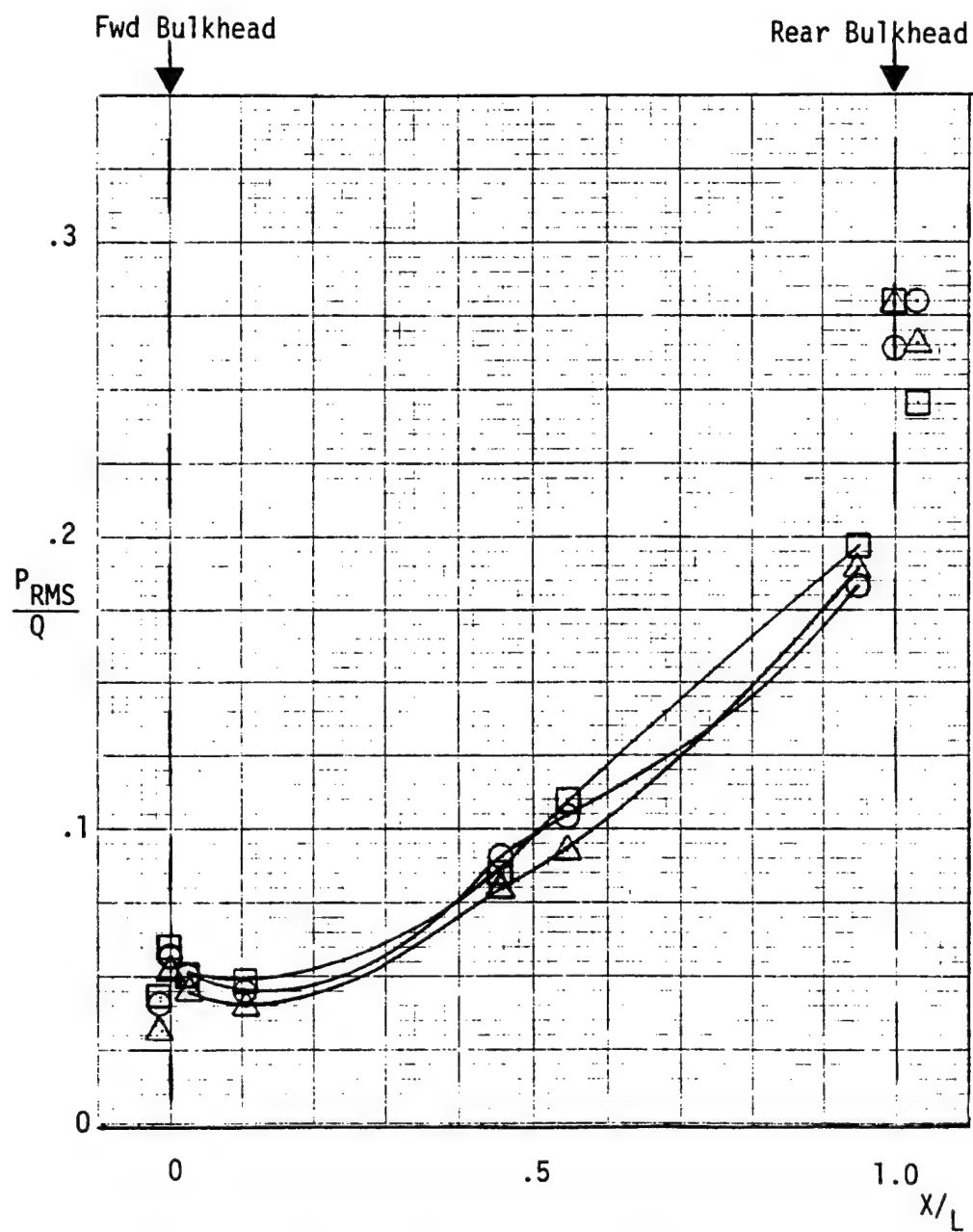


Figure 20. Mach Effects on Turbulence Distribution, Configuration 1.

SYM	TP	MACH	ALPHA(DEG)	$R_N \times 10^{-6}/Ft$
○	34	.69	3	5.0
□	38	.8	3	5.0
△	48	.9	3	5.0

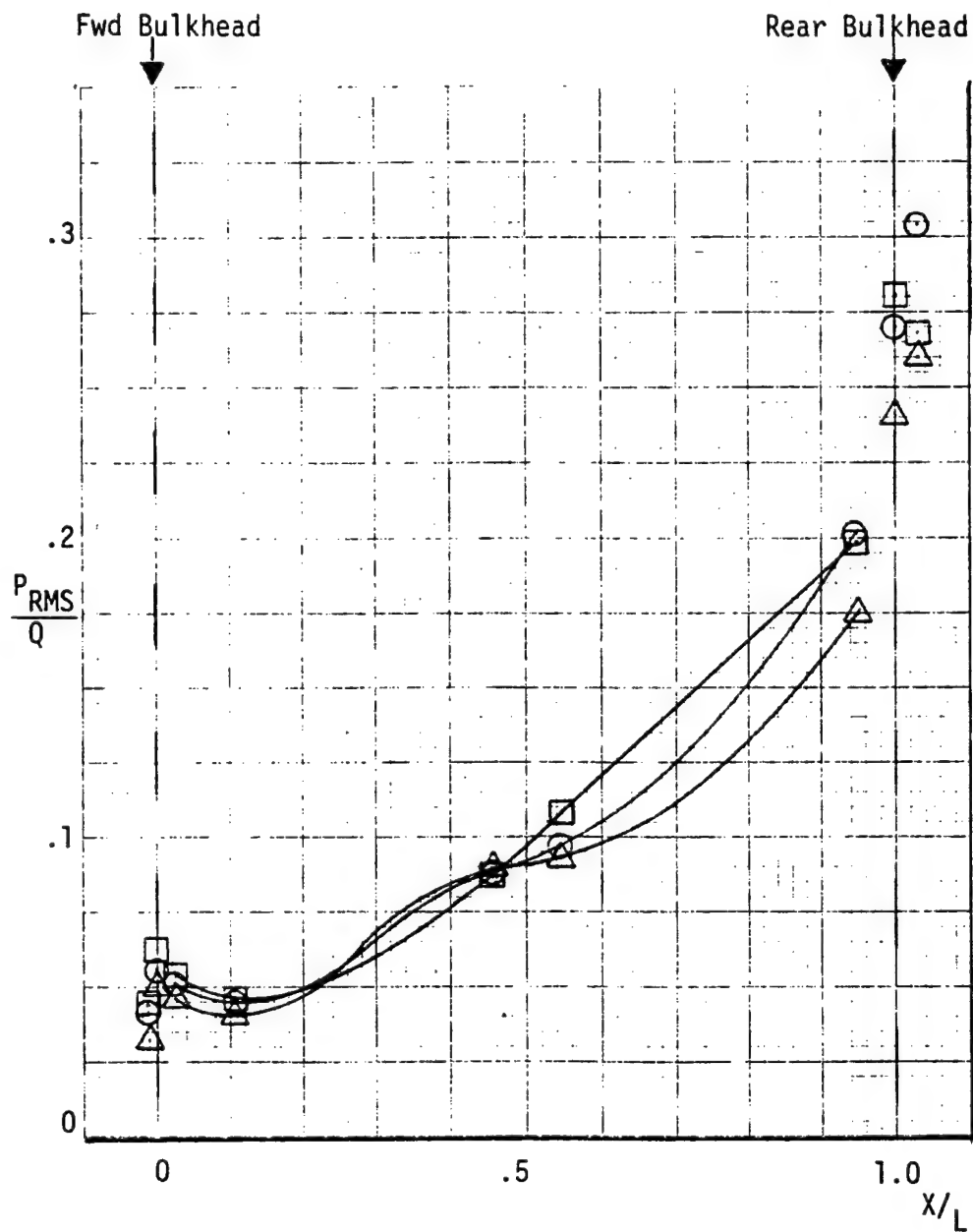


Figure 21. Mach Effects on Turbulence Distribution, Configuration 1.

SYM	TP	MACH	ALPHA(Deg)	$R_N \times 10^{-6}/Ft$
□	41	.7	3	3.0
◇	34	.69	3	5.0
◊	44	.8	3	3.0
◊	38	.8	3	5.0
△	30	.88	3	3.0
○	48	.9	3	5.0

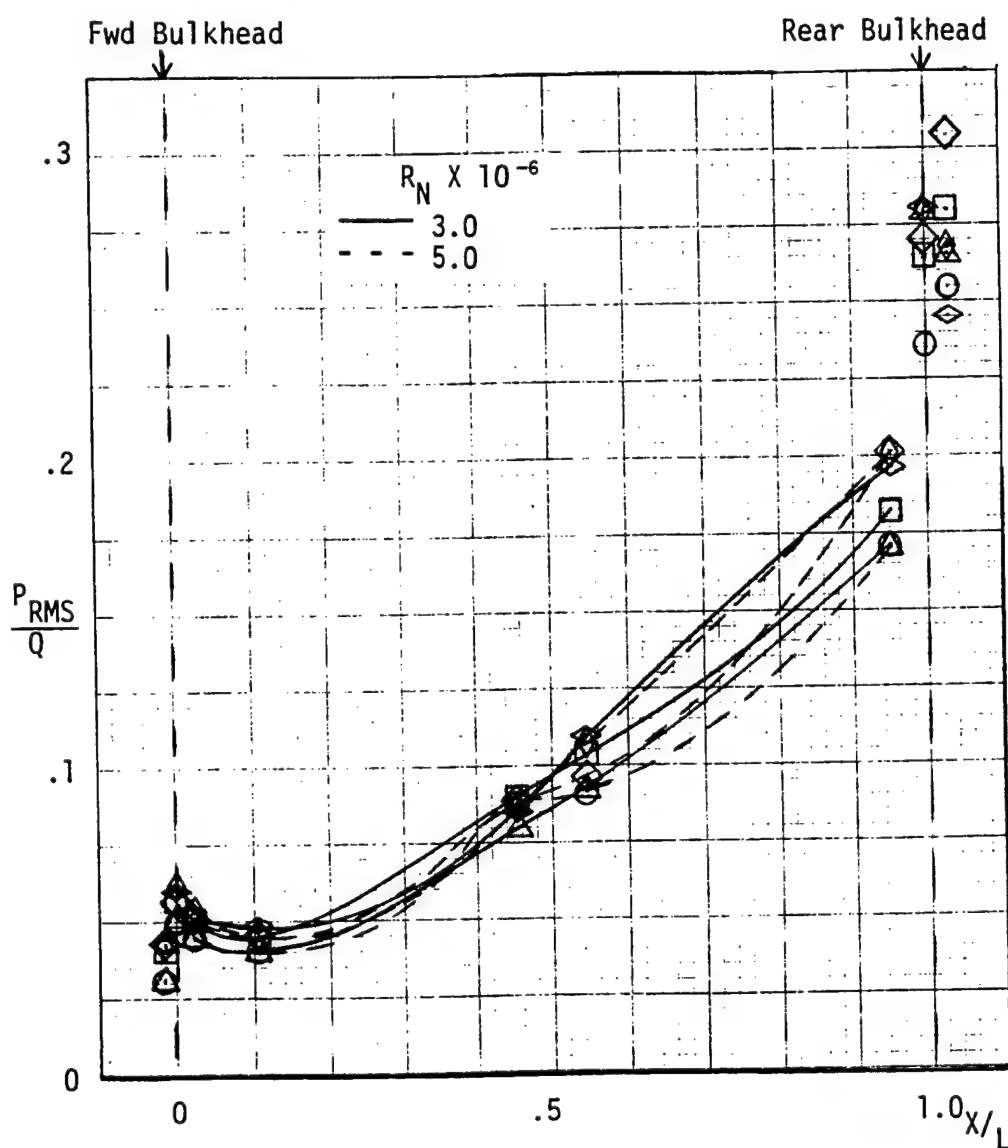


Figure 22. Overlay of Cavity Turbulence Distributions at Three Mach Numbers and Two R_N 's, Config. 1.

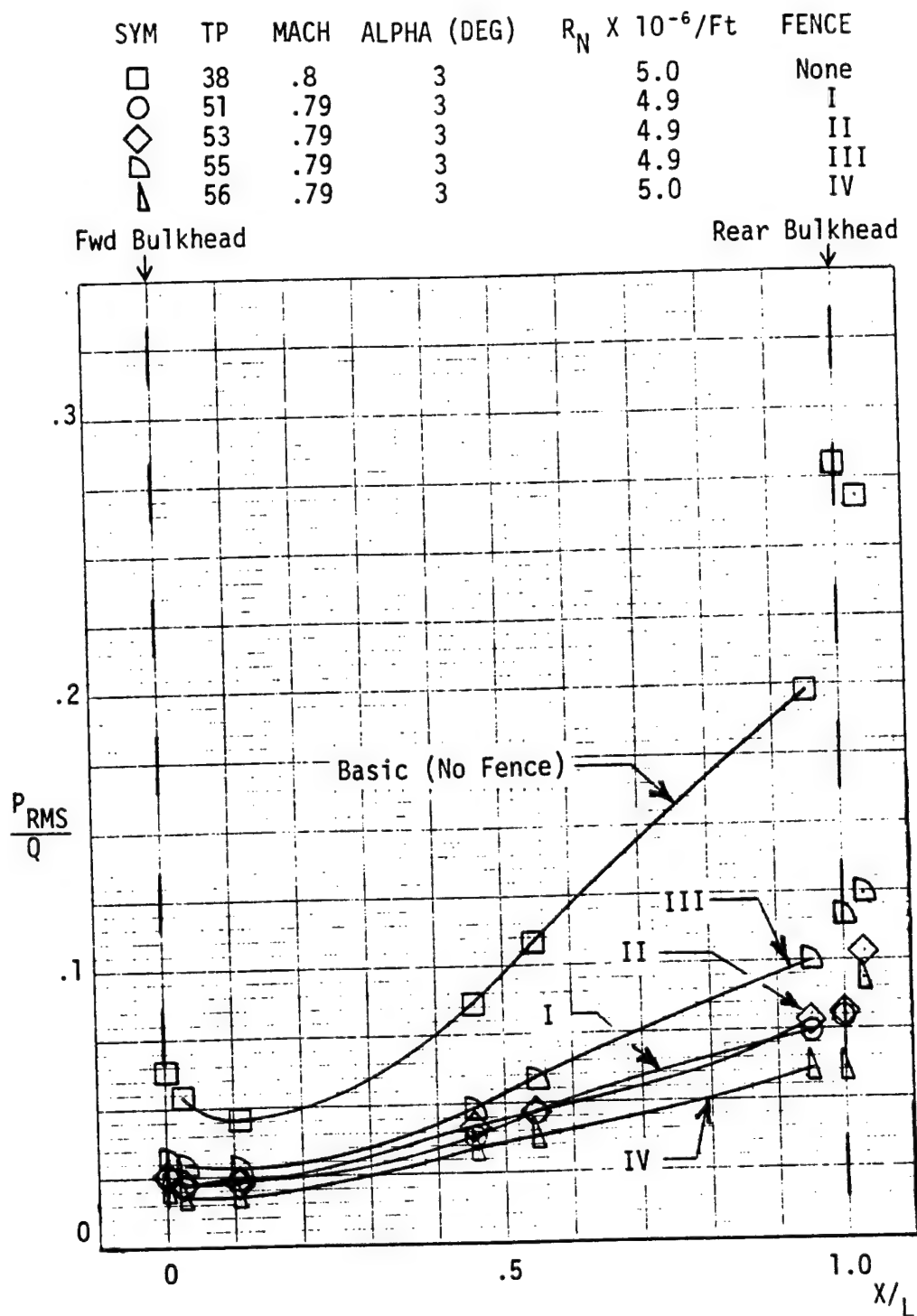


Figure 23. Comparison of Fences I - IV with the Basic (No Fence) Turbulence Distribution of Configuration 1.

SYM	TP	MACH	ALPHA(DEG)	$R_N \times 10^{-6}/\text{Ft}$
○	81	.69	3	5.0
◐	76	.70	3	5.0
◑	34	.69	3	5.0

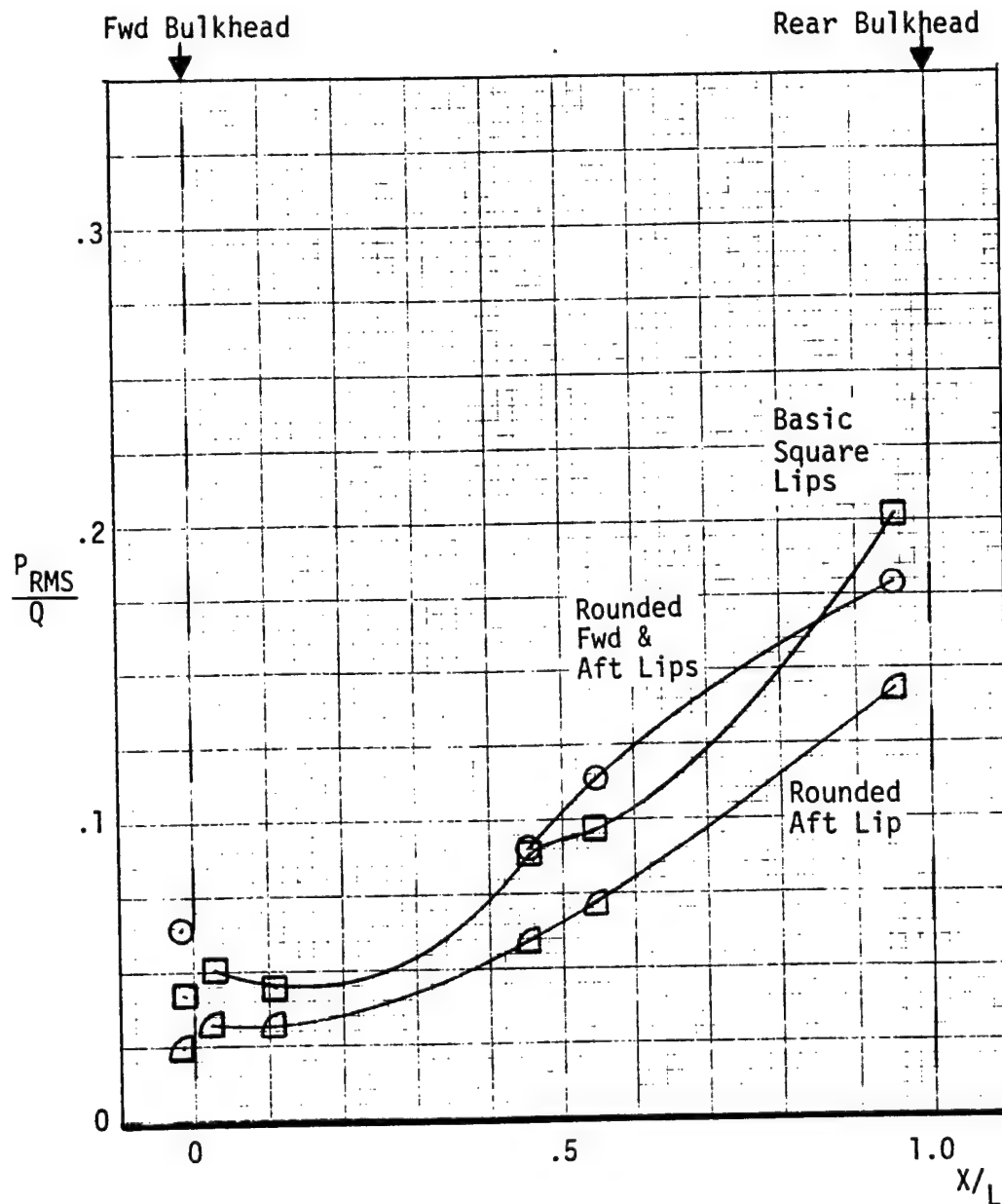


Figure 24. Effect of Cavity Lip Shape on Cavity Turbulence Distribution, Configuration 1.

SYM	TP	MACH	ALPHA(DEG)	$R_N \times 10^{-6}/Ft$
○	80	.79	3	4.9
△	72	.79	3	5.0
□	38	.8	3	5.0

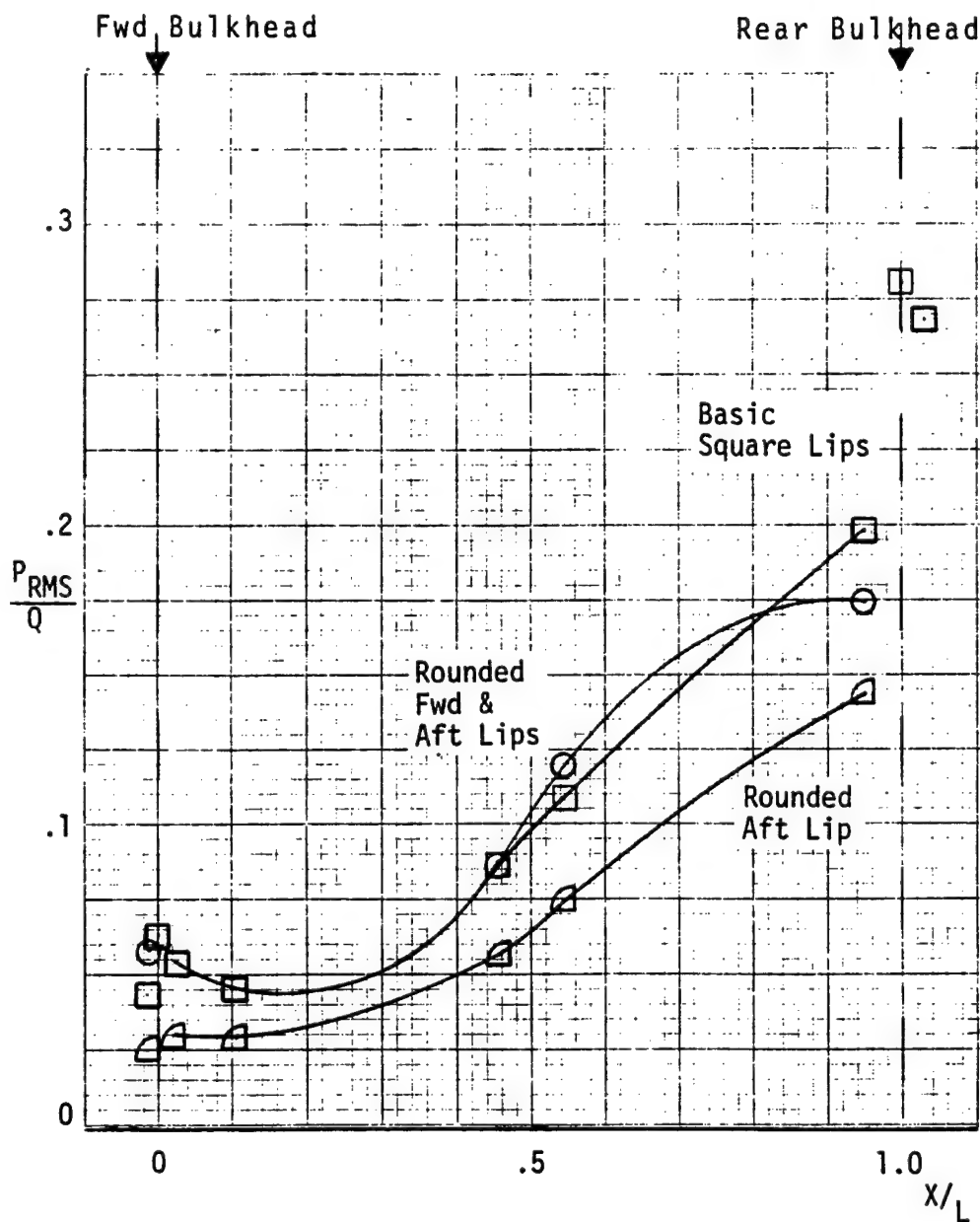


Figure 25. Effect of Cavity Lip Shape on Turbulence Distribution, Configuration 1.

SYM	TP	MACH	ALPHA(DEG)	$R_N \times 10^{-6}/\text{Ft}$	FENCE
○	78	.79	0	5.0	I
□	77	.79	3	5.0	I
△	79	.79	6	5.0	I

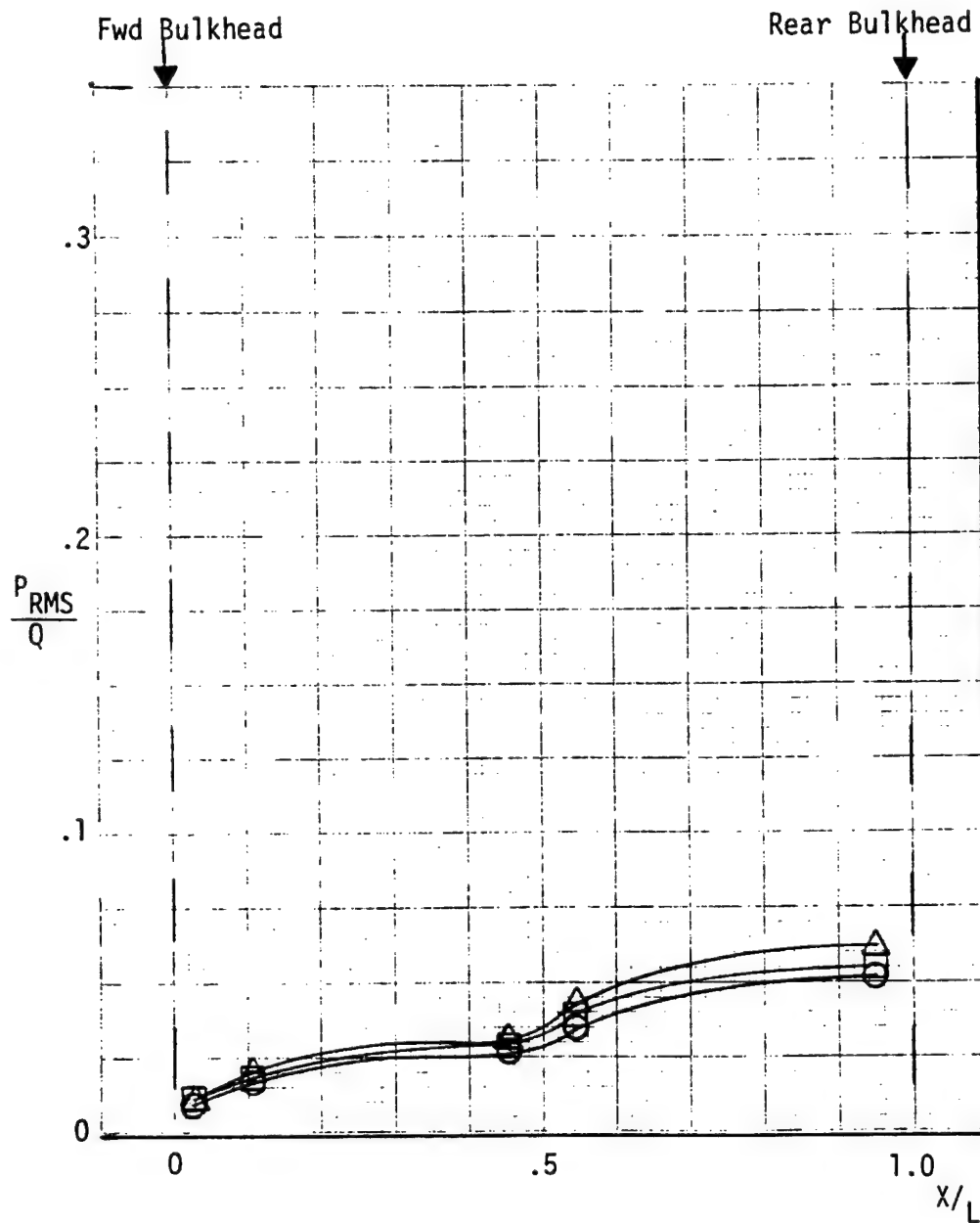


Figure 26. Angle of Attack Effect on Cavity With Rounded Aft Lip and Fence I at Leading Edge of Cavity.

SYM	TP	MACH	ALPHA(DEG)	$R_N \times 10^{-6}/Ft$	FENCE
□	51	.79	3	4.9	I
△	77	.79	3	5.0	I

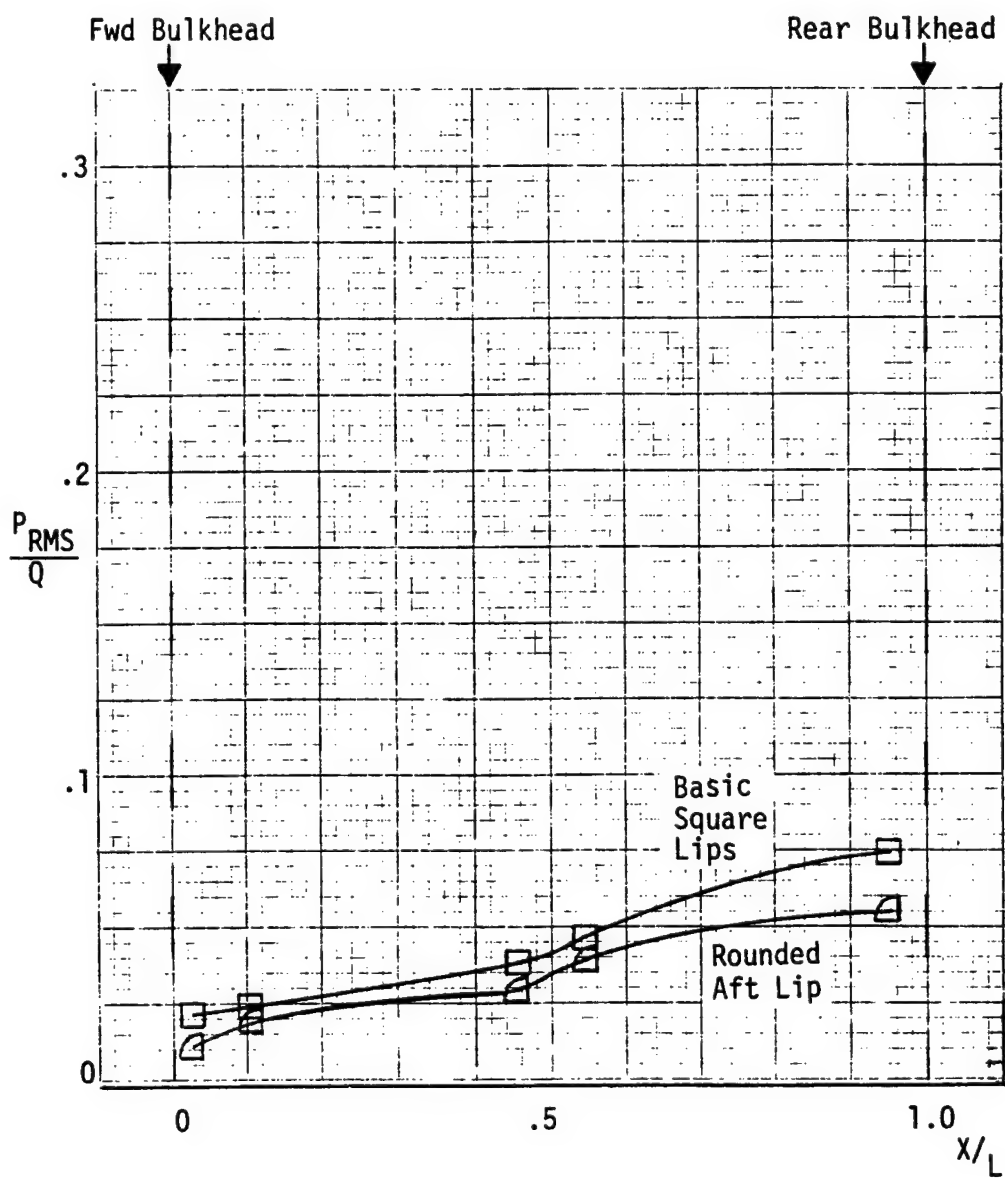


Figure 27. Effect of Aft Lip Shape Turbulence Distribution with Fence I at Leading Edge of Cavity.

SYM	TP	MACH	ALPHA(DEG)	$R_N \times 10^{-6}/Ft$	C_J
○	38	.8	3	5.0	0
□	62	.79	3	4.9	.101
△	61	.79	3	5.0	.152

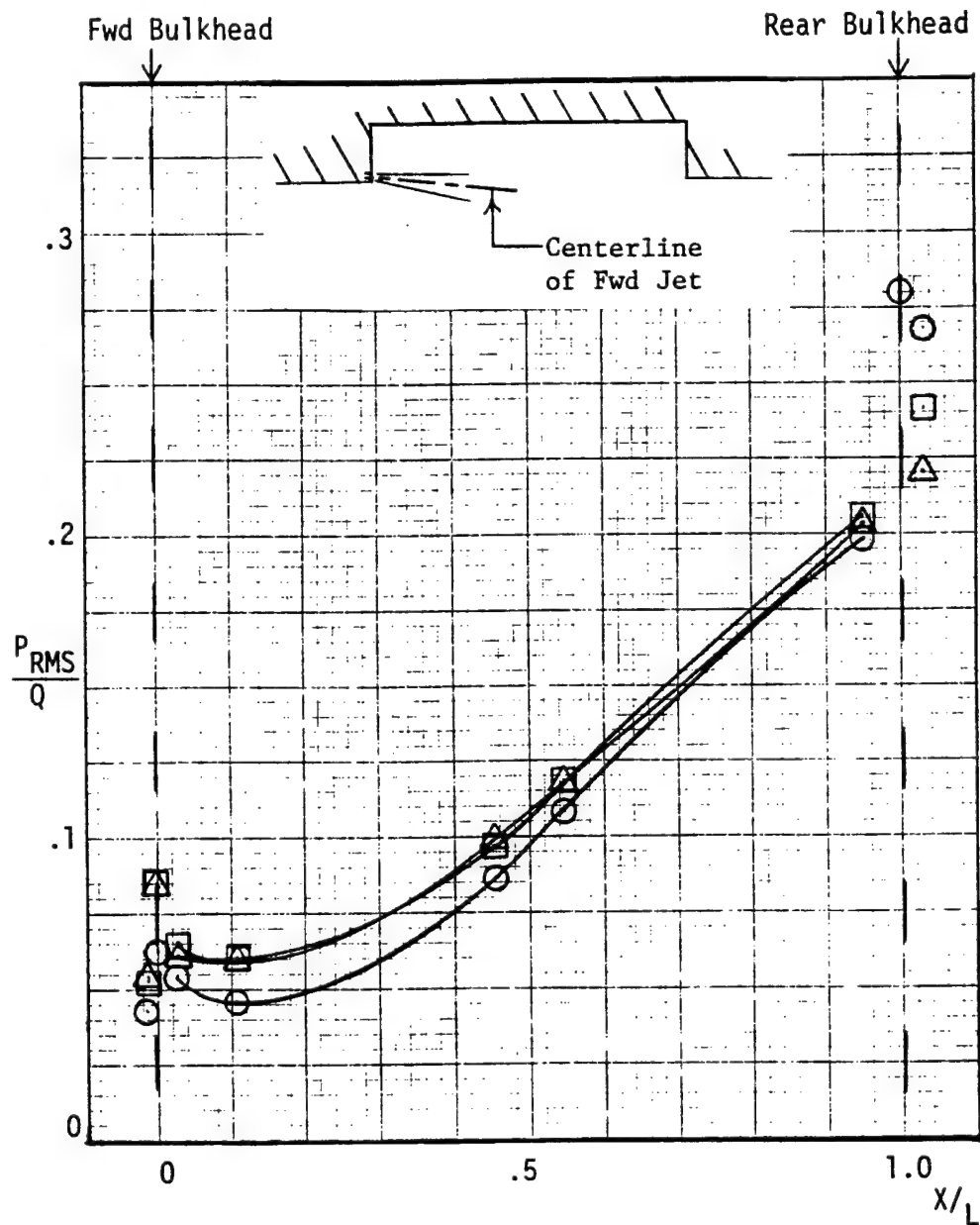


Figure 28. Effect of Blowing at the Forward Lip on Turbulence Distribution, Configuration 1.

SYM	TP	MACH	ALPHA(DEG)	$R_N \times 10^{-6}/Ft$	C_J
○	38	.8	3	5.0	0
□	69	.79	3	4.9	.107
△	70	.79	3	4.9	.142

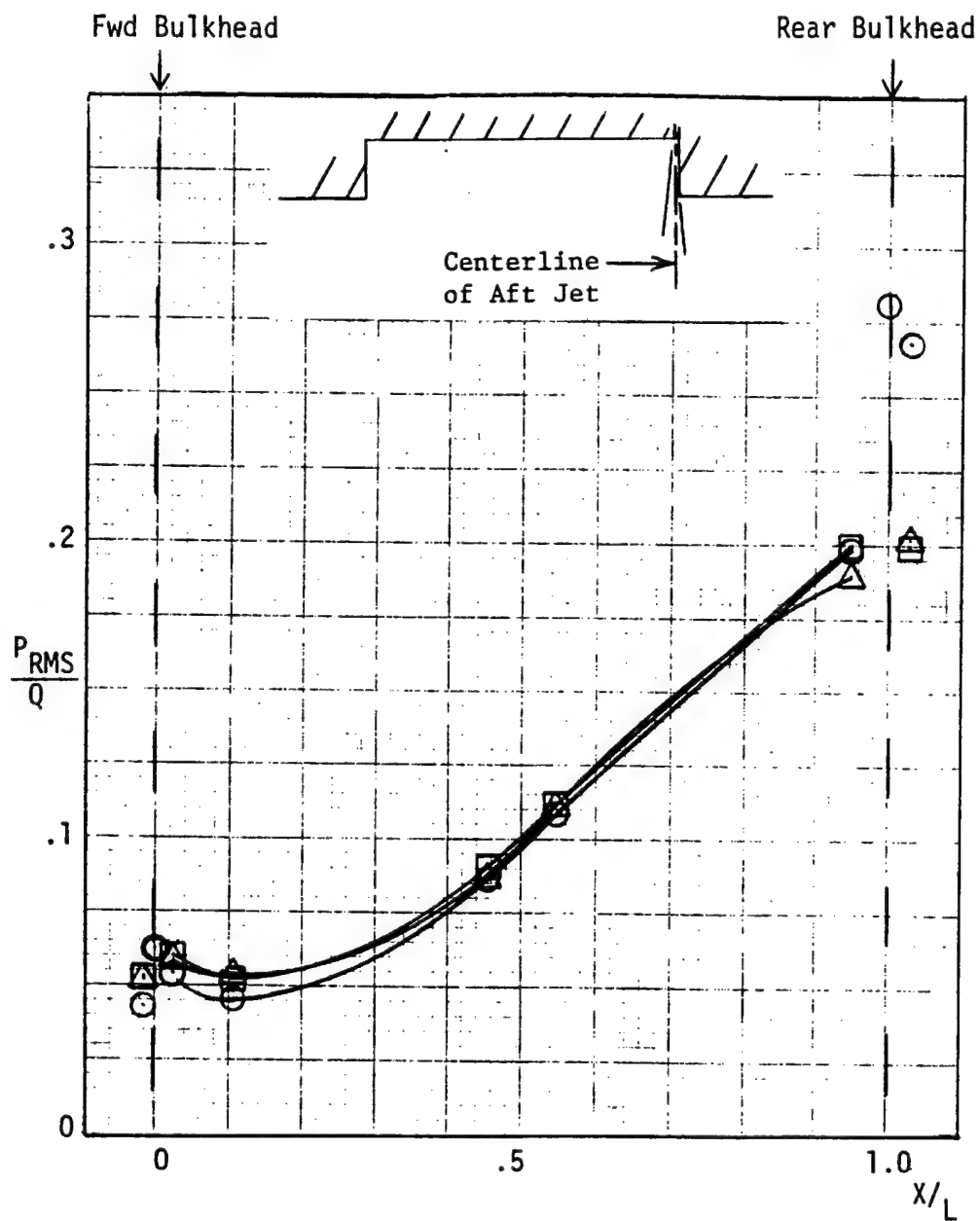


Figure 29. Effect of Blowing Over Aft Bulkhead on Turbulence Distribution, Configuration 1.

SYM	TP	MACH	ALPHA (DEG)	$R_N \times 10^{-6}/\text{Ft}$	C_J
○	72	.79	3	5.0	0
□	73	.79	3	4.9	.034
△	74	.79	3	4.9	.072
◻	75	.79	3	5.0	.124

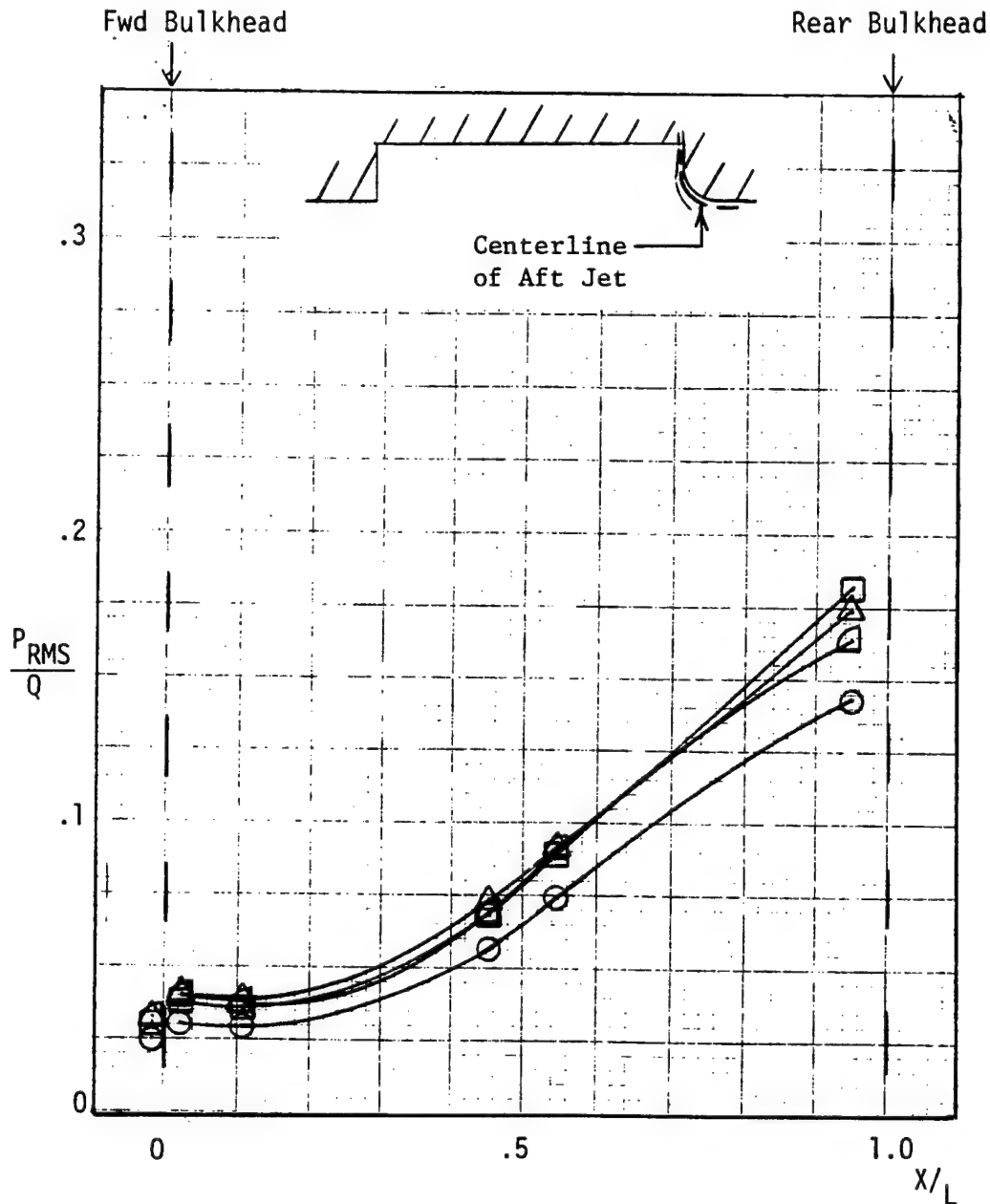


Figure 30. Effect of Blowing Over Aft Bulkhead with Rounded Lip, Configuration 1.

SYM	TP	MACH	ALPHA(DEG)	$R_N \times 10^{-6}/\text{Ft}$	FENCE
□	38	.8	3	5.0	None
◻	77	.79	3	5.0	I

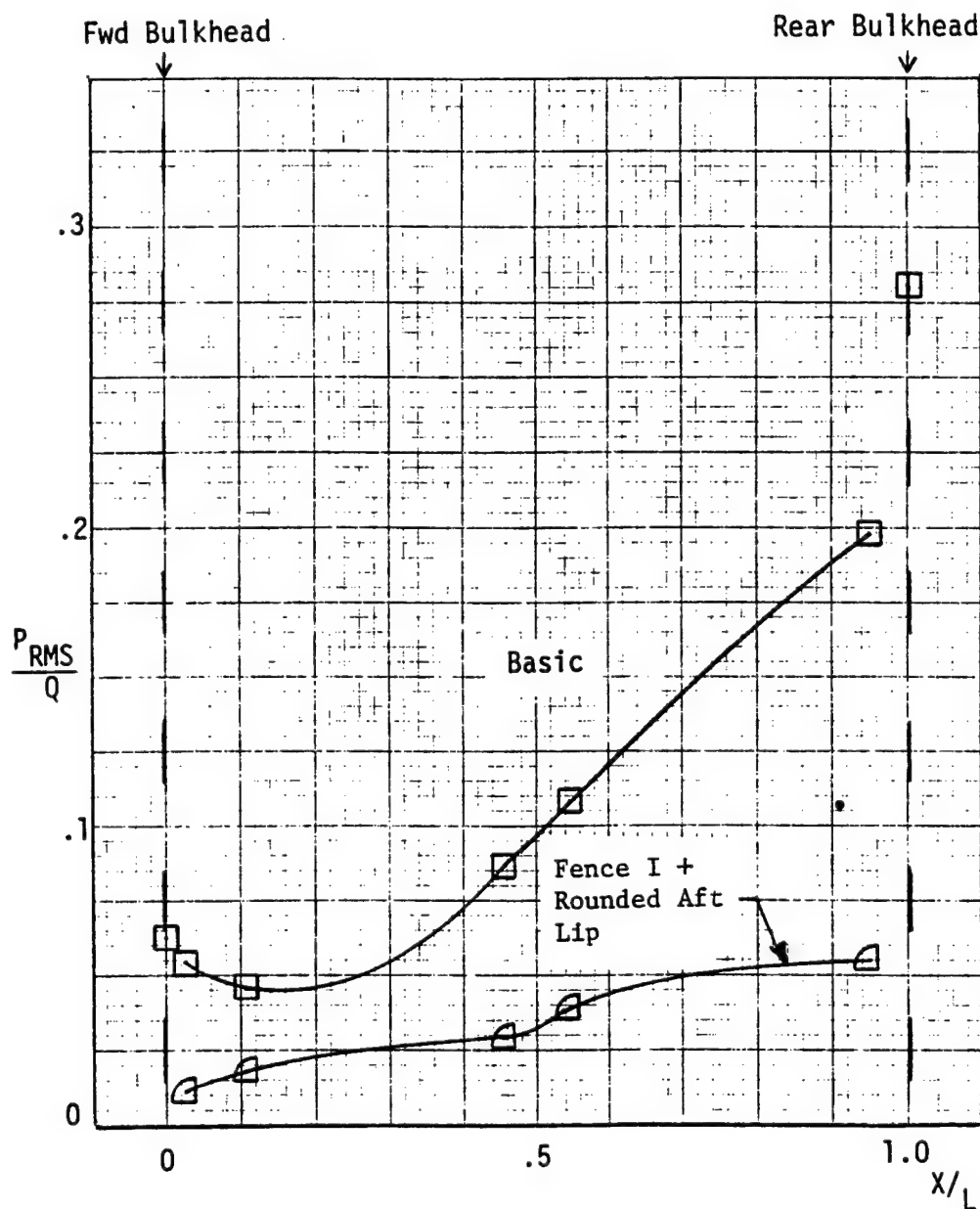
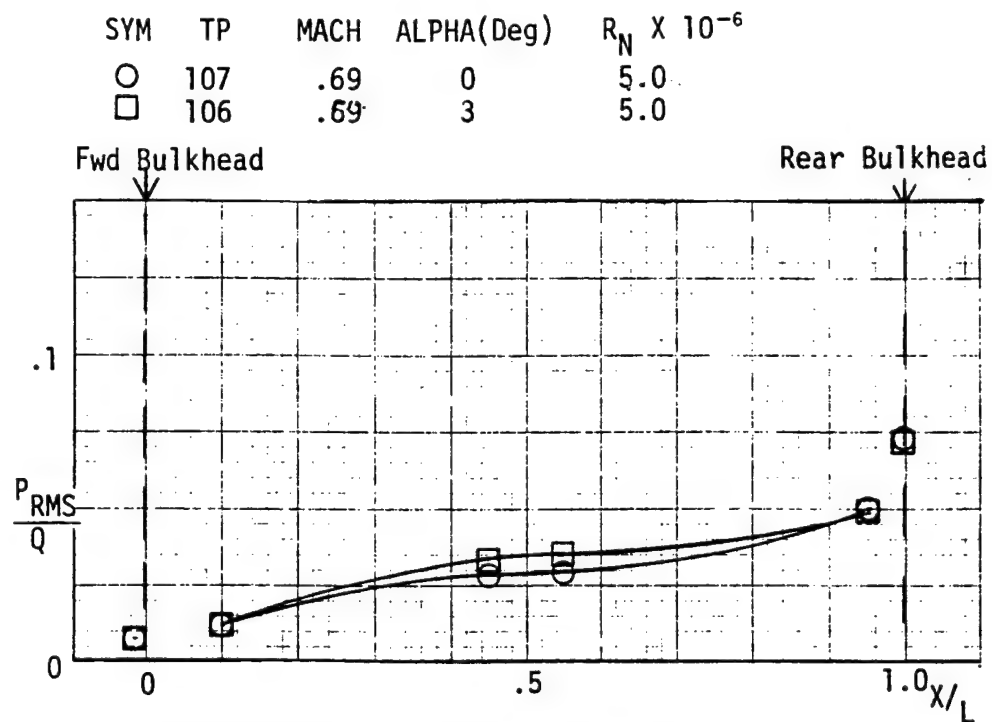
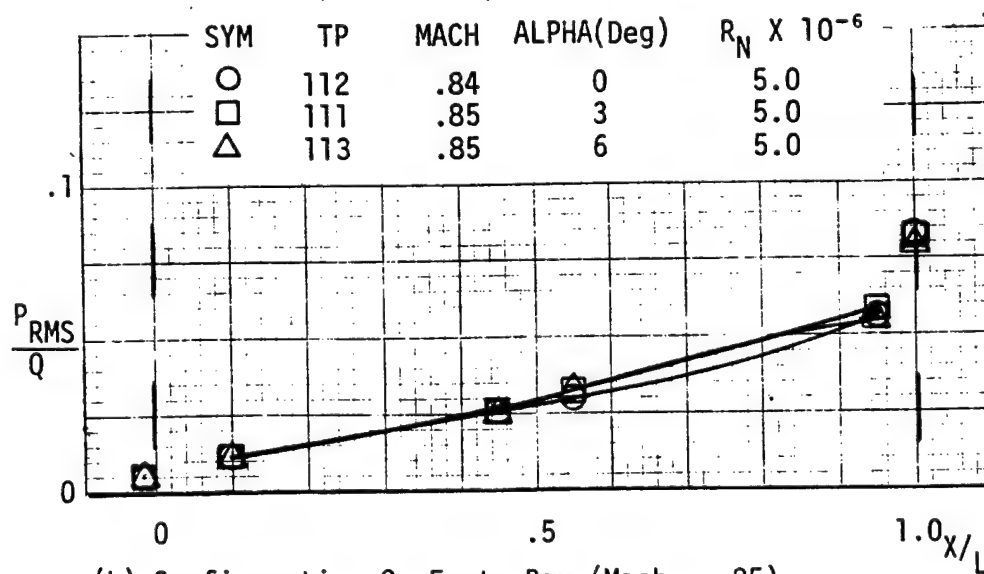


Figure 31. Combined Effect of Fence I with Rounded Aft Lip



(a) Configuration 2, Empty (Mach \approx .69)



(b) Configuration 2, Empty Bay (Mach \approx .85)

Figure 32. Angle of Attack Effects on Turbulence Distribution, Configuration 2.

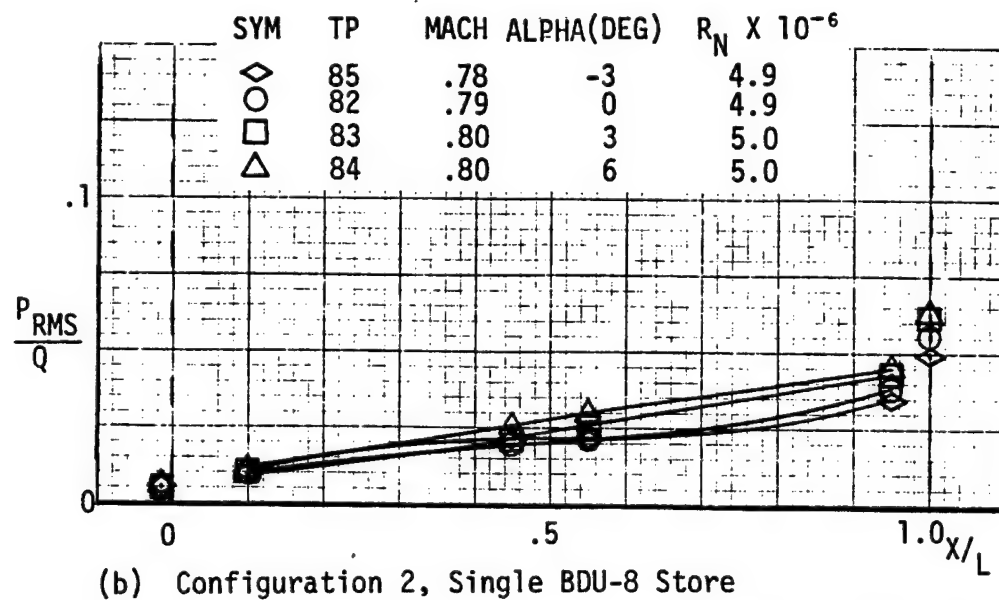
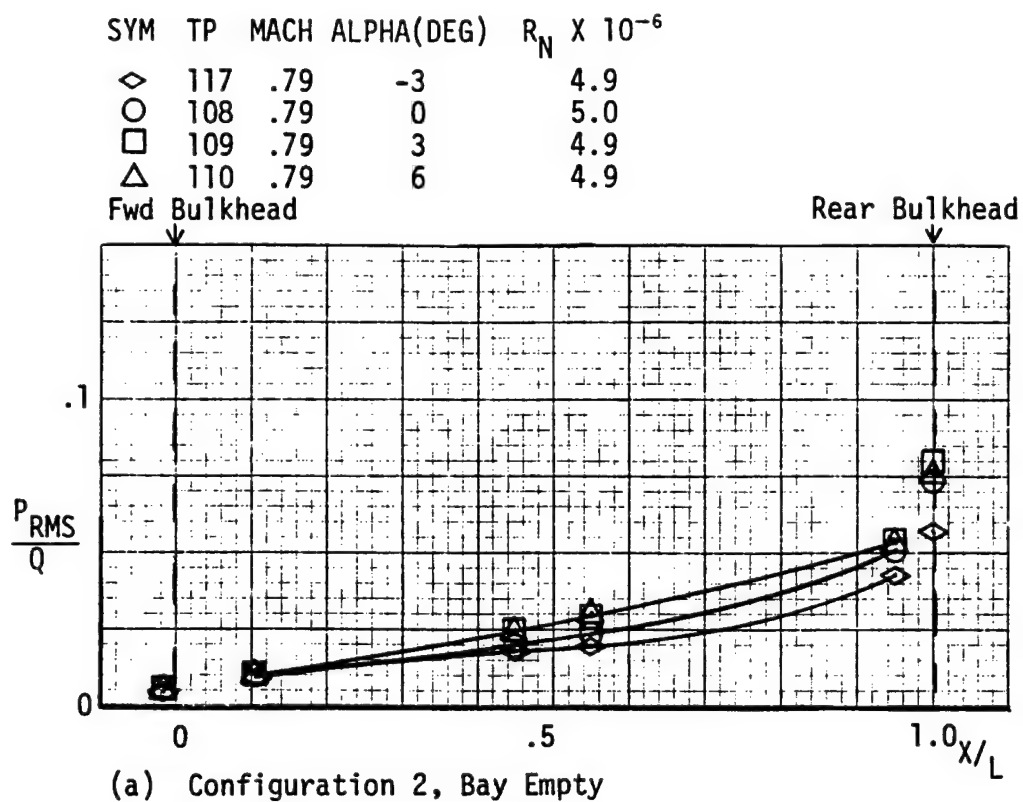


Figure 33. Angle of Attack Effects on Turbulence Distribution with and without Store Installed on Left Side of Bay.

SYM	ALPHA (DEG)	$R_N \times 10^{-6}$	BAY
○	3	3.0	Empty
□	3	5.0	Empty

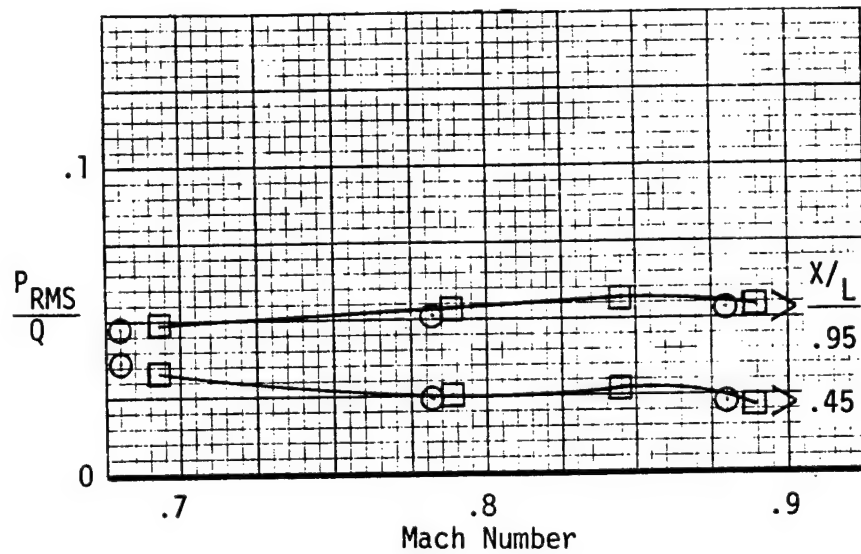
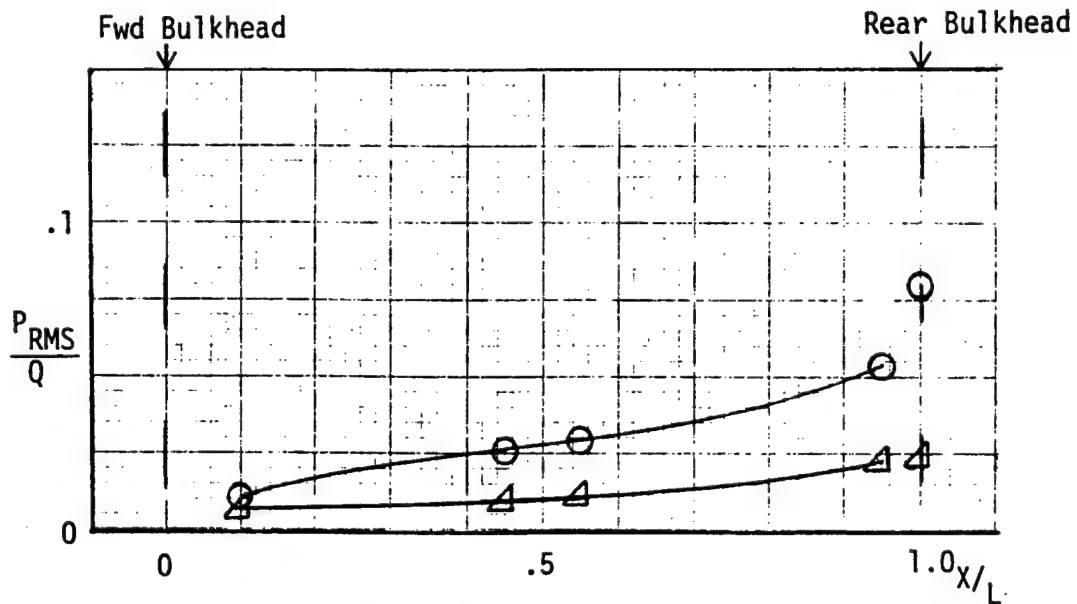
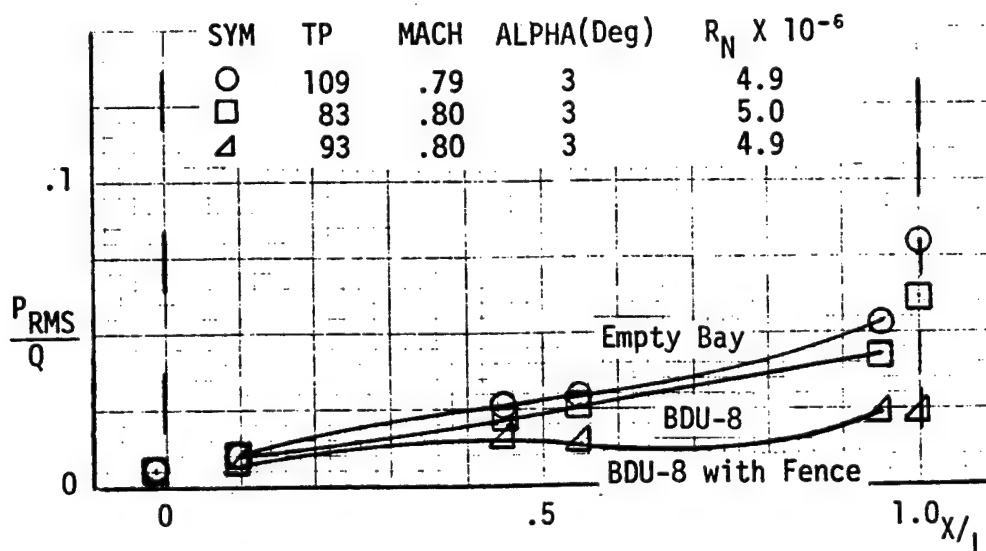


Figure 34. Reynold's Number Effect on Turbulence Level, Configuration 2.

SYM	TP	MACH	ALPHA(Deg)	$R_N \times 10^{-6}$
○	109	.79	3	4.9
△	100	.80	3	4.9



(a) Comparison of Empty Bay with and without Fence I at Leading Edge of Bay.



(b) Effect of BDU-8 with and without Fence I at Leading Edge of Bay.

Figure 35. Turbulence Distributions in Configuration 2.

SYM	ALPHA(DEG)	$R_N \times 10^{-6}$	BAY
○	3	5.0	Empty
□	3	5.0	Single BDU-8

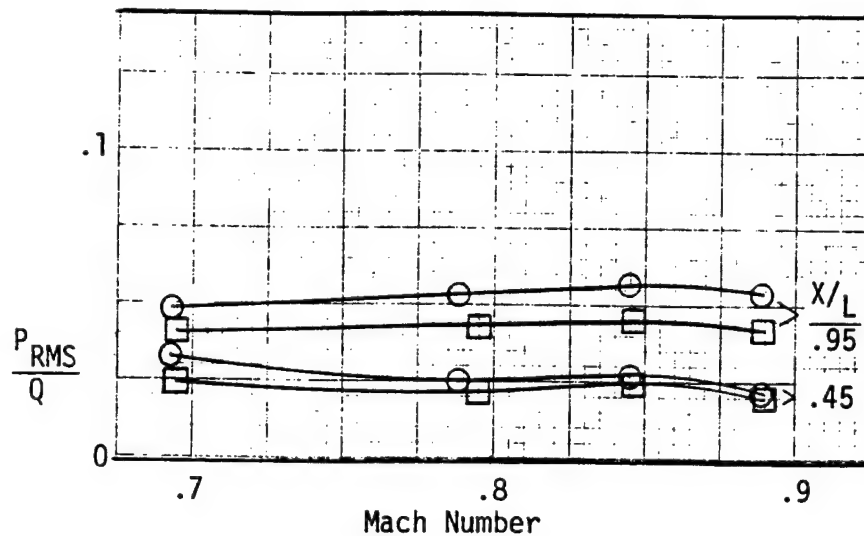


Figure 36. Mach Effects on Turbulence with and Without Single BDU-8 Store, Config.2.

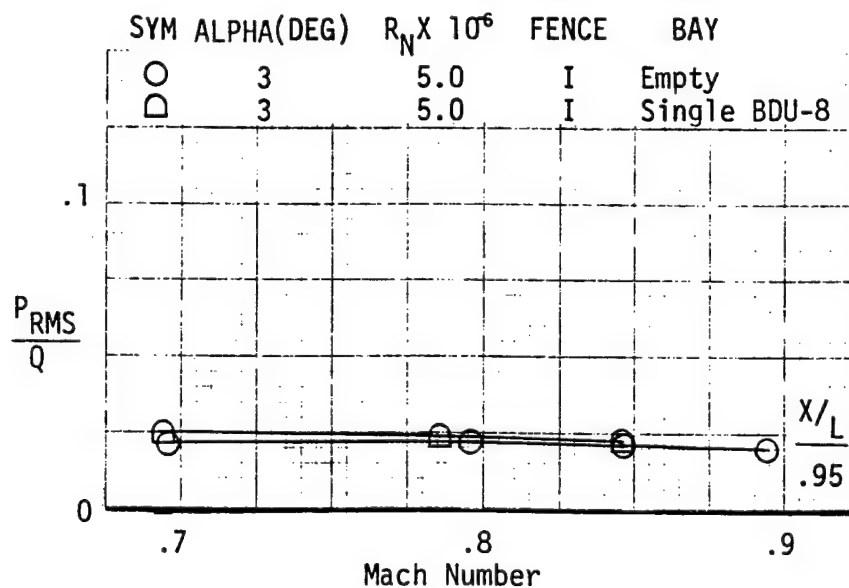


Figure 37. Mach Effects on Turbulence with Fence I, with and Without BDU-8 in Bay; Configuration 2.

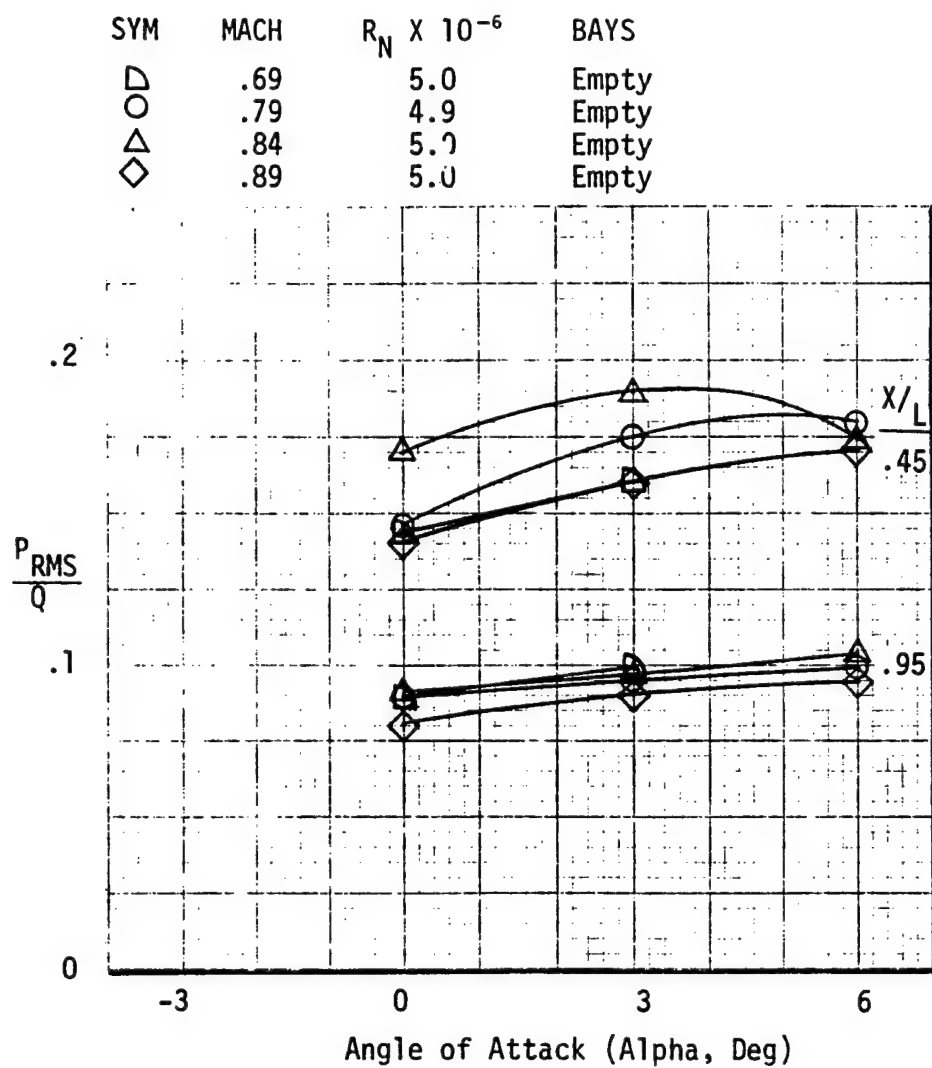


Figure 38. Angle of Attack Affects on Turbulence Level in Forward and Aft Bays of Configuration 3.

SYM	ALPHA(Deg)	$R_N \times 10^{-6}$
○	3	3.0
□	3	5.0

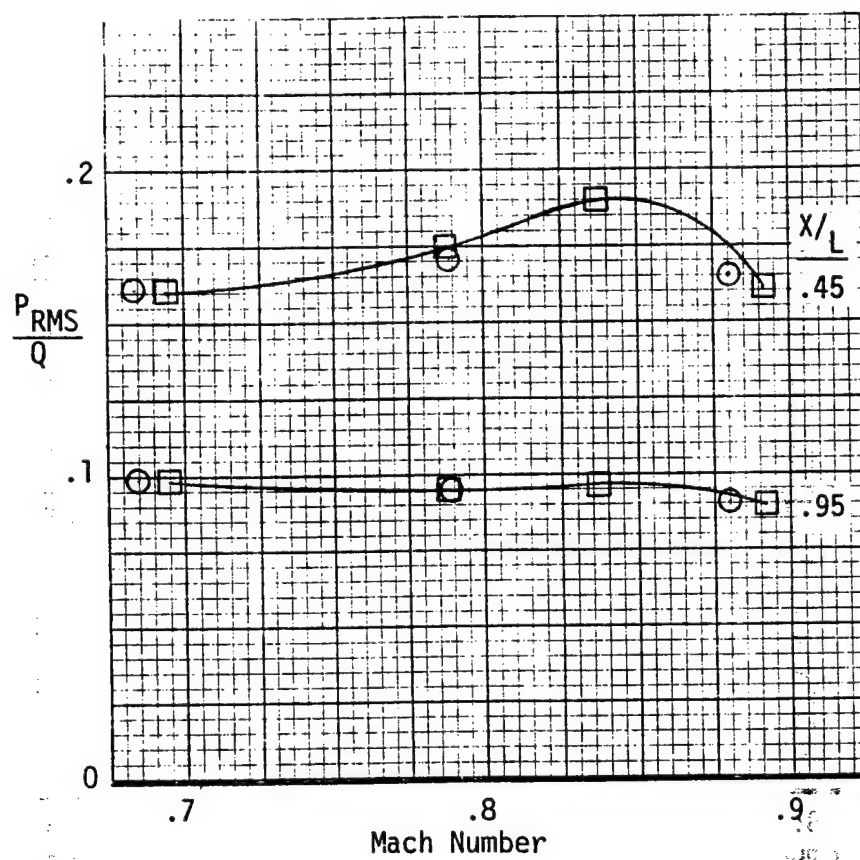


Figure 39. Reynold's Number Effects on Turbulence Level, Configuration 3; Bays Empty.

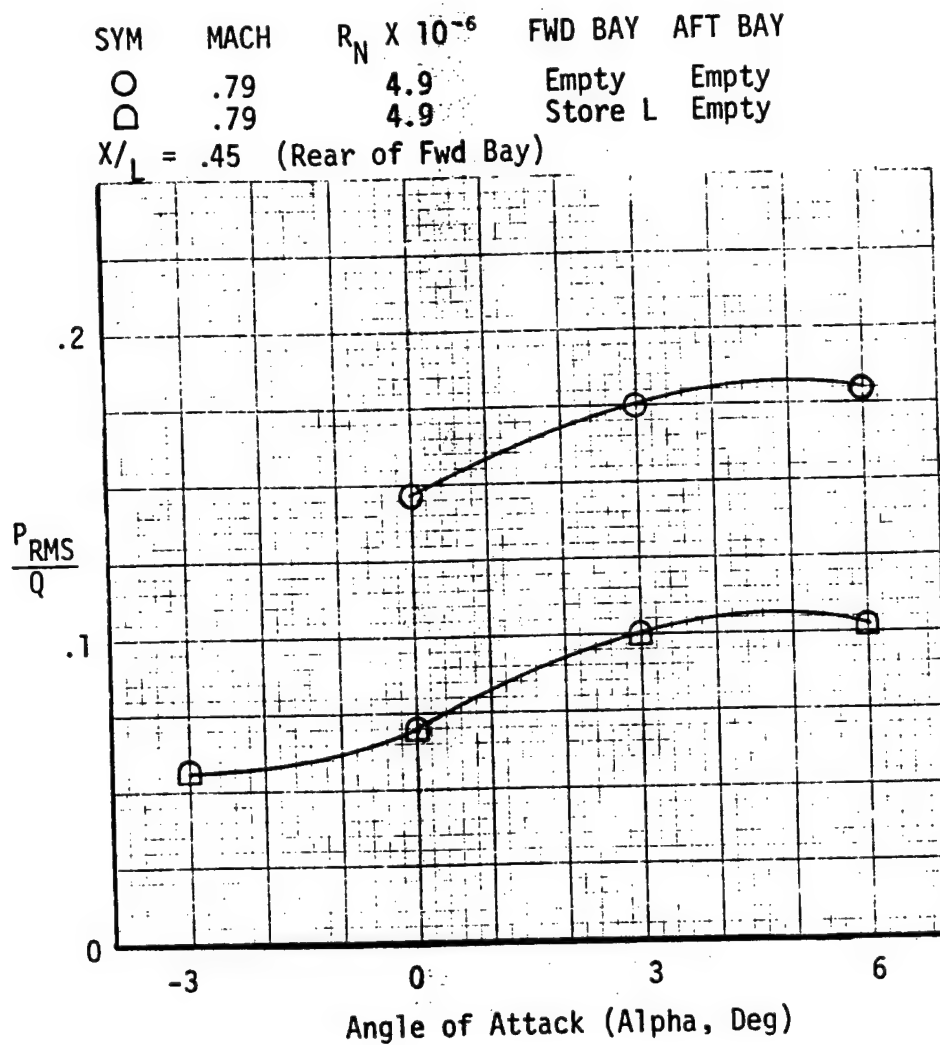


Figure 40. Angle of Attack Effects on Turbulence with and without Store L in Forward Bay, Configuration 3.

SYM	ALPHA(Deg)	$R_N \times 10^{-6}$	FENCE	FWD BAY	AFT BAY
O	3	5.0	None	Empty	Empty
D	3	5.0	None	Store L	Empty
Δ	3	5.0	I	Store L	Empty
△	3	5.0	I	Empty	Empty

$X/L = .45$ (Peak level observed near rear bulkhead in fwd bay of Configuration 3.)

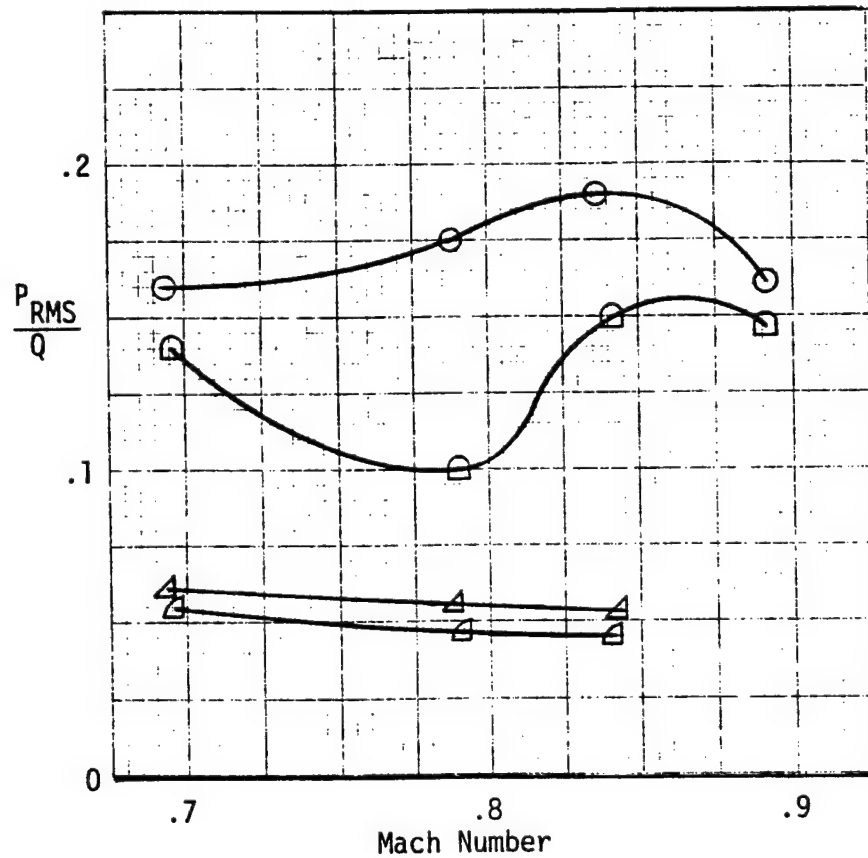


Figure 41. Mach Effects on Peak Turbulence Level in Forward Bay of Configuration 3, with and without Store L and Fence I.

SYM	ALPHA(DEG)	$R_N \times 10^{-6}$	FENCE	FWD BAY	AFT BAY
○	3	5.0	None	Empty	Empty
◻	3	5.0	None	Store L	Empty
◻	3	5.0	I	Empty	Empty
△	3	5.0	I	Store L	Empty

$$X/L = .45$$

Flagged Symbols are for Left Side Wall

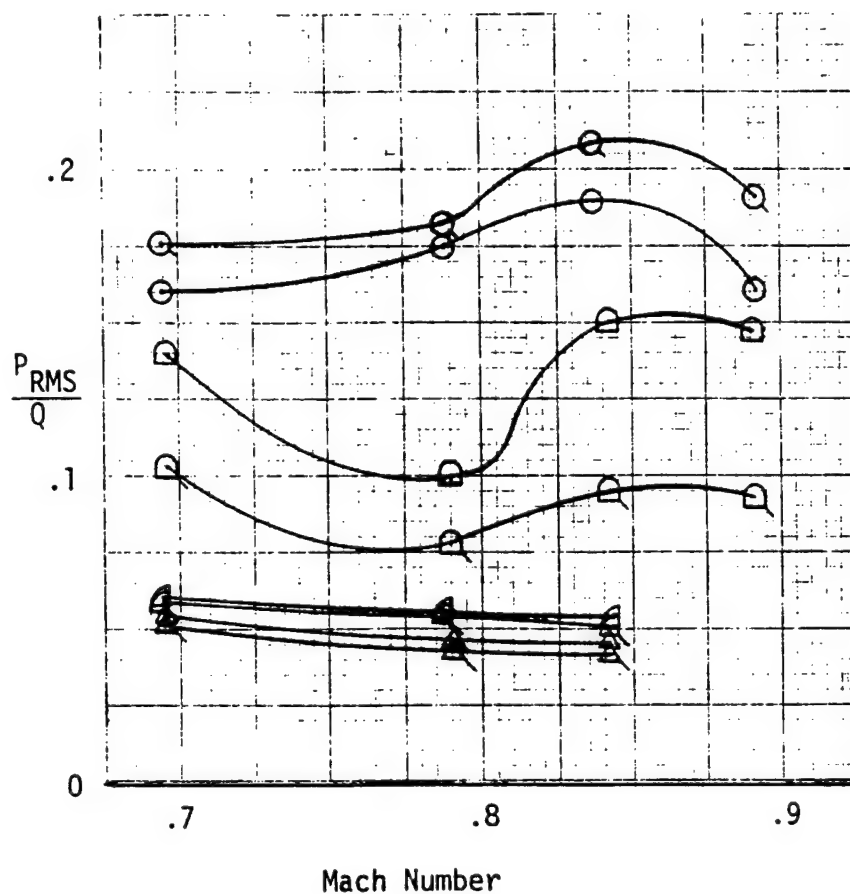


Figure 42. Comparison of Turbulence Levels Measured on Centerline (Roof) with Sidewall of Configuration 3.

SYM	CONFIG.	MACH	$R_N \times 10^{-6}$	X/L
○	1	.8	5.0	.95
△	3	.79	5.0	.45 (Rear of Fwd Bay)
▽	3	.79	5.0	.95 (Rear of Aft Bay)
□	2	.79	5.0	.95

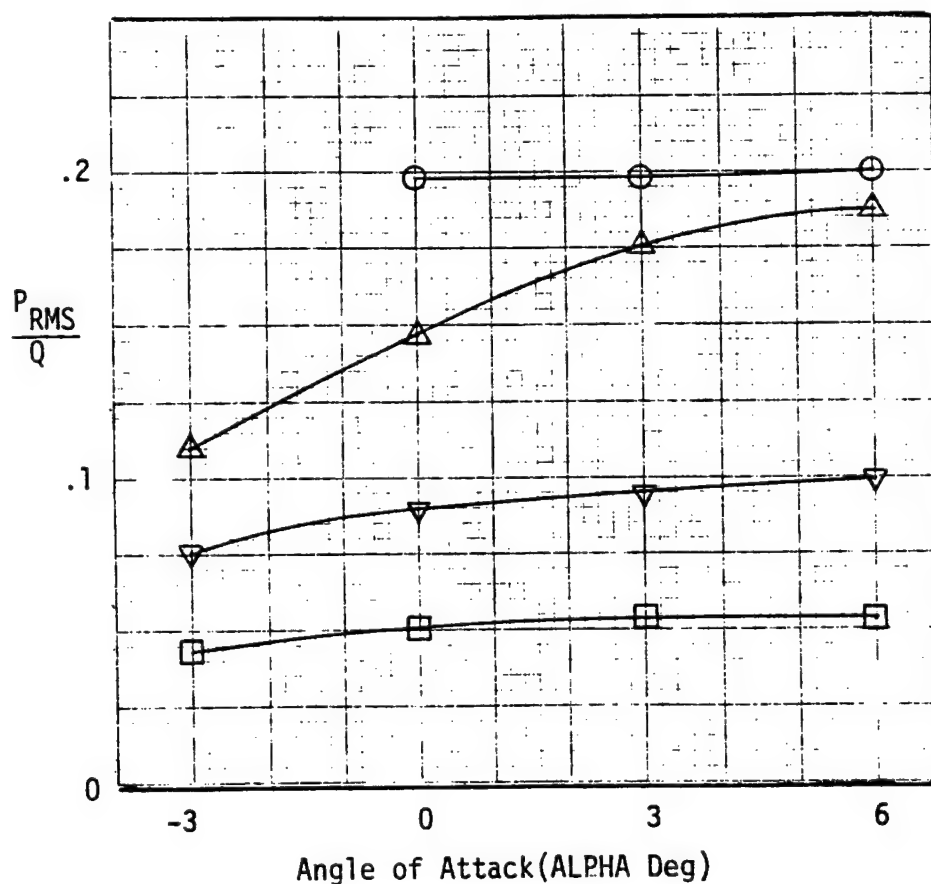


Figure 43. Summary of Angle of Attack Effects (Mach $\approx .8$) Comparing Representative Turbulence Levels in the Three Bay Configurations, Bays Empty.

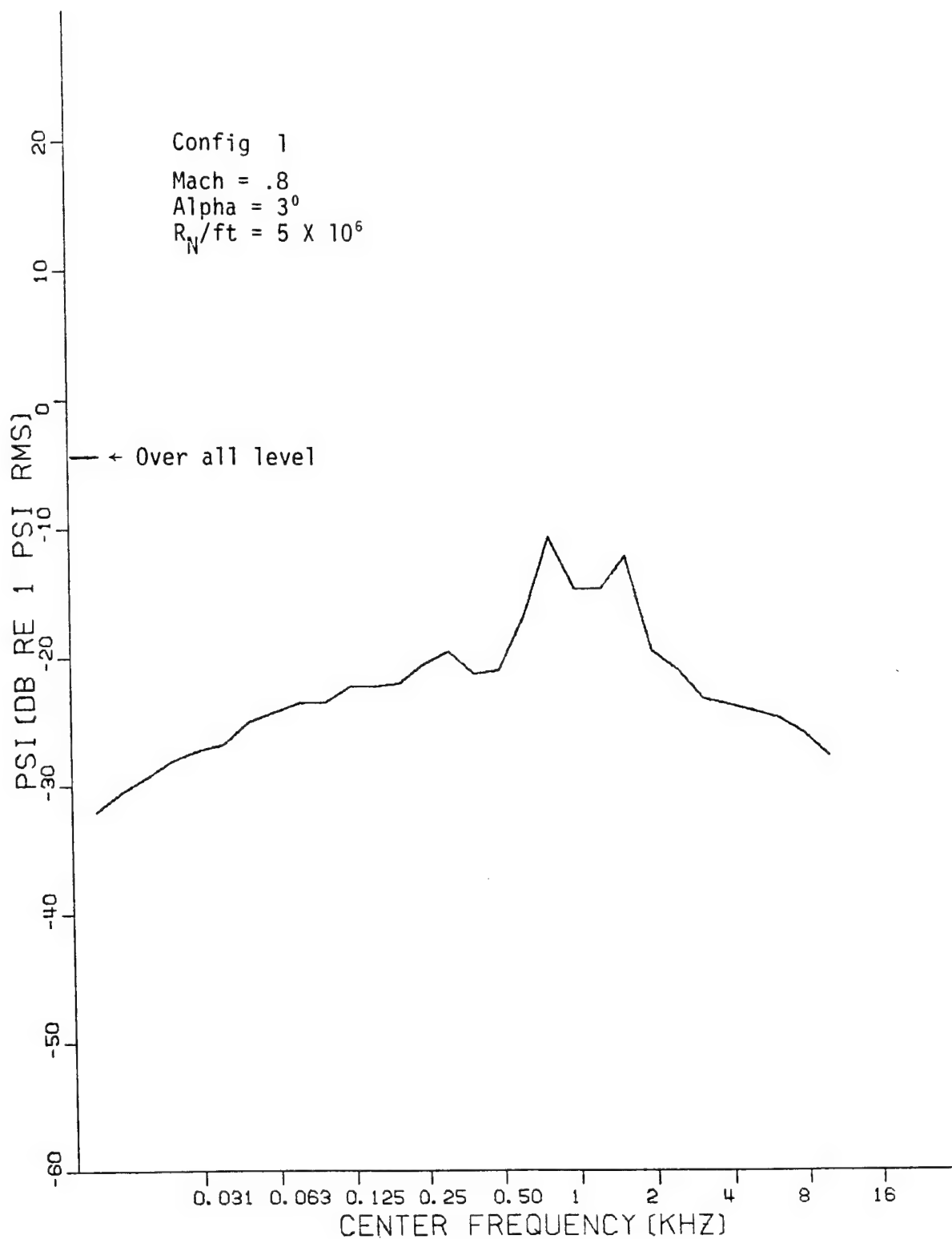


FIGURE 44. ONE THIRD OCTAVE BAND SPECTRA
FROM TEST POINT NR 38,
TRANSDUCER NR 6, $X/L = .55$.

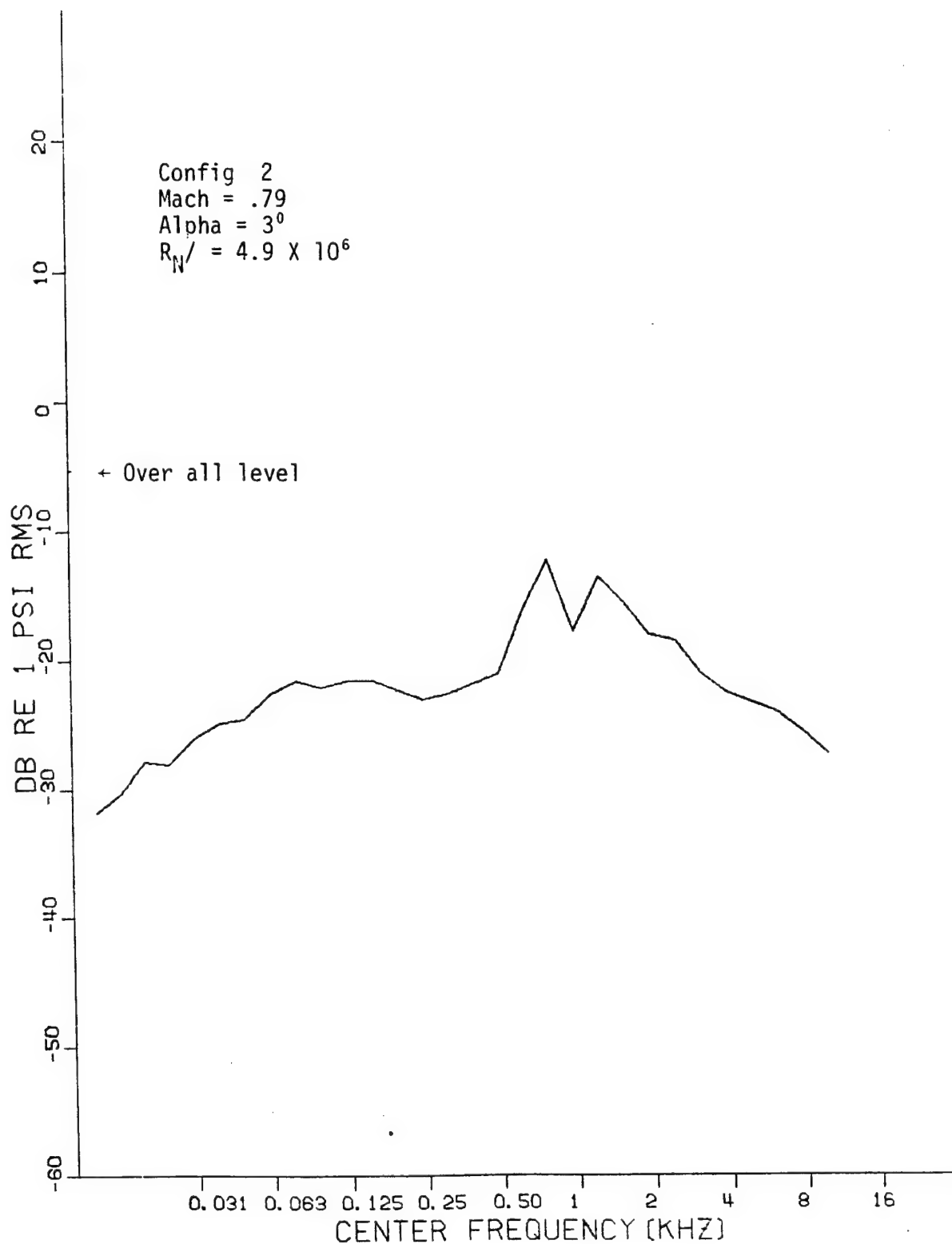


FIGURE 45. ONE THIRD OCTAVE BAND SPECTRA
FROM TEST POINT NR 109,
TRANSDUCER NR 6, $X/L = .55$.

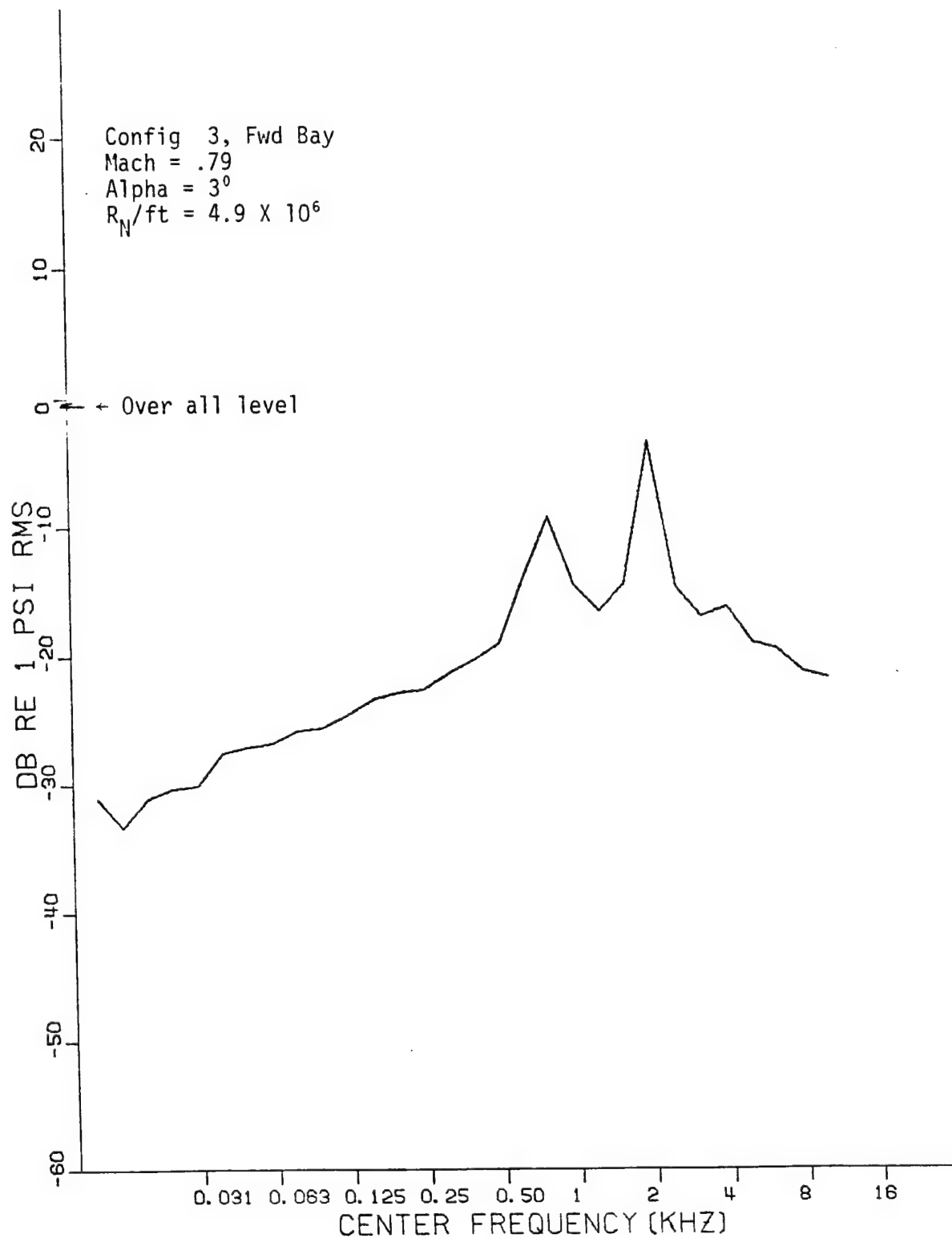


FIGURE 46a. ONE THIRD OCTAVE BAND SPECTRA
FROM TEST POINT NR 140,
TRANSDUCER NR 5, $X/L = .45$.

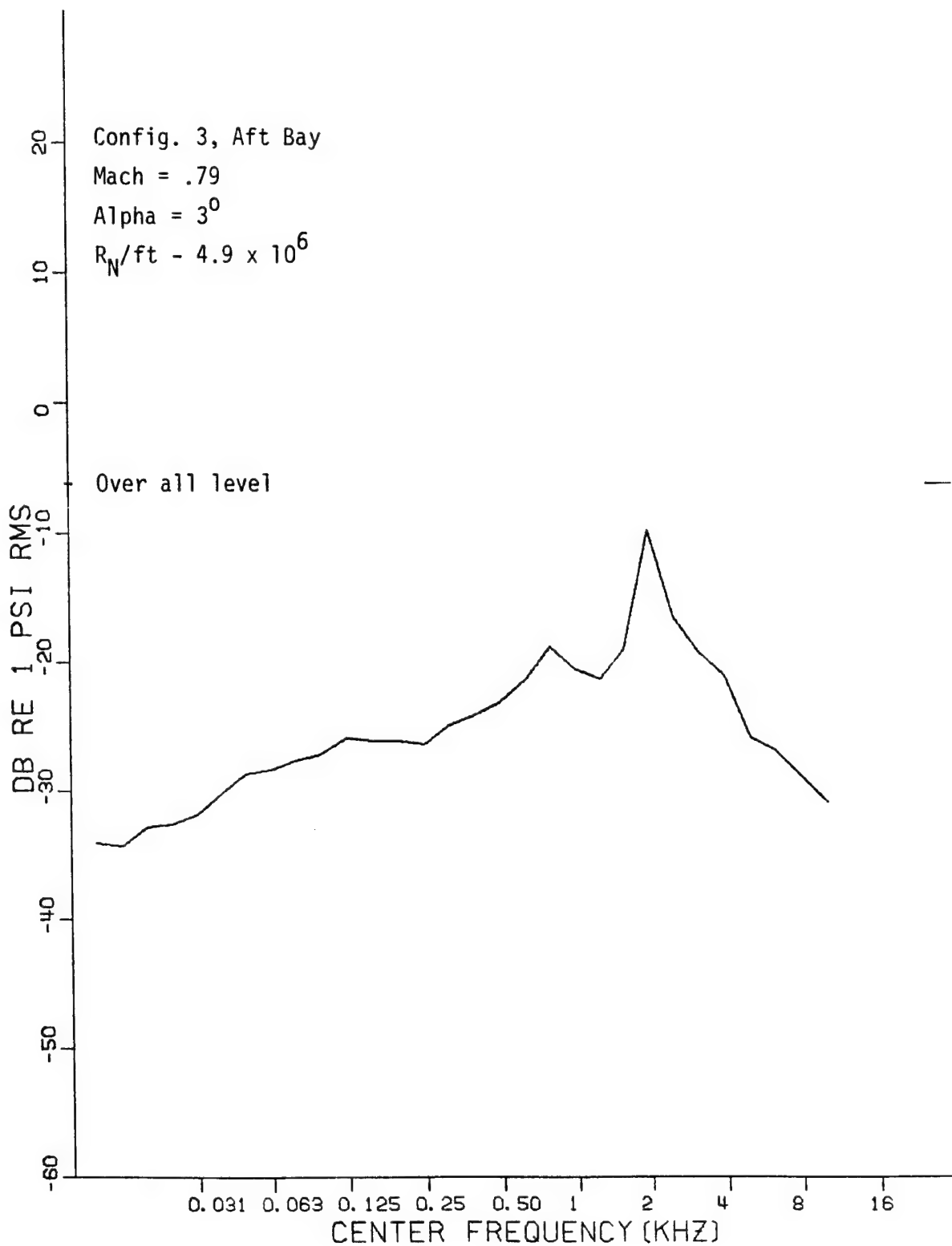


FIGURE 46b. ONE THIRD OCTAVE BAND SPECTRA
FROM TEST POINT NR 140,
TRANSDUCER NR 39, $x/L = .55$

Sym	Config	X/L	Bay	Fence
○	1	.45	Empty	None
□	1	.55	Empty	None

Alpha = 3°

Reynold's Number = 5 X 10⁶/Ft

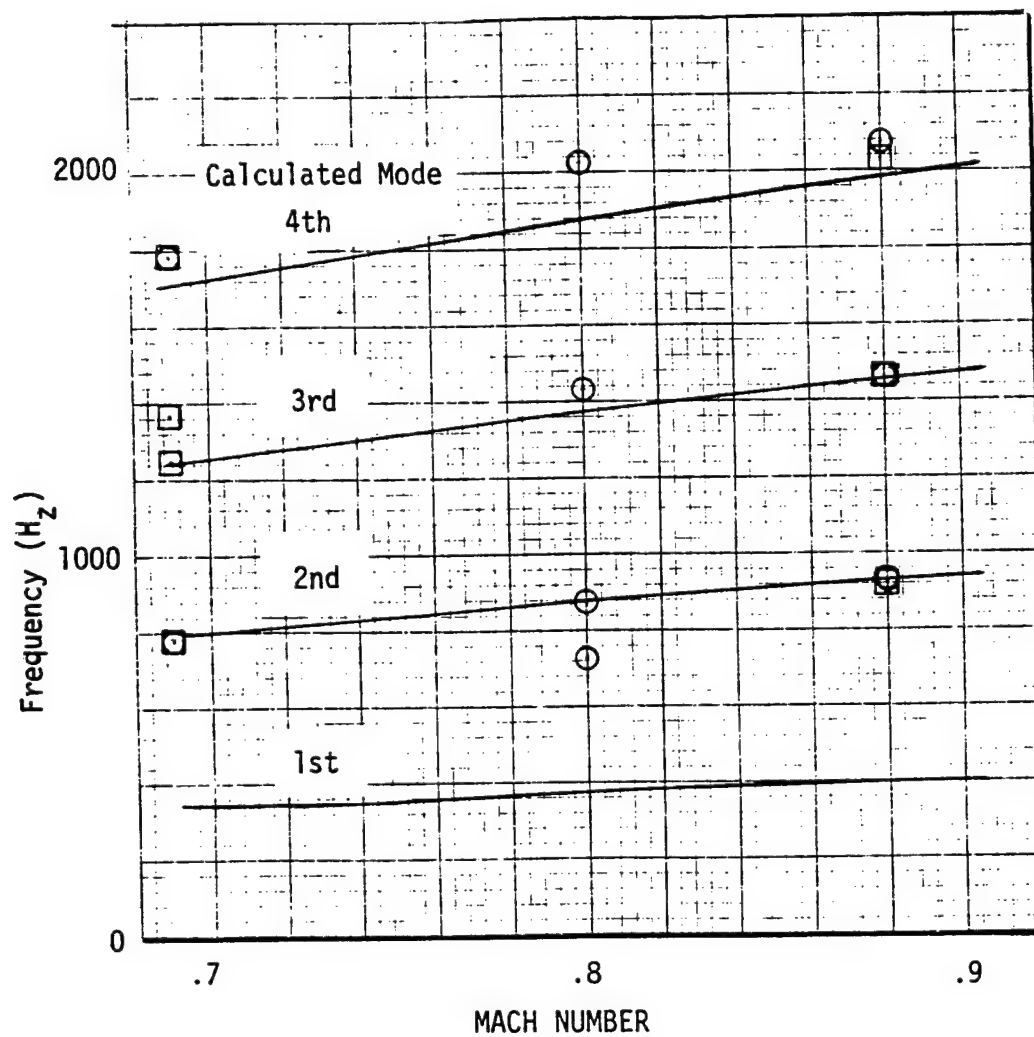


Figure 47a. Cavity Resonant Modes, Comparison of Calculated with Experimental Results

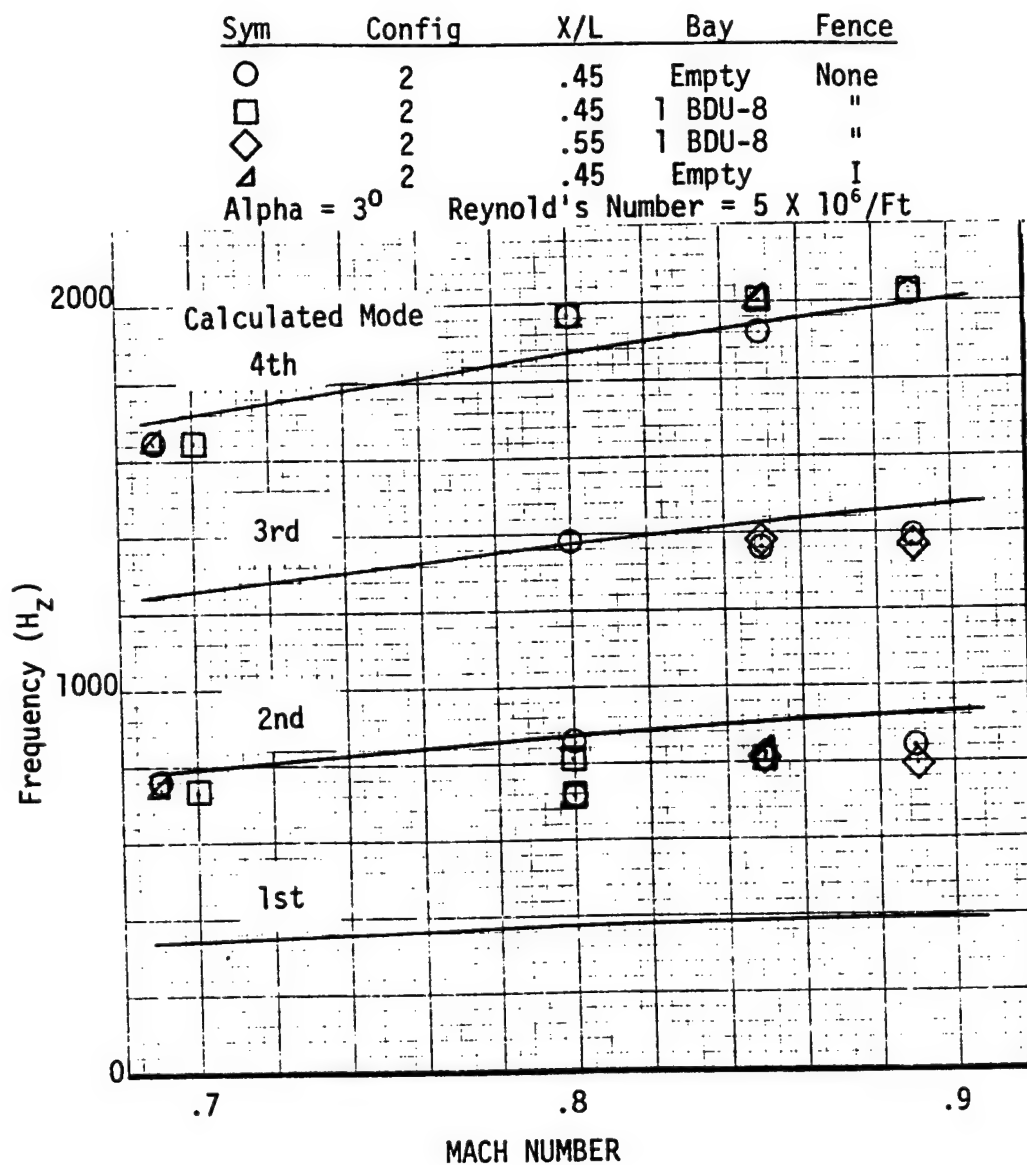


Figure 47b. Cavity Resonant Modes, Comparison of Calculated with Experimental Results

Sym	Config	Xducer Location	Fwd	Aft Bay
○	3	Rear of Fwd Bay	Empty	Empty
△	3	Rear of Aft Bay	Empty	Empty
□	3	Rear of Fwd Bay	Store L	Empty
◇	3	Rear of Aft Bay	Store L	Empty

Alpha = 3° Reynold's Number = 5 X 10⁶/Ft

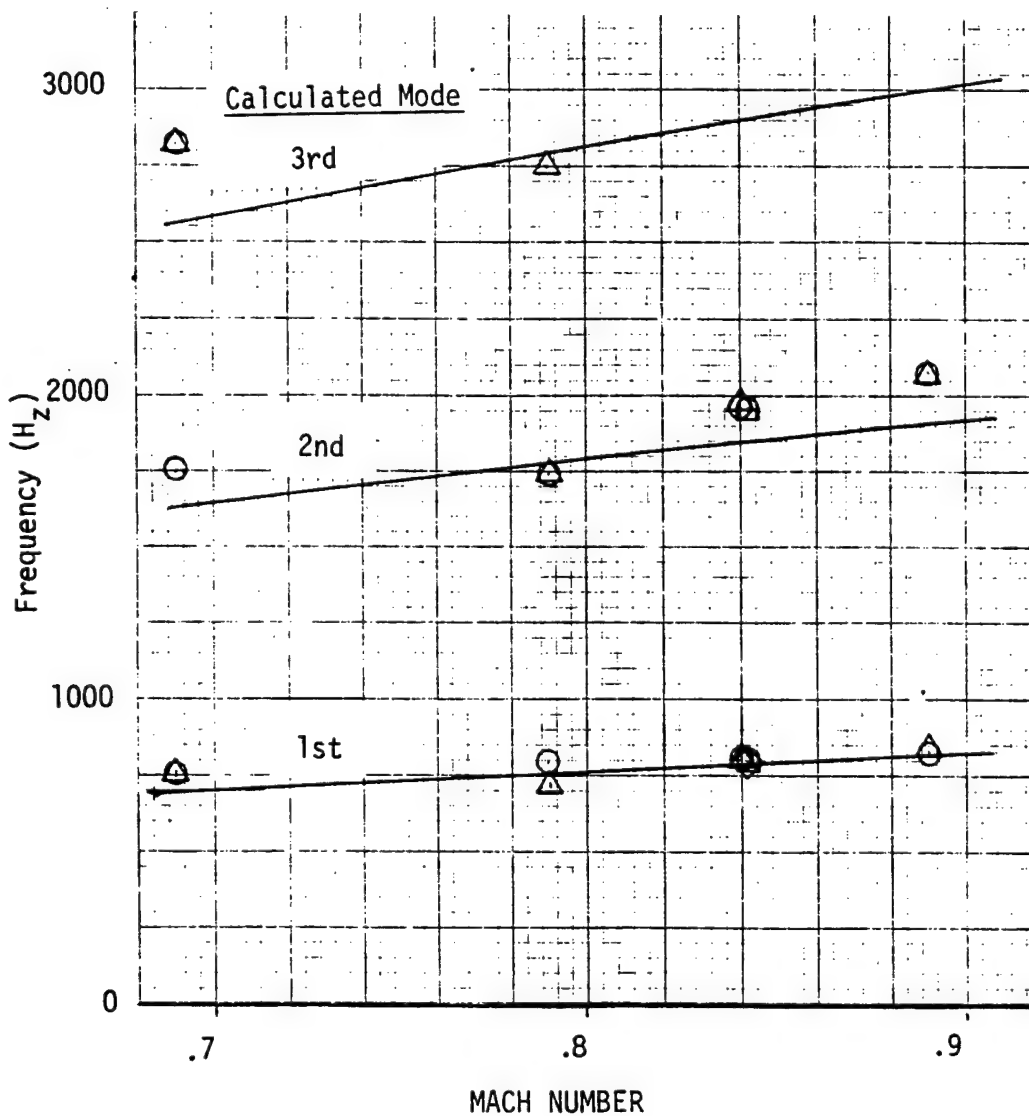


Figure 47c. Cavity Resonant Modes (Tandem Bays), Comparison of Calculated with Experimental Results

IV CONCLUSIONS

1. The effect of angle of attack on cavity turbulence level over the range of 0 to 6 degrees is not significant for shallow cavities ($L/D > 5$); however, a significant angle of attack effect was observed in the forward bay of Configuration 3 with an L/D of 2.7.

2. Over the Mach number range of .7 to .9, Mach number produces only a minor effect on turbulence level of the weapons bay configurations investigated.

3. No significant changes are observed in the turbulence levels between Reynolds numbers of 3 and 5 million/ft.

4. Turbulence levels are significantly reduced by rounding the aft cavity lip.

5. Installation of a turbulence reduction fence at the leading edge of the weapons bay is the most effective single turbulence reduction technique; however, the combination of rounded aft lip plus fence produced a further reduction in turbulence level.

6. Comparison of Configurations 1 and 2 turbulence levels indicates that bay geometry; L/D , width distribution and roof slope from front to back have significant effects on turbulence level; however, the isolated effect of each of these features can not be determined from the available data.

7. Good agreement between measured frequency modes and those calculated using the Rossiter equation is observed.

REFERENCES

1. Anderson, C.F., "Static and Fluctuating Pressures in the Weapons Bay of a 1/15 - Scale F-111F Model at Transonic Speeds", AEDC-TR-75-113, Arnold Engineering Development Center, AFSC, August 1975.
2. Rossiter, J. E., "Wind Tunnel Experiments on the Flow Over Rectangular Cavities at Subsonic and Transonic Speeds", RAE Rep Nr 64037, R&M Nr 3438, October 1964.
3. Heller, H. H., et al, "Flow-Induced Pressure Oscillations in Shallow Cavities", AFFDL-TR-70-104, Bolt, Beranek and Newman, Inc. December 1970.

APPENDIX

Static Pressure Data

Typical static pressure distributions are presented in the following figures. Only a limited analysis of this data has been attempted to date. No significant correlation is observed between turbulence level and the level of static pressure in the form of pressure coefficient.

No significant angle of attack, Mach number or Reynolds number effects are noted over the range of these variables investigated.

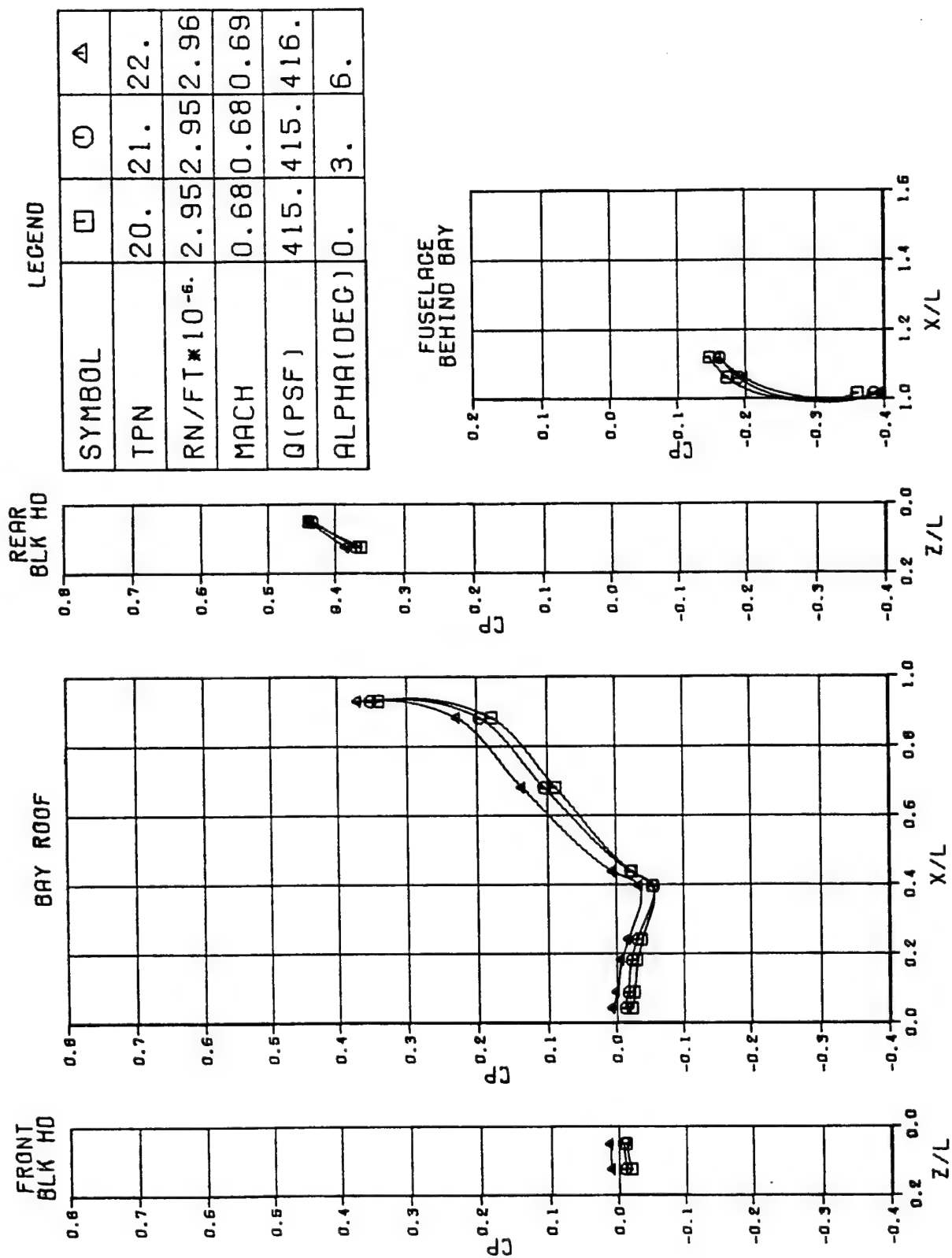


Figure 1A. Angle of Attack Effects on Static Pressure Distribution, Configuration 1.

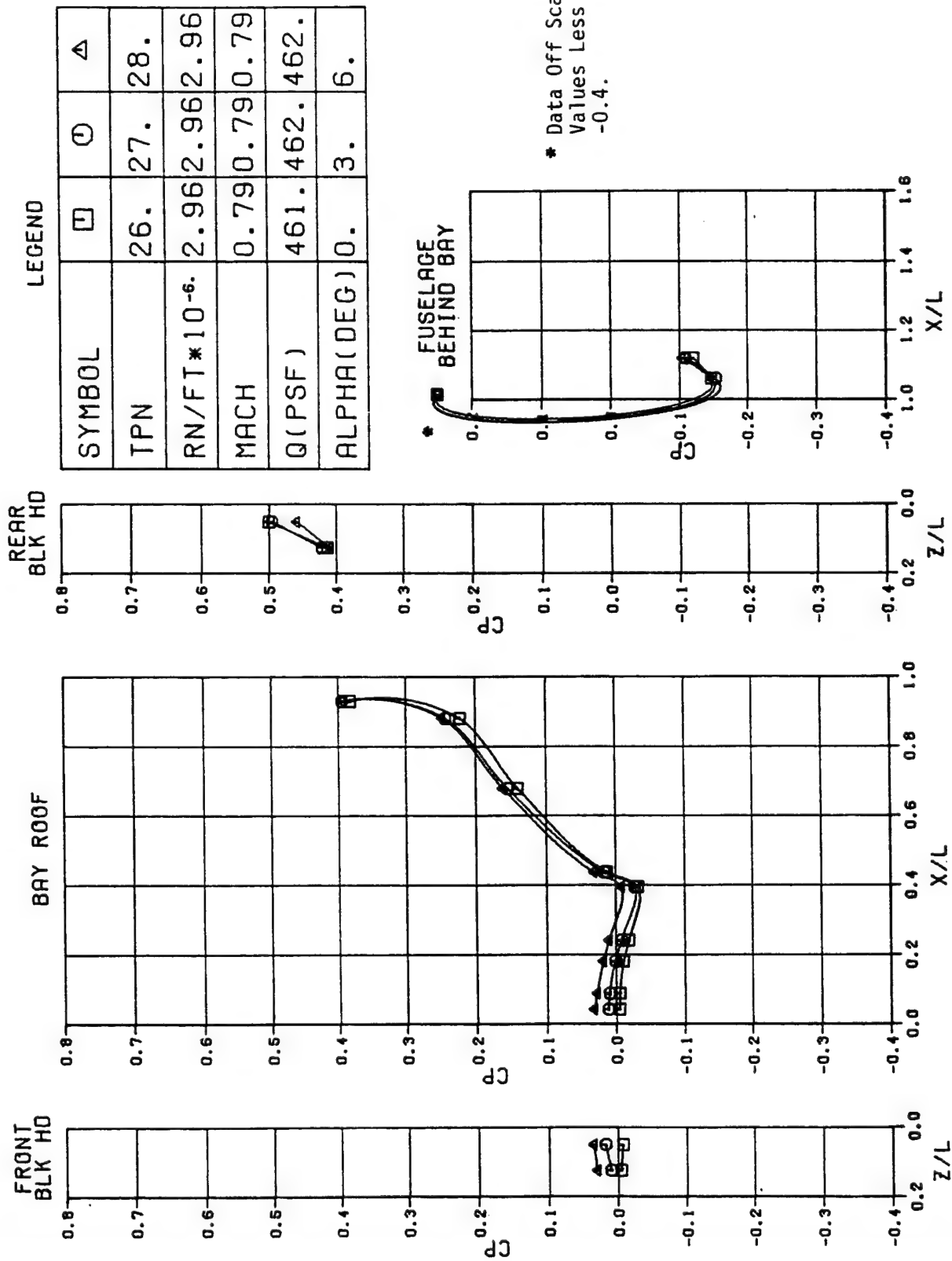


Figure 2A. Angle of Attack Effects on Static Pressure Distribution, Configuration 1.

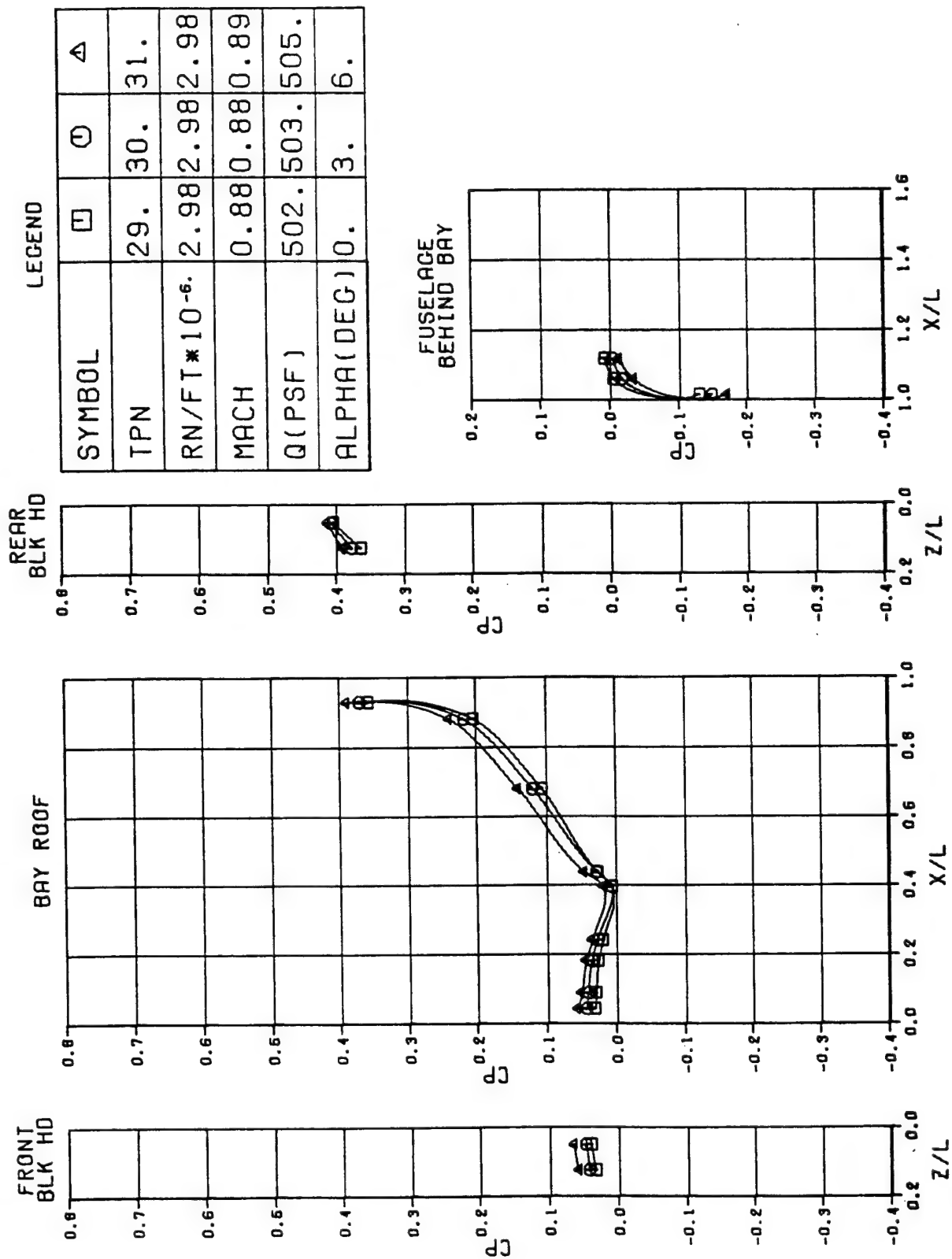


Figure 3A. Angle of Attack Effects on Static Pressure Distribution, Configuration 1.

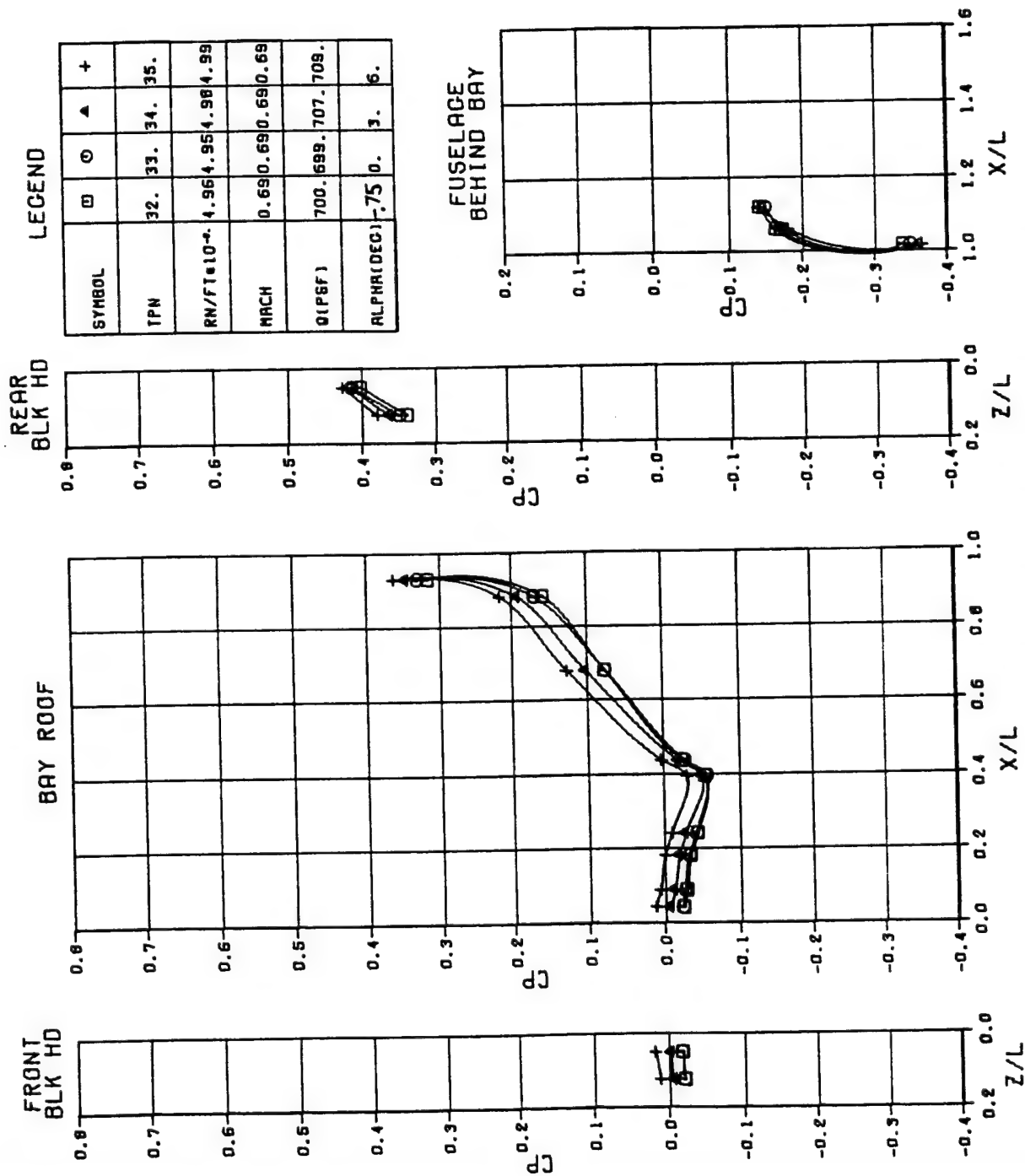


Figure 4A. Angle of Attack Effects on Static Pressure Distribution, Configuration 1.

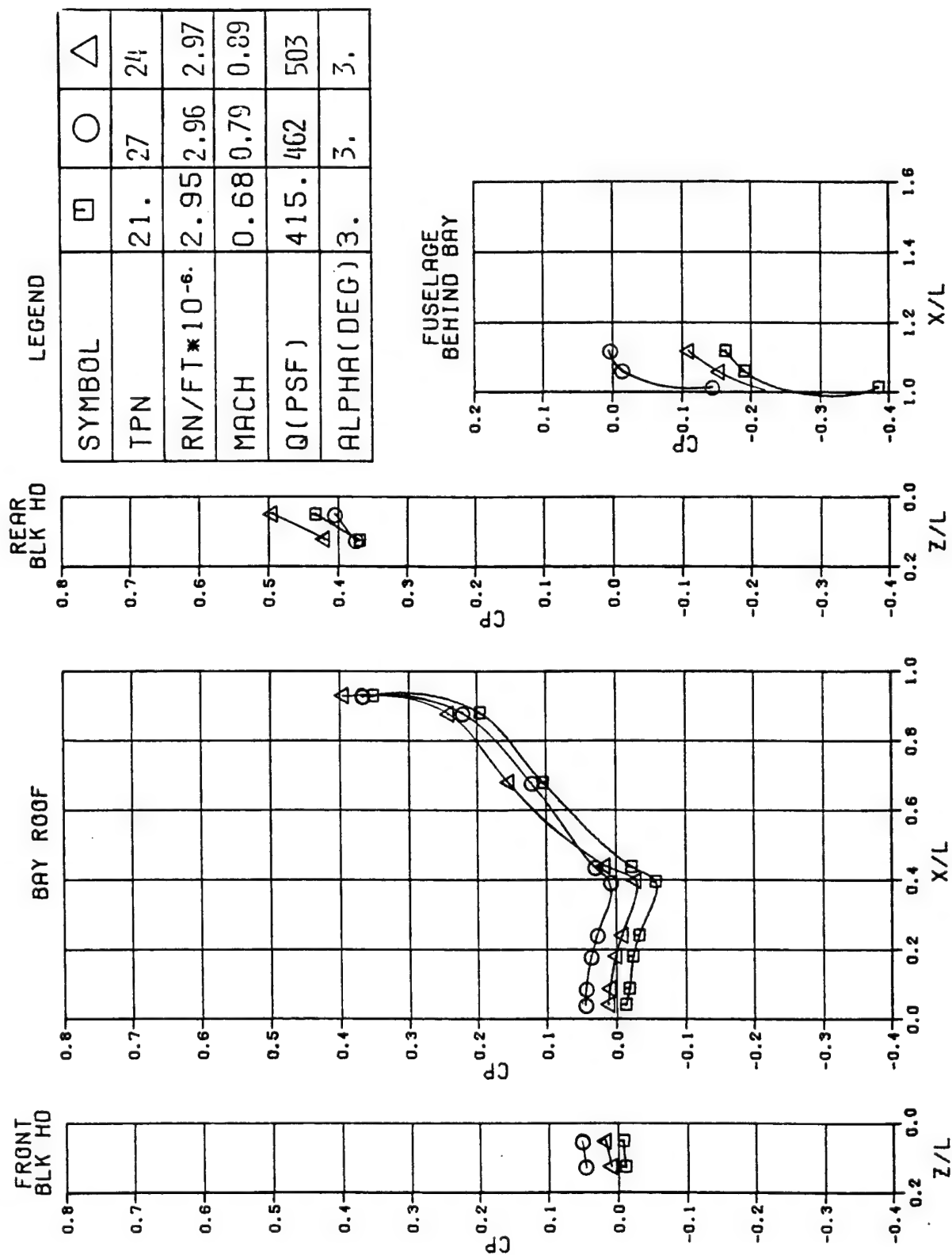


Figure 5A. Mach Effects on Static Pressure Distribution, Configuration 1.

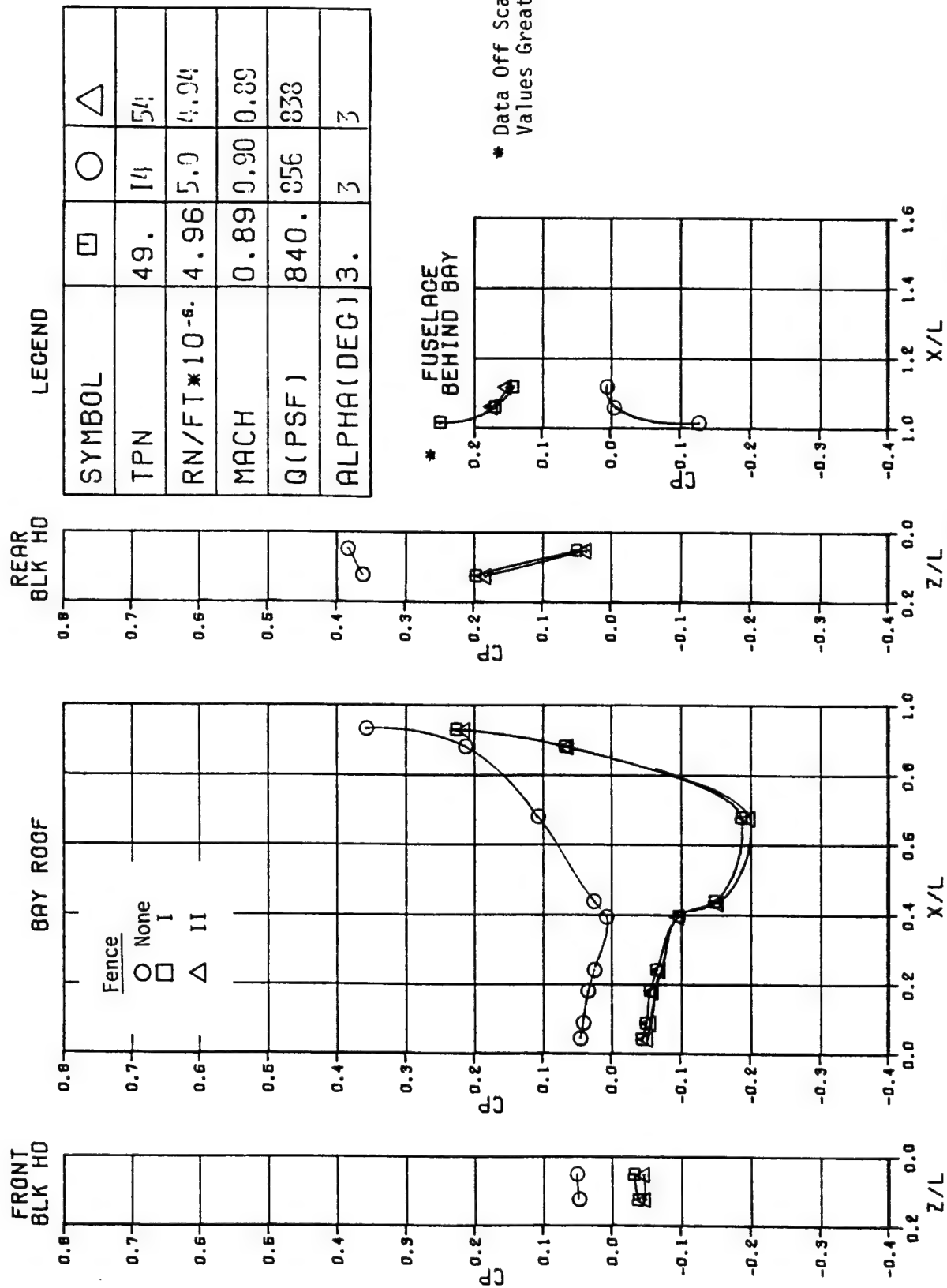


Figure 6A Effect of Fences on Static Pressure Distribution, Configuration 1.

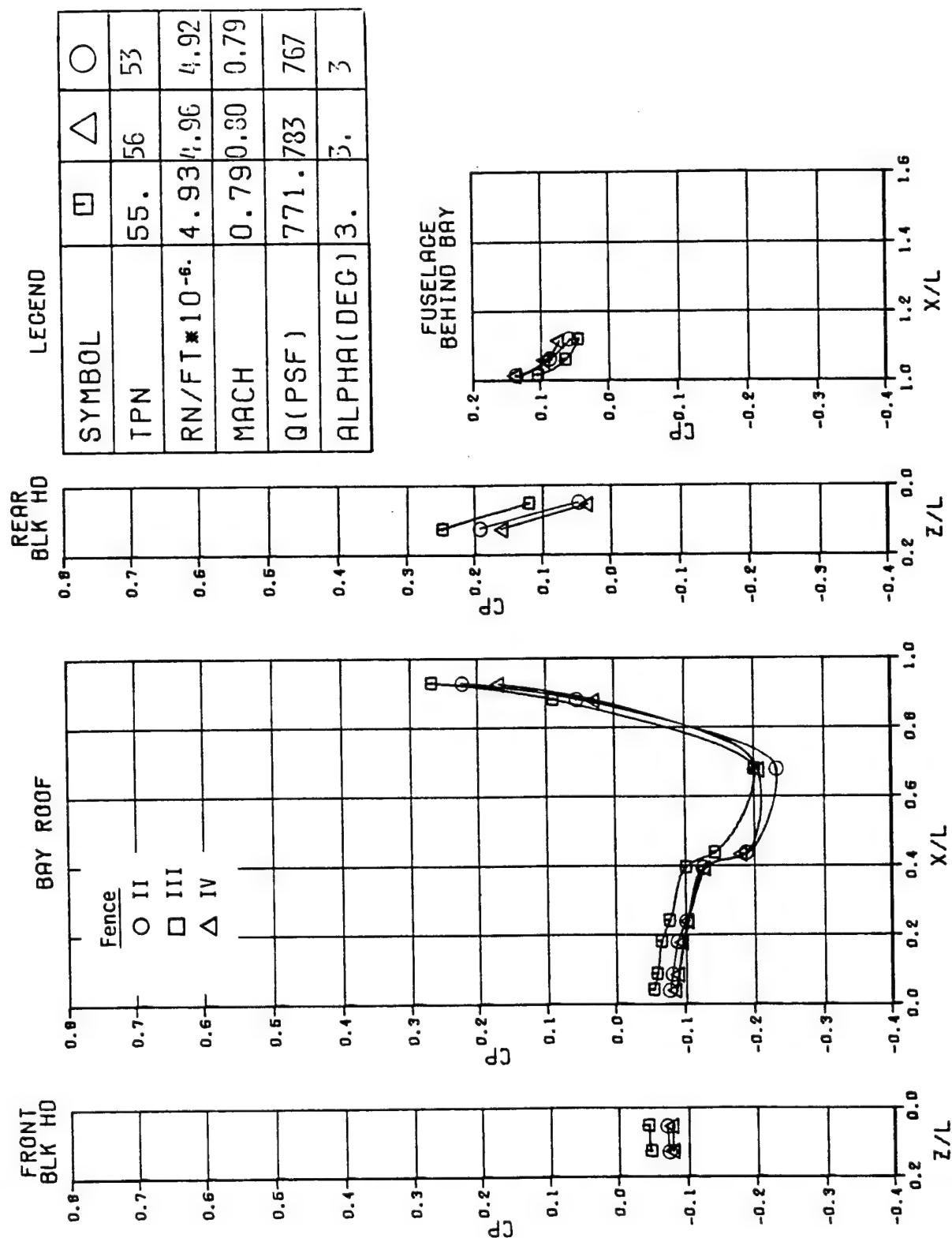


Figure 7A. Comparison of Fences II, III, and IV, Configuration 1.

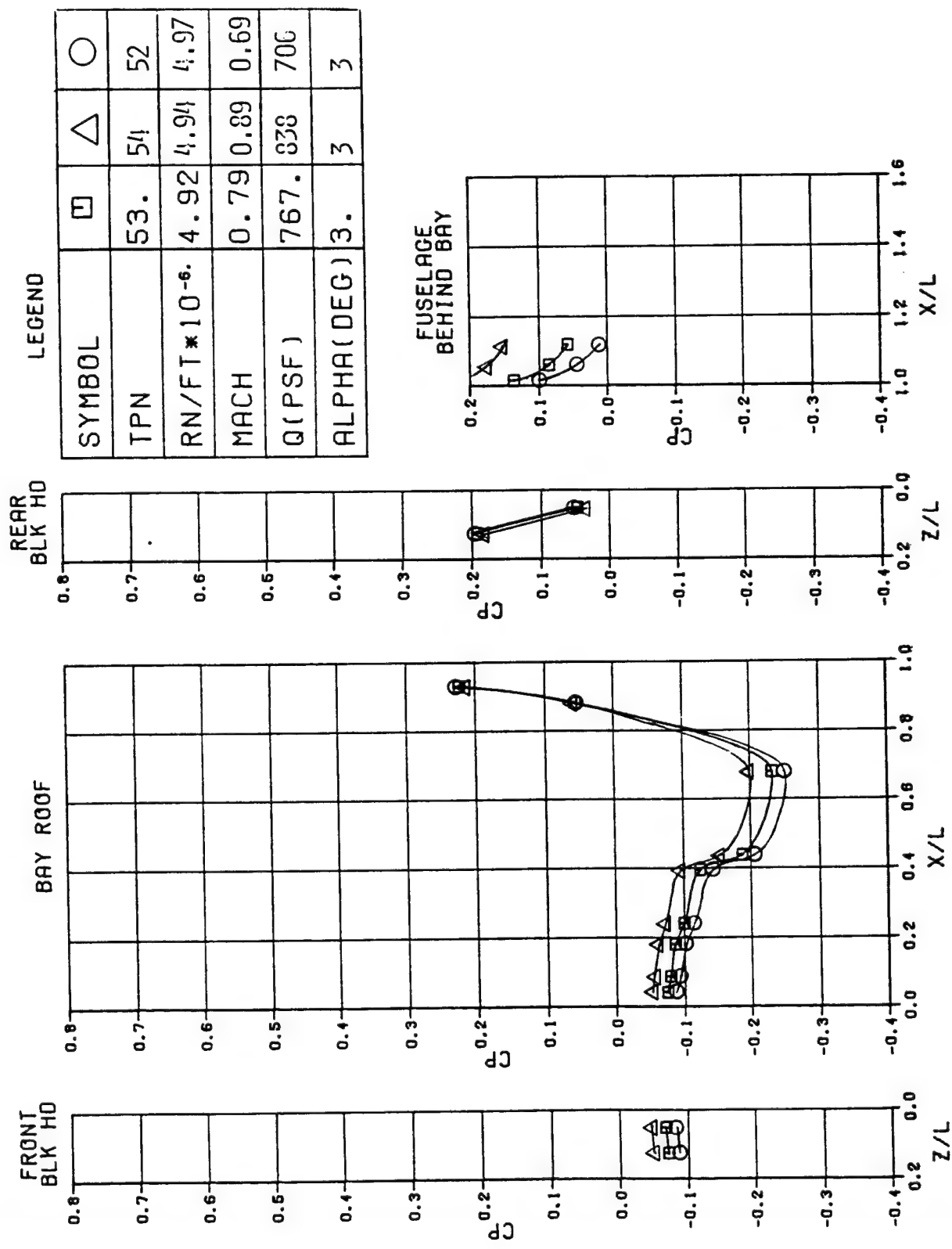


Figure 8A. Mach Effects on Static Pressure Distribution with Fence II installed at L. E. of Bay, Configuration 1.

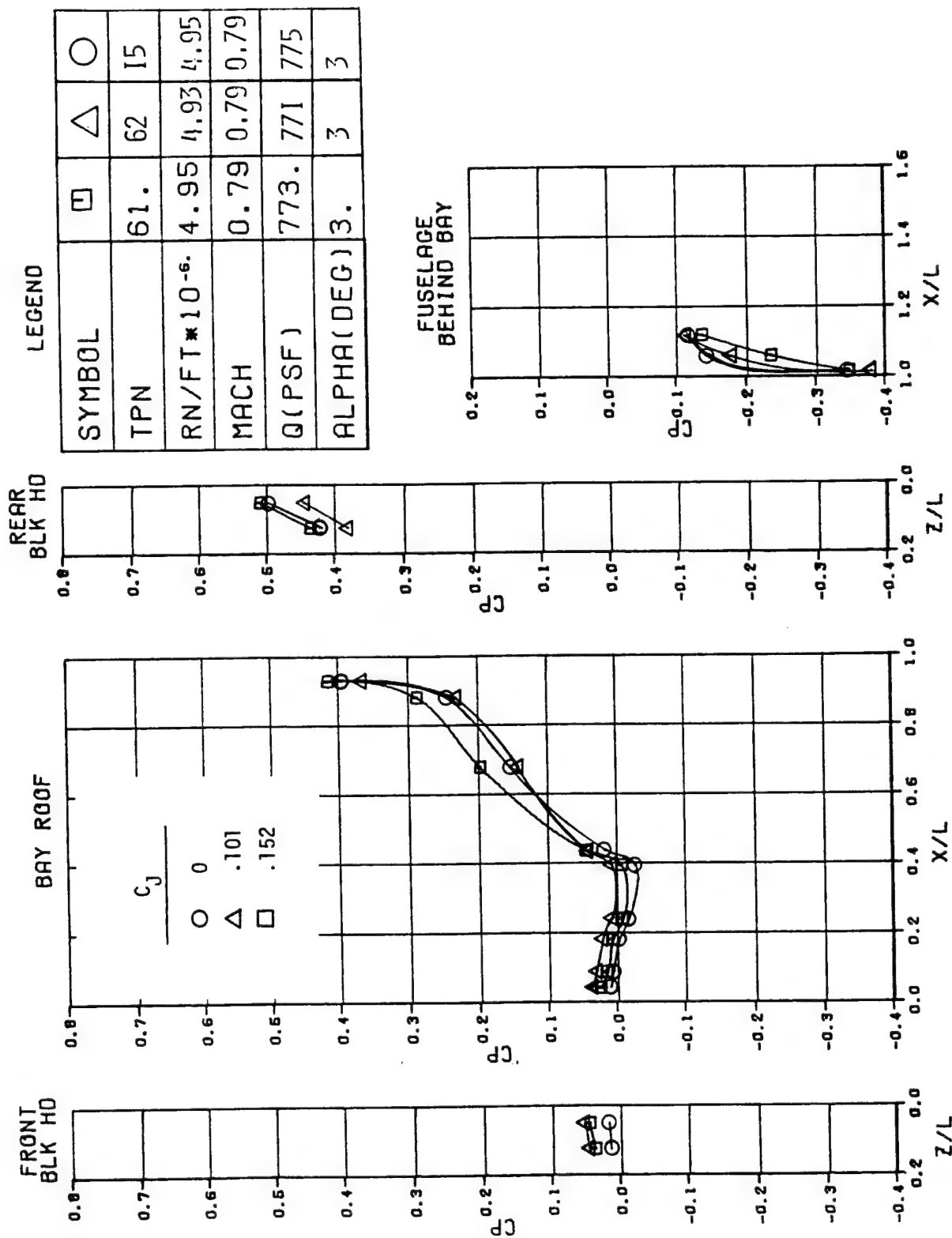


Figure 9A. Effect of Blowing at the Forward Lip on Static Pressure Distribution, Configuration 1.

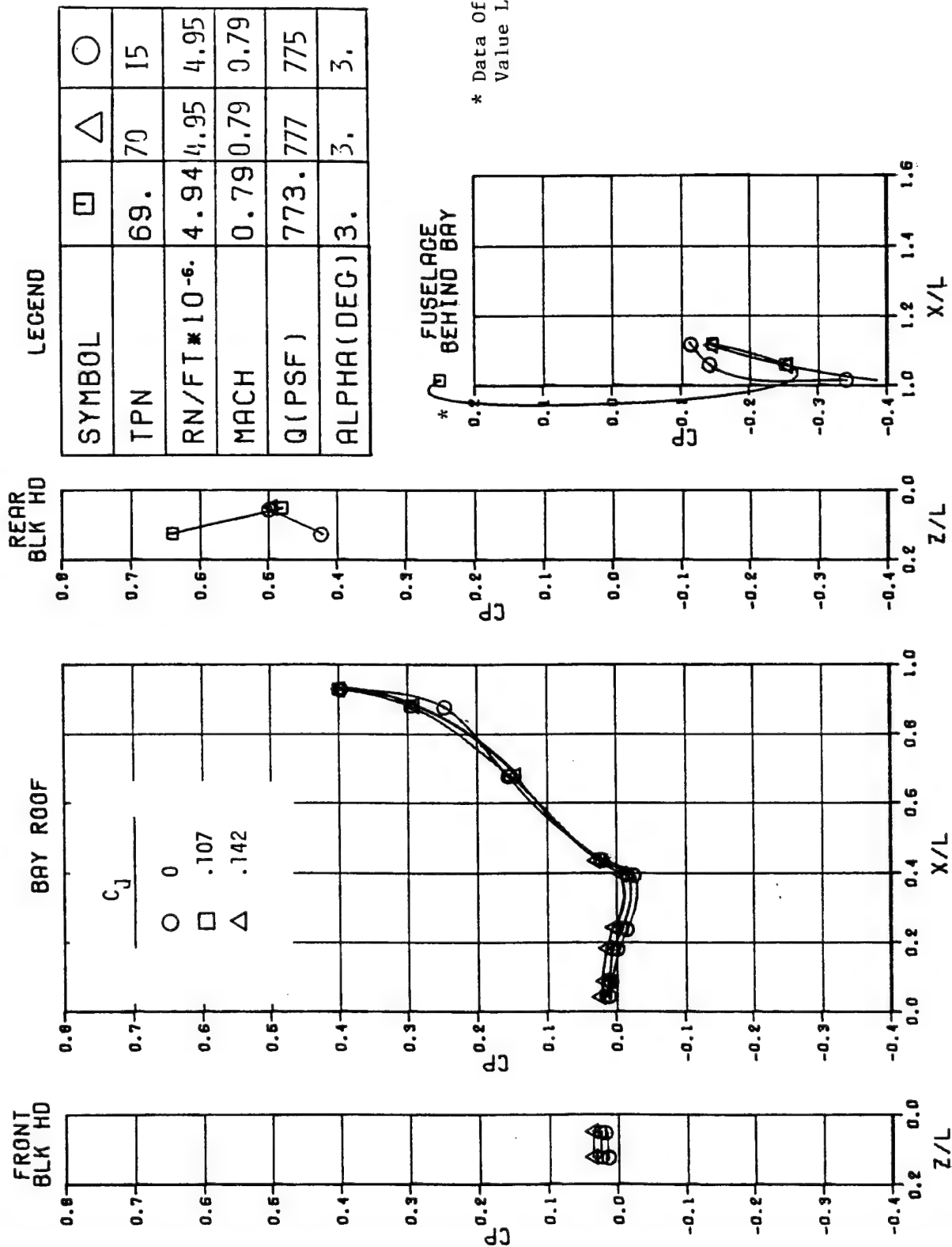


Figure 10A. Effect of Blowing over Aft Lip on Static Pressure Distribution, Configuration 1.

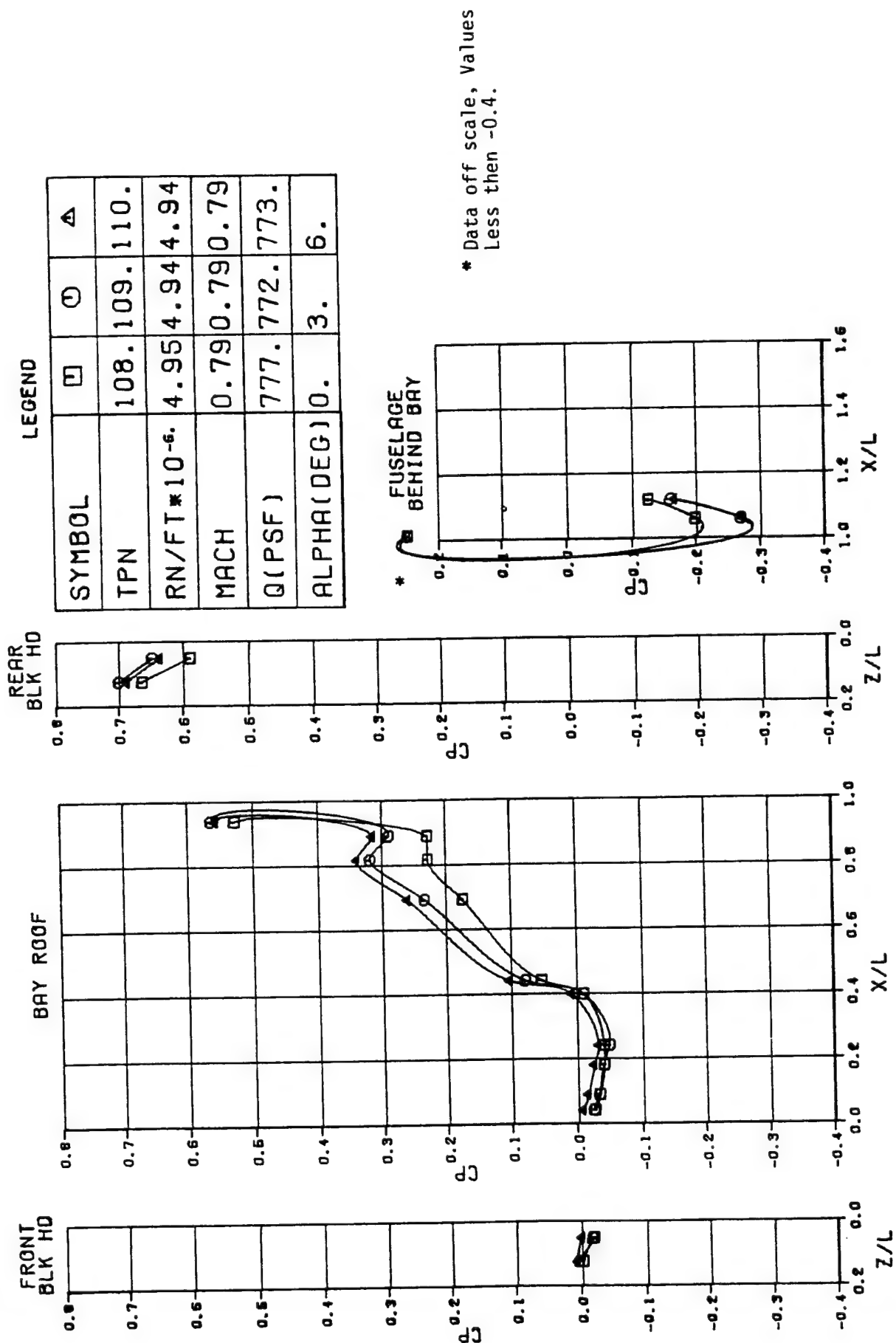


Figure 12A. Angle of Attack Effects on Static Pressure Distribution of Empty Bay, Configuration 2:

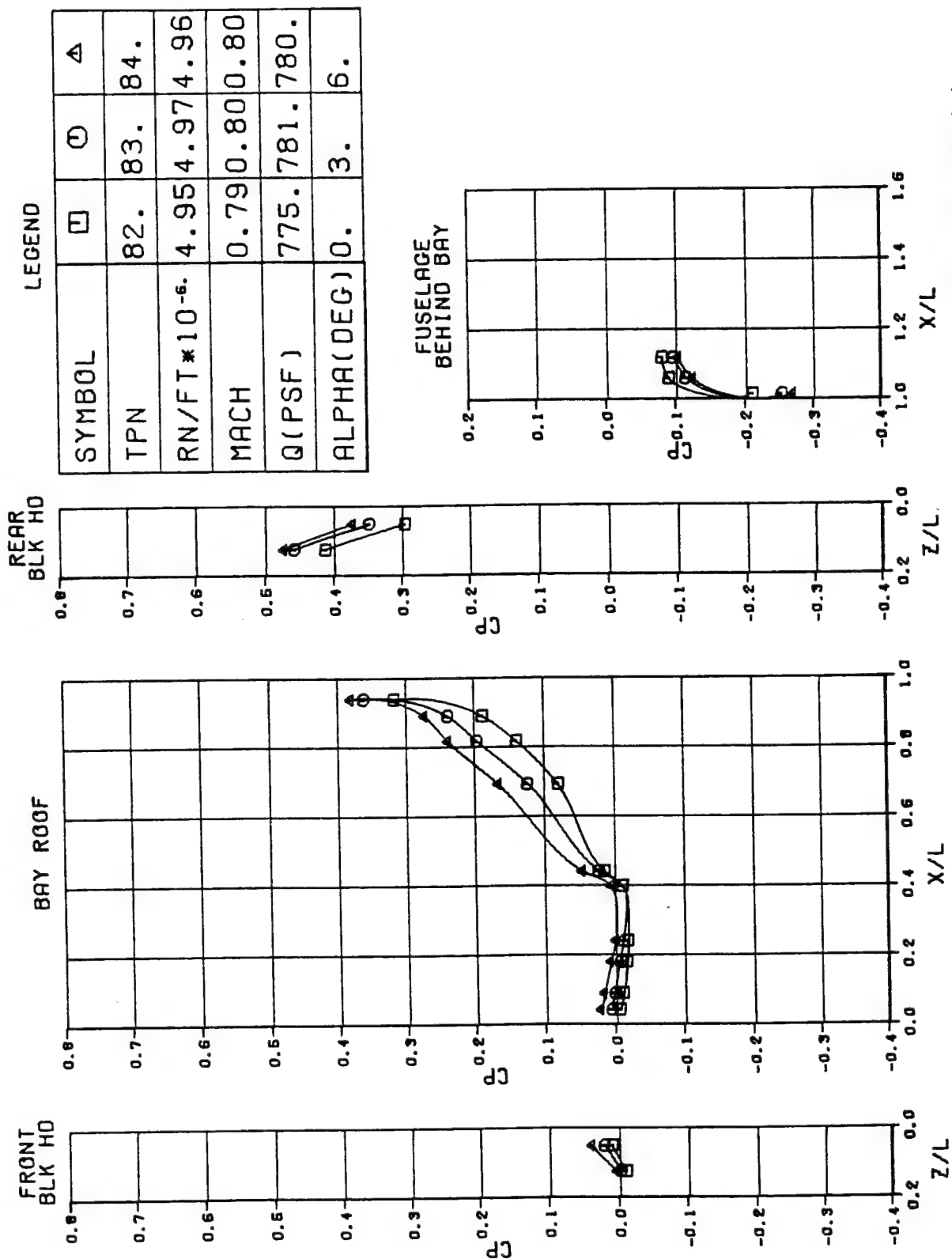


Figure 13A. Angle of Attack Effects on Static Pressure Distribution with Single BDU-8 in Bay, Configuration 2.

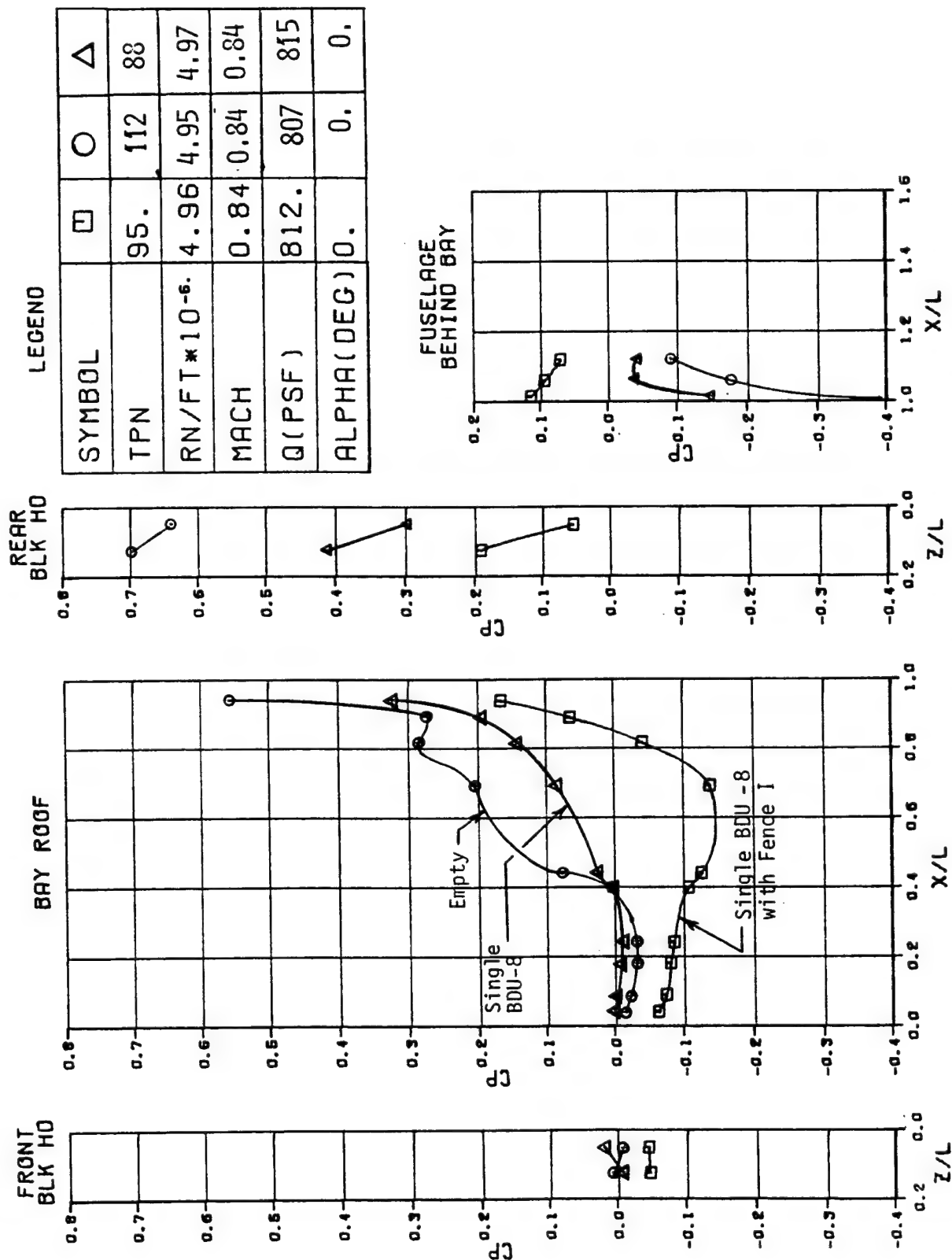


Figure 14A. Static Pressure Distribution, Configuration 2/BDU-8 with & without Fence I

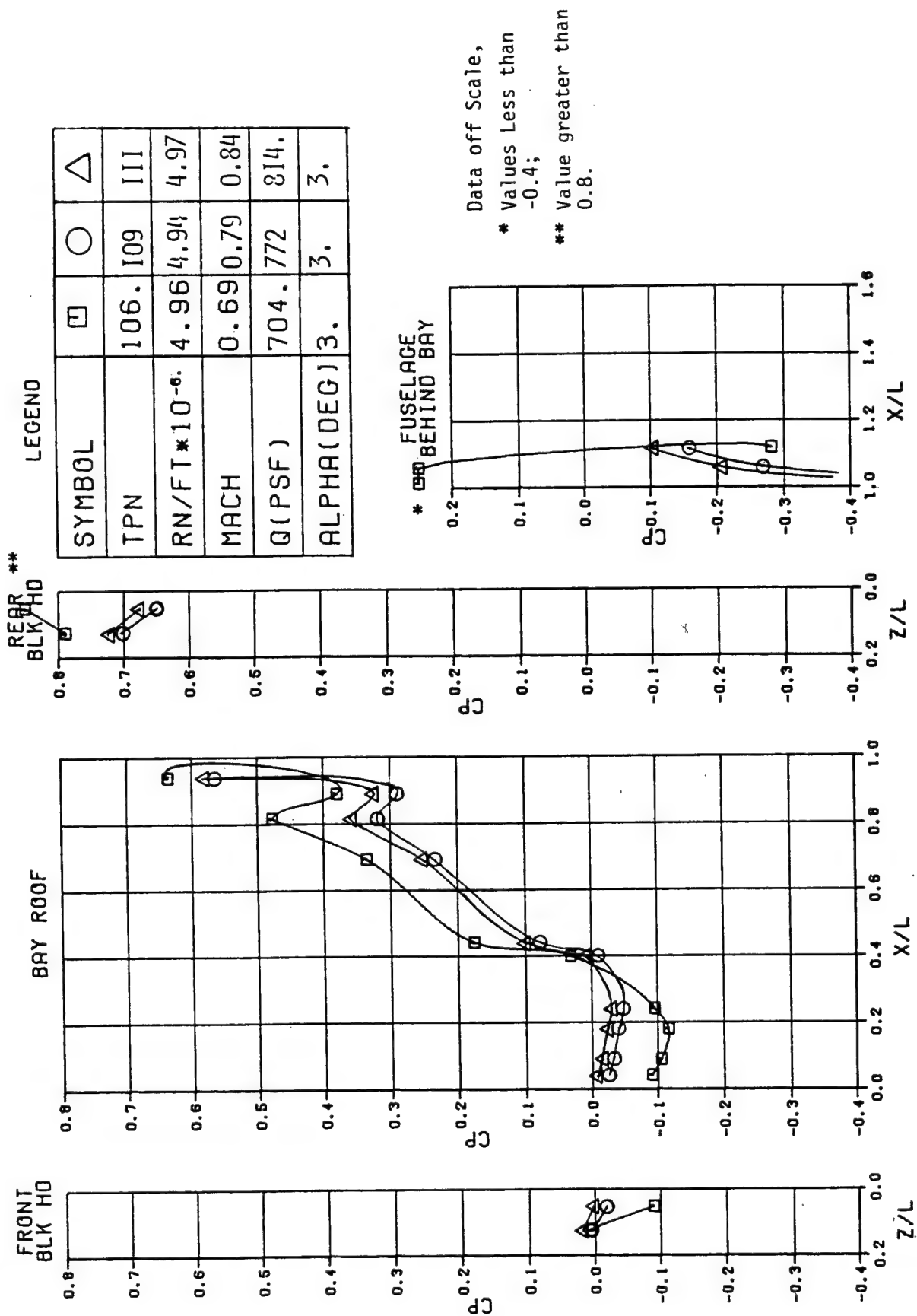


Figure 15A. Mach Effects on Static Pressure Distribution of Empty Bay, Configuration 2.

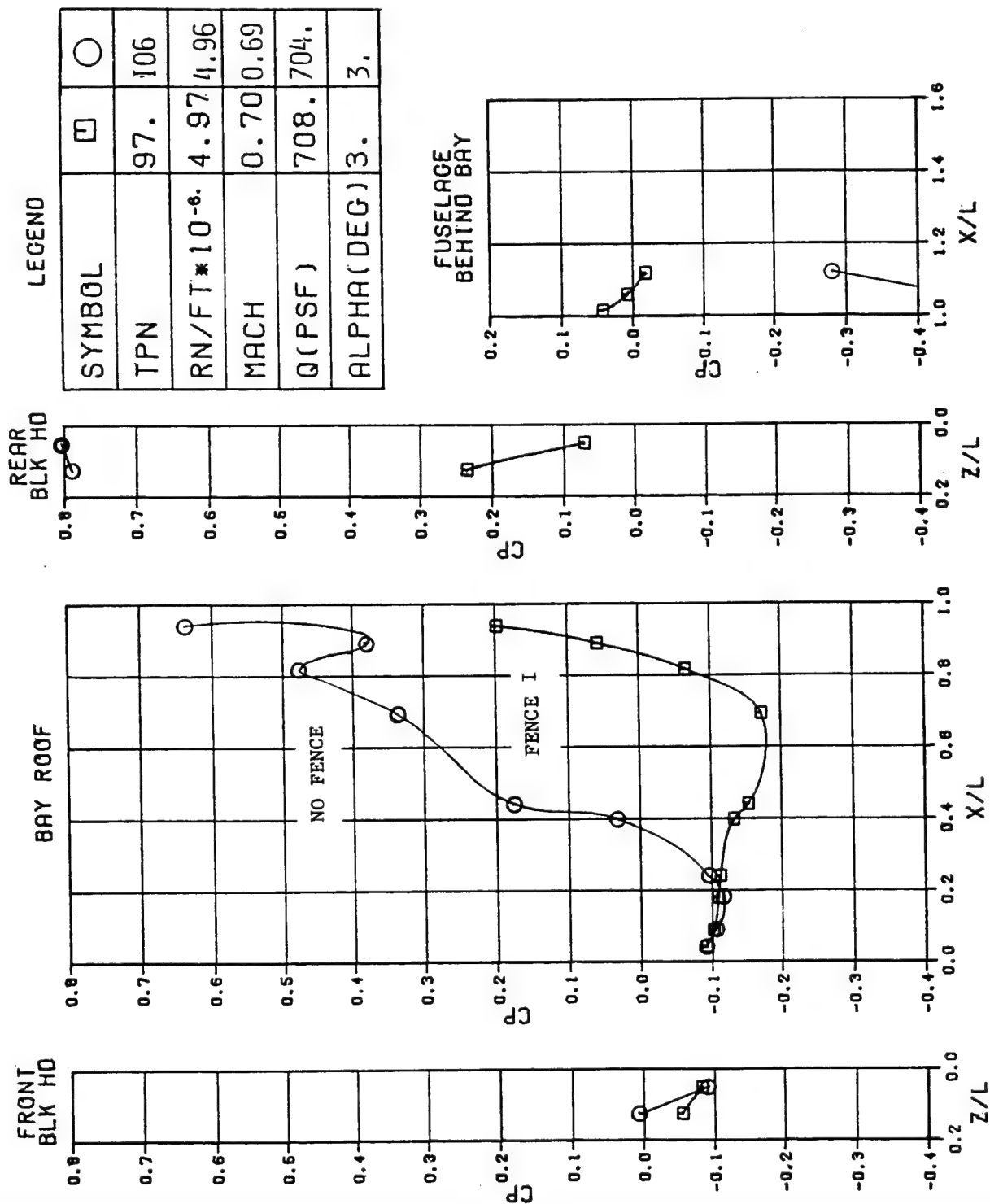


Figure 16A. Effect of Fence I on Static Pressure Distribution of Empty Bay, Configuration 2.

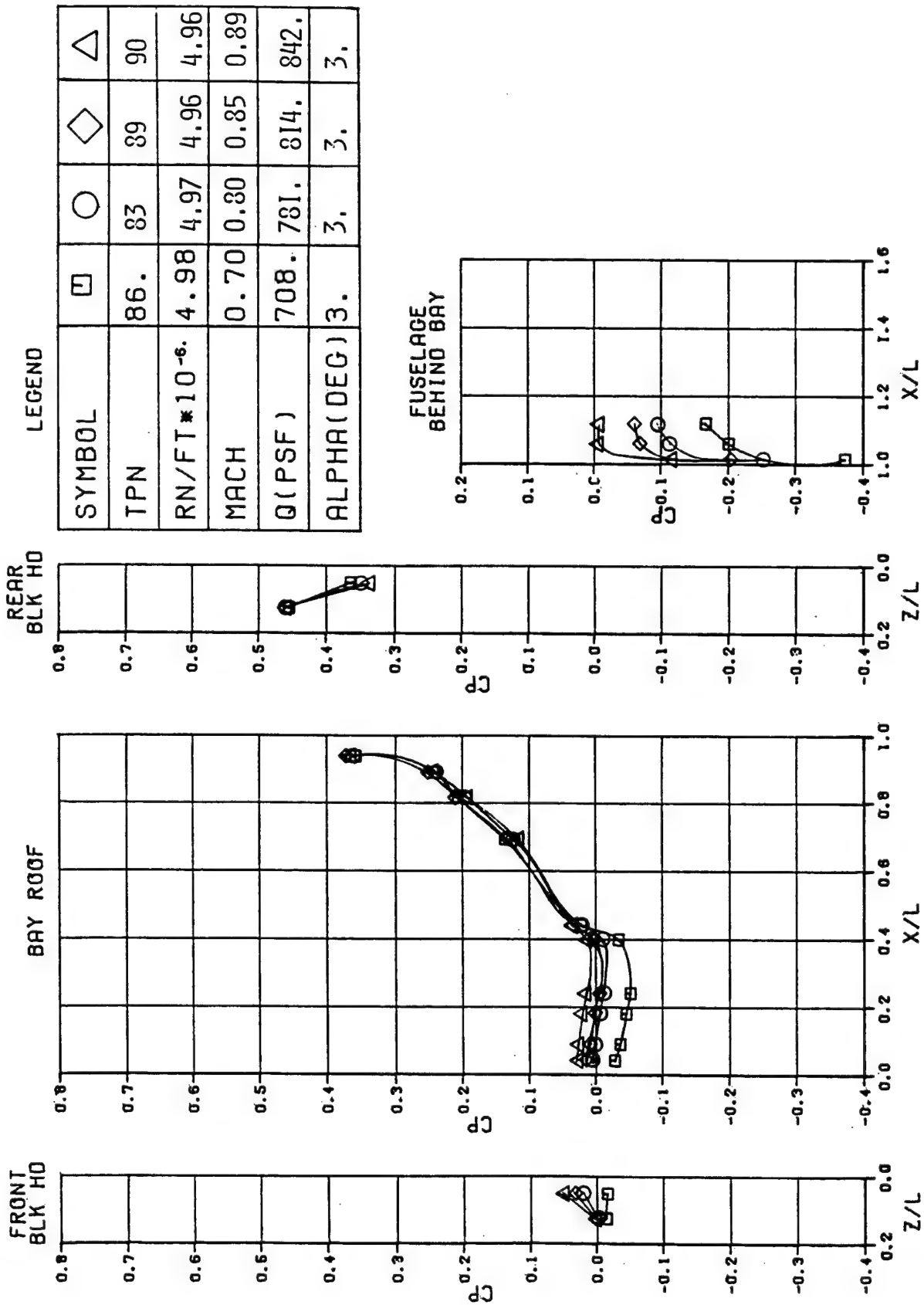
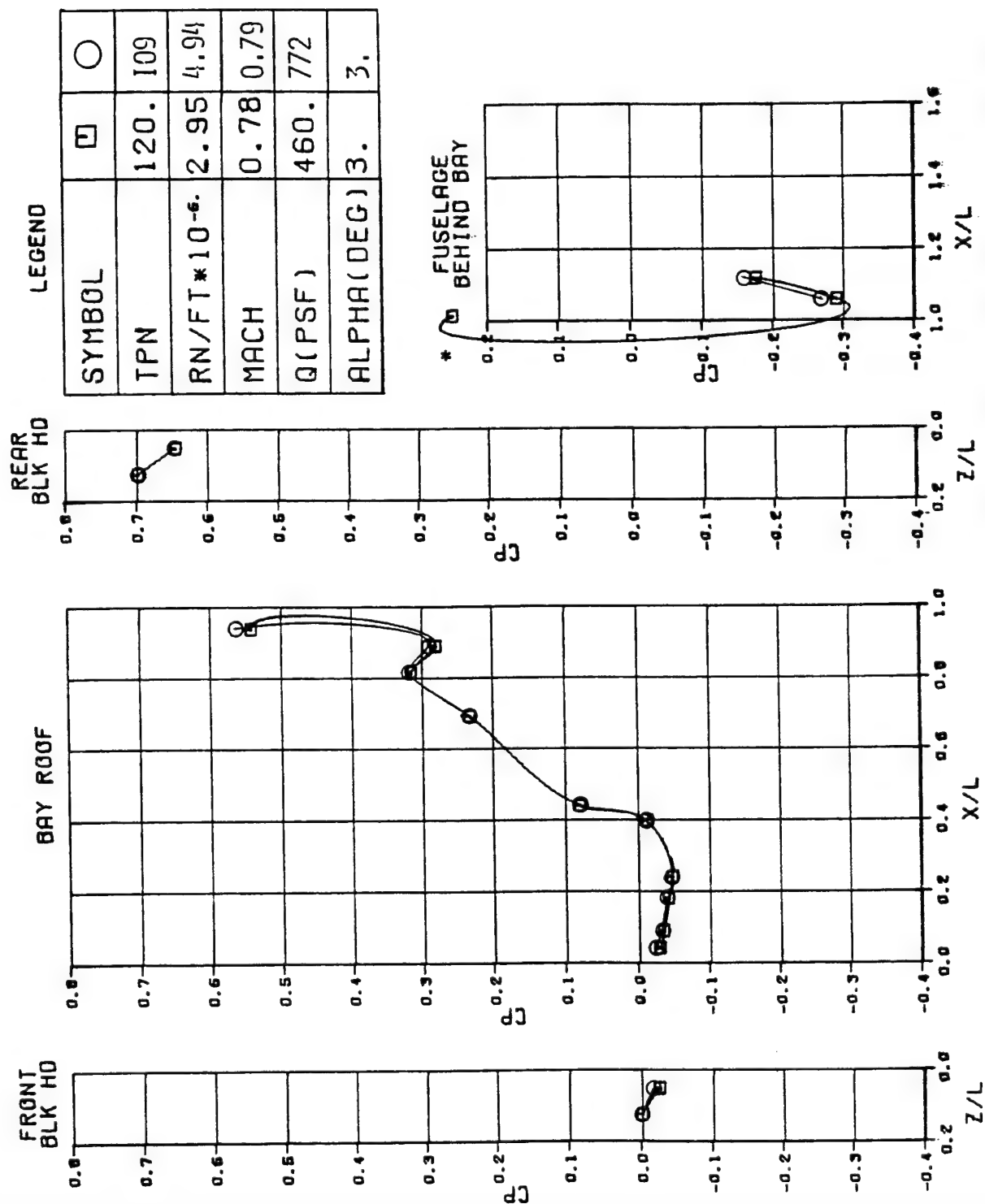
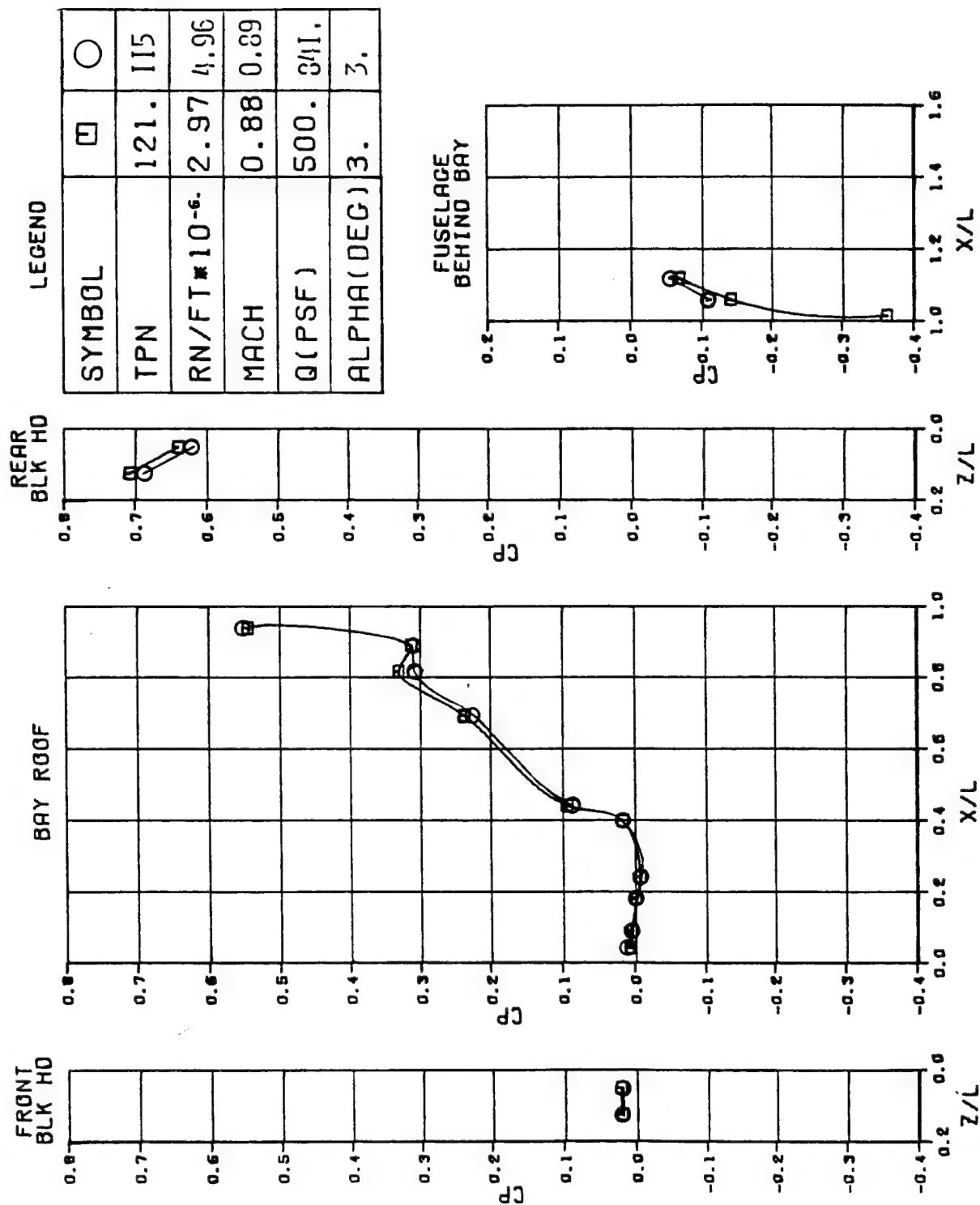


Figure 17A. Mach Effects on Static Pressure Distribution with Single BDU-8 in Bay, Configuration 2.





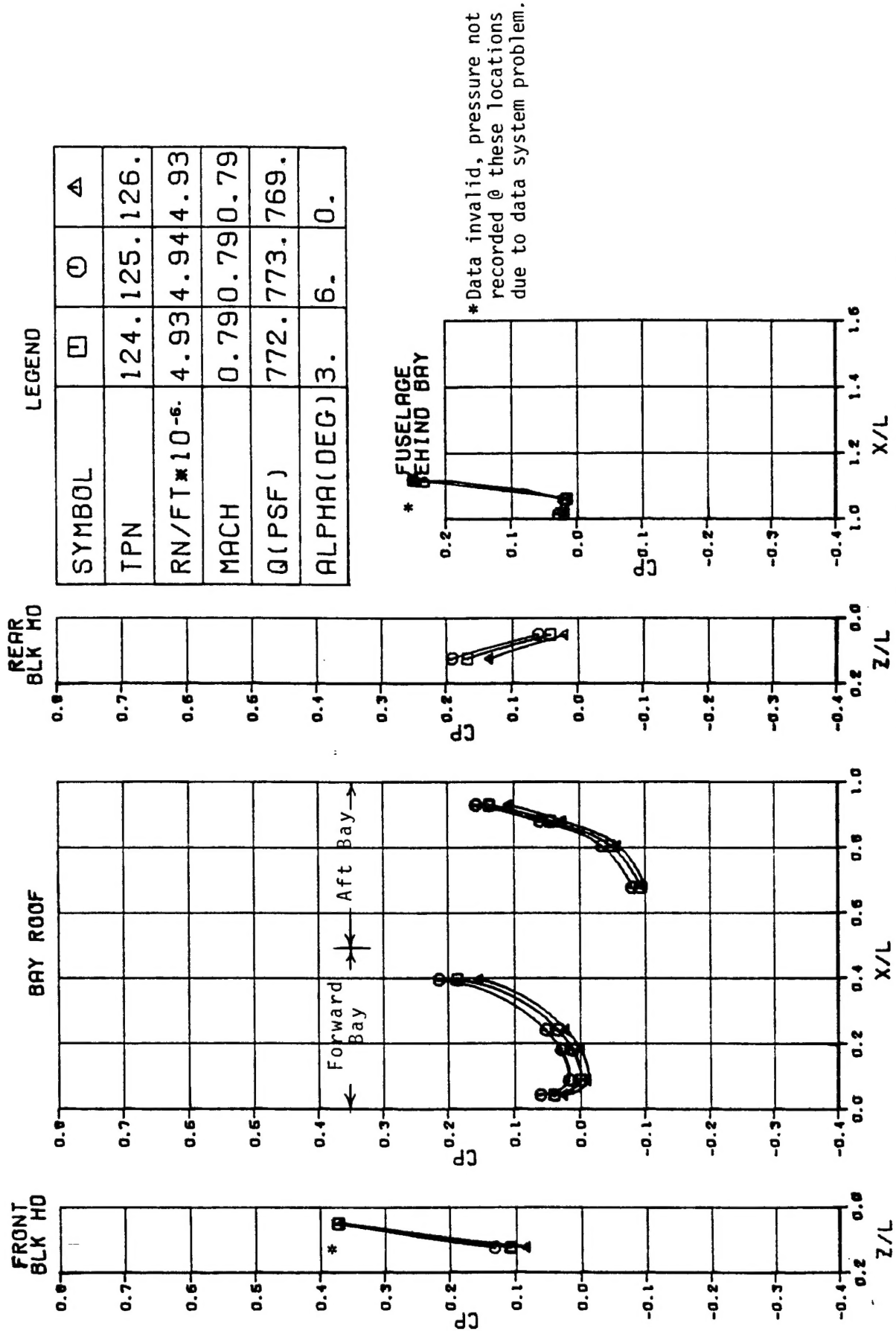


Figure 20A. Angle of Attack Effects on Static Pressure Distribution with Store L in Forward Bay, Configuration 3.

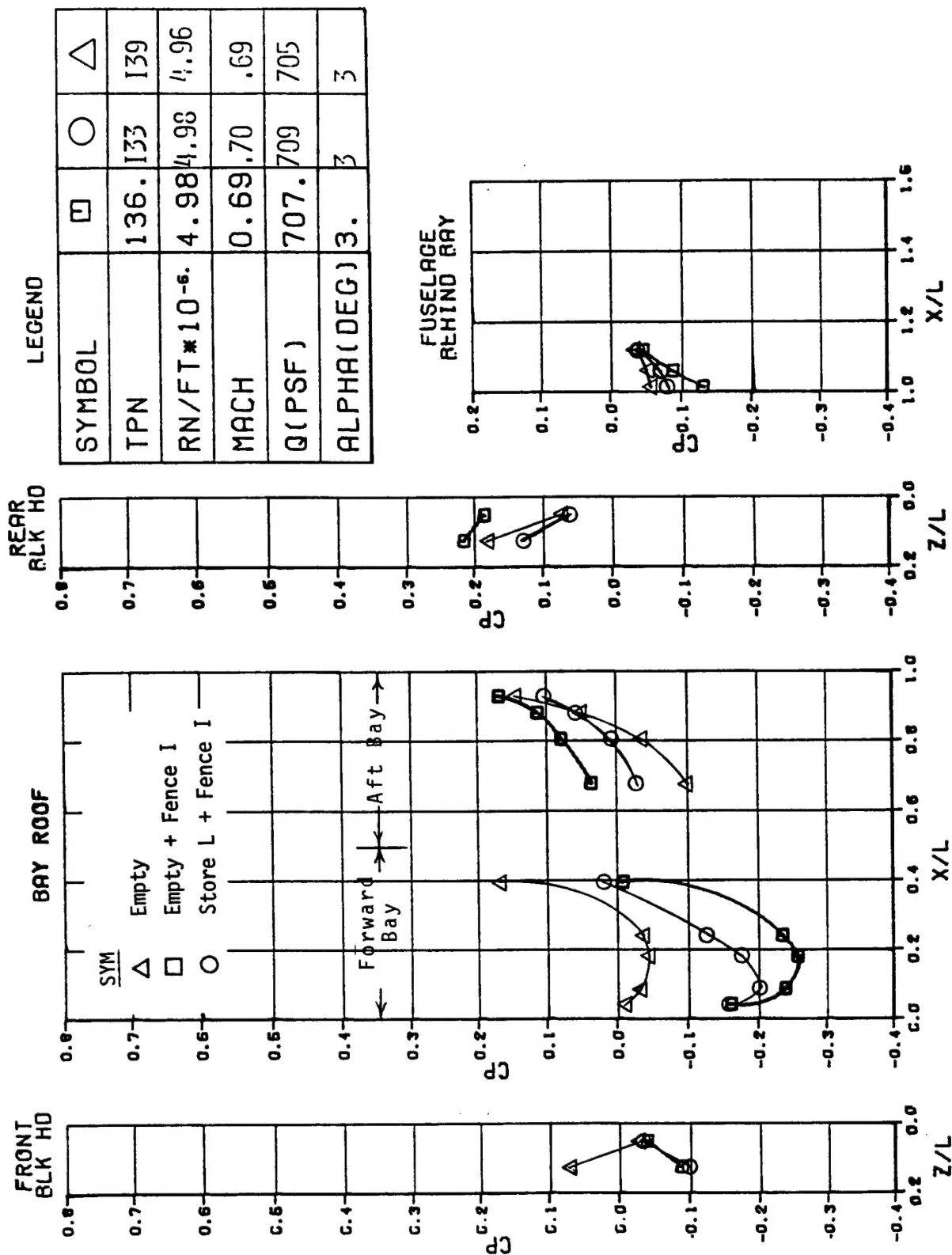


Figure 21A. Effect of Fence I on Configuration 3 with and without Store L in Forward Bay

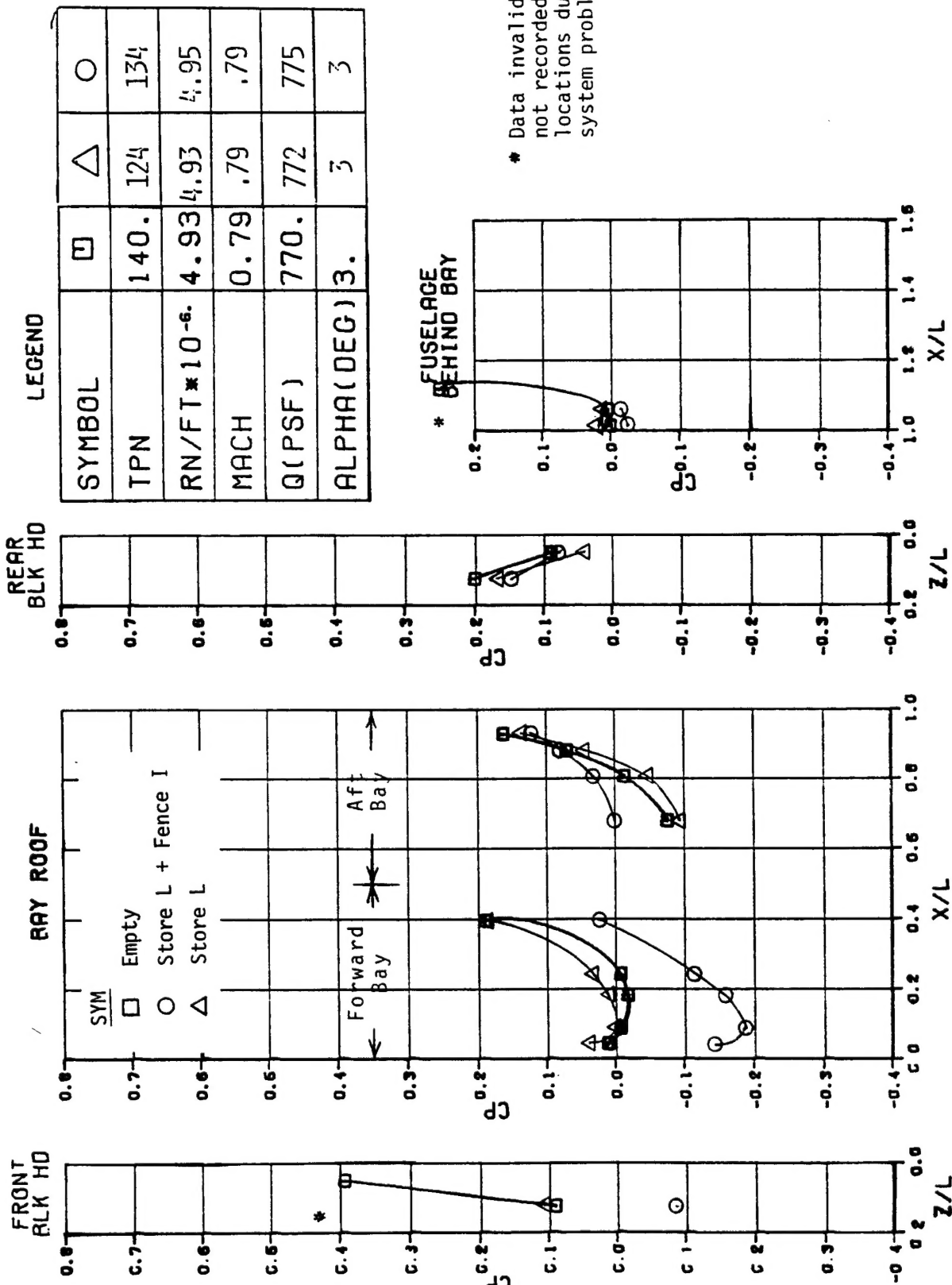


Figure 22A. Effect of Store L in Forward Bay with and without Fence I, Configuration 3.

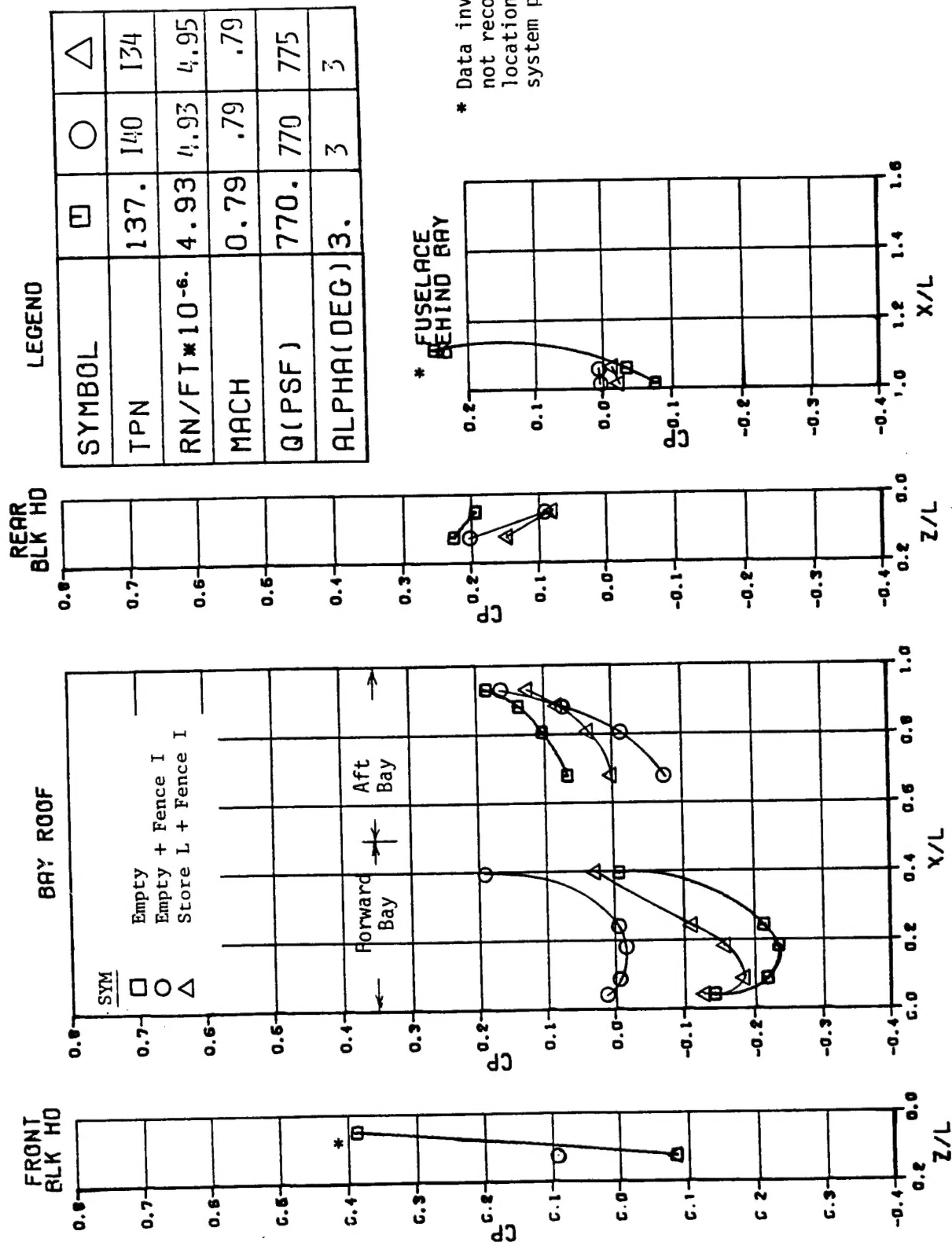


Figure 23A. Effect of Fence I with and without Store L in Forward Bay, Configuration 3.